Passive Components Technology Roadmap

(Version 1.1 EN, Preliminary English Edition)

MEXT
Basic Technology Research and Development Project for Innovative Power Electronics

Passive Components Technology Roadmap Working Group, ed.

March 2026

Preface

The Ministry of Education, Culture, Sports, Science and Technology's (MEXT) "Basic Technology Research and Development Project for Innovative Power Electronics (hereinafter referred to as INNOPEL)" is a national project for research and development aimed at innovating power electronics (power electronics) technology, a key technology for energy conservation and high performance, in order to contribute to the realization of a carbon-neutral, highly digital society. INNOPEL considers the insufficient research and development of power devices that fully utilize the excellent material properties of next-generation semiconductors such as GaN, passive components and power electronics circuit systems that can support higher performance (e.g., high-speed operation) to be an important issue, and is developing individualized products that take advantage of the characteristics of power devices, passive components and power electronics circuit systems. In addition to the individual research and development that takes advantage of the characteristics of power devices, passive components, and power electronics circuit systems, we are promoting research and development that focuses on the "integration" of power electronics devices as a whole.

When I was appointed Program Director (PD) at the start of INNOPEL, I had a meeting with Program Officers (PO) Dr. Shimizu, Dr. Matsumoto, Dr. Yamaguchi, and MEXT officials to discuss INNOPEL's management policy, etc. As the management policy, research themes in the three technical areas of power electronics circuit systems, power devices, and passive components The operating policy is that research themes in the three technical areas of power electronics circuit systems, power devices, and passive components will basically be researched and developed in each of these areas, including the investigation of academic principles. In addition, based on the principle of "bringing together the power electronics as a whole," and in accordance with the policy of "building innovative power electronics technology through information exchange and collaboration while respecting fairness and originality as a gentleman researcher," we will exchange opinions with the Theme Leader, and under the advice of the PD and PO, we will, for example, discuss the requirements of power electronics circuits, power devices, and passive components with the Theme Leader and the PD and PO. For example, requests for power electronics circuits are fed back to the research area of power devices and passive components, and requests from power devices and passive components are fed back to the power electronics circuit system area, and the research content, goals, milestones, etc. of the theme are reviewed as necessary from the viewpoint of application to power electronics devices. In this way, the technical areas will collaborate with each other. In this way, we aim to establish integrated innovative power electronics technology by promoting collaborative research across technical areas.

In order to promote such collaborative research smoothly, it is important for research themes in the power electronics circuit system area, power device area, and passive device area to fully understand and grasp each other's technological features, issues, and future directions, etc., and to promote each other's research and development. However, since there has been little interaction between the different technology areas, the meanings of each other's words and the direction of each other's technology are not well understood. However, although there are many technology roadmaps for power devices such as Si and SiC, there are few technology roadmaps that refer to passive components, and in particular, there are no technology roadmaps for passive components from the viewpoint of "integrating them as power electronics devices.

For this reason, we have decided to present a technology roadmap from the viewpoints of power electronics circuit system researchers and passive device material and device researchers, and while understanding each other's words, discuss the current status and issues in each technical area, research directions and future challenges, and consider and construct a passive device technology roadmap as a collaborative theme for INNOPEL as a whole. We have decided to implement this activity as a collaborative theme for INNOPEL as a whole.

Thanks to the continuous activities of the PO, theme leaders, working committee members and experts from various fields, and the cooperation and support of many people over the past five years since the start of the project, we have been able to release "Passive Device Technology Roadmap Version 1". We would like to express our sincere gratitude to all those involved. Although there may be many points of concern, such as inadequacies and uncertainties in this first effort, we hope that it will be of some use to you in your research and development. I also hope that this passive device technology roadmap will be a catalyst for more active discussions among the various technical fields of power electronics, and that the passive device technology roadmap will be revised based on your discussions in the future.

March 2026
INNOPEL Program Director
Tatsuo Omori

Passive Device Technology Roadmap List of Working Group Members

<Program Director and Program Officer>

Tatsuo Omori	Mitsubishi Electric Corporation
Masahiro Yamaguchi	Tohoku University
Toshihisa Shimizu	Tokyo Metropolitan University
Isao Matsumoto	Nagoya University

<Committee members>

Kan Akatsu	Yokohama National University
Takanori Isobe	University of Tsukuba
Takaaki Ibuchi	Osaka University
Yoshinao Iwaji	Ibaraki University
Yasushi Endo	Tohoku University
Satoshi Okamoto	Tohoku University/National Institute for Materials Science
Kenichi Onda	Nippon Chemi-Con Corporation
Shuji Kato	Tohoku University
Shin Saito	Tohoku University
Toshiro Sato	Shinshu University
Yukihiko Sato	Chiba University
Keita Suzuki	Tohoku University
Hiroo Sekiya	Chiba University
Naoki Takagi	Tohoku University
Yoshikazu Takahashi	Tohoku University
Hiroki Taniguchi	Nagoya University
Kazunori Hasegawa	Kyushu Institute of Technology
Hiroki Habazaki	Hokkaido University
Hiroaki Matsumori	Nagoya Institute of Technology
Tsutomu Mizuno	Shinshu University
Daisuke Miyagi	Chiba University
Kosuke Miyaji	Shinshu University
Mai Phuong Nguyen	Tamura CorporationKeiji Wada　Tokyo Metropolitan University

(Titles omitted, chapters in alphabetical order)

Passive Device Technology Roadmap Author List

<Chapter 0>

Toshihisa Shimizu	Tokyo Metropolitan University
Masahiro Yamaguchi	Tohoku University

<Chapter 1>

Kan Akatsu	Yokohama National University
Takanori Isobe	University of Tsukuba
Takaaki Ibuchi	Osaka University
Yoshinao Iwaji	Ibaraki University
Ryosuke Ota	Tokyo Metropolitan University
Hiroo Sekiya	Chiba University
Shotaro Takahashi	Akita University
Kazunori Hasegawa	Kyushu Institute of Technology
Hiroaki Matsumori	Nagoya Institute of Technology
Keiji Wada Tokyo	Metropolitan University

<Chapter 2>

Takaaki Ibuchi	Osaka University
Yasushi Endo	Tohoku University
Motoki Ota	Shimane University
Tadakatsu Okubo	National Institute for Materials Science
Satoshi Okamoto	Tohoku University/National Institute for Materials Science
Tsuyoshi Ogasawara	National Institute of Advanced Industrial Science and Technology
Ryuhei Koyama	Sashizuki Electric Mfg.
Toshiro Sato	Shinshu University
Yuki Sato	Aoyama Gakuin University
Hiroki Taniguchi	Nagoya University
Shingo Tamaru	National Institute of Advanced Industrial Science and Technology
Kazuhiro Nagahara	Nippon Chemi-Con Corporation
Manabu Hagiwara	Keio University
Kazunori Hasegawa	Kyushu Institute of Technology
Sakyo Hirose	Murata Manufacturing Co.
Kenji Machida	Nippon Chemi-Con Corporation
Tetsuji Matsuo	Kyoto University
Tsutomu Mizuno	Shinshu University
Kosuke Miyaji	Shinshu University
Mai Phuong Nguyen	Tamura Corporation
Hideto Yanagihara	University of Tsukuba

<Chapter 3>

Jun Suda	Nagoya University

<Chapter 4>

Masato Kotsugi	Tokyo University of Science
Hiroo Sekiya	Chiba University
Sho Muroga	Tohoku University
Takahiro Yamazaki	Tokyo University of Science

<Chapter 5>

Takanori Isobe	University of Tsukuba
Yasushi Endo	Tohoku University
Ryuhei Koyama	Sashizuki Electric Mfg.
Ryota Kunieda	Tamura Corporation
Shin Saito	Tohoku University
Toshiro Sato	Shinshu University
Hiroki Taniguchi	Nagoya University
Manabu Hagiwara	Keio University
Kazunori Hasegawa	Kyushu Institute of Technology
Hiroki Habazaki	Hokkaido University
Sakyo Hirose	Murata Manufacturing Co.
Hiroaki Matsumori	Nagoya Institute of Technology
Mai Phuong Nguyen	Tamura Corporation
Masahiro Yamaguchi	Tohoku University
Shigeyoshi Yoshida	Tohoku University
Keiji Wada	Tokyo Metropolitan University

(Titles omitted, chapters in alphabetical order)

Table of Contents

Chapter 0 Introduction 1
Section 1 Positioning of this roadmap 1
1.1 Objective 1
1.2 Guideline 1
1.3 Policy 1
1.4 Methodology 3
1.5 Public Outreach 5
Section 2 Composition of this Roadmap 5
2.1 Chapter Structure 5
2.2 Relationship between chapters 6
Chapter 1 Passive components viewed from circuit side 9
Section 1 Magnetic element 9
1.1 How to use passive components used in power electronics circuits 9
1.2 Gap 21
1.3 Insulation performance of transformer, ratio of iron loss to copper loss, capacitance between windings 25
1.4 Review of Magnetic Materials Used in Transformers and Inductors 29
1.5 High Flux Density Materials and Low-Loss Magnetic Elements 35
1.6 Factors in design accuracy required for magnetic components 41
Section 2 Capacitor 44
2.1 Requirements for capacitors per application (including tan δ) 44
2.2 Capacitors applied for smoothing 48
2.3 AC capacitor 49
2.4 Bottlenecks in circuit application 53
2.5 Lifetime, Reliability, and Safety 56
Section 3 Benchmark 60
3.1 Inductor 60
3.2 Common mode inductor 65
3.3 Transformers for SST 70
3.4 Capacitors for DC link 74
Chapter 2 Power electronics from the viewpoint of passive components 78
Section 1 Magnetic 78
1.1 Fundamentals of Magnetic Materials for Power Electronics 78
1.2 Thin strip, sintered 85
1.3 Powdered magnetic cores and fine particle composite cores 90
1.4 Magnetic Property Measurements 107
1.5 Transformers and inductors 132
1.6 Examples of Steinmetz coefficients 160
1.7 Tradeoffs in Materials and Manufacturing Processes for Magnetic Components 162
1.8 Modeling of Magnetic Elements 164
Section 2 Capacitors 171
2.1 Differentiating the Use of Capacitors for Power Electronics 171
2.2 Ceramic Capacitors 173
2.3 Film capacitors 175
2.4 Electrolytic Capacitors 179
Chapter 3 Development of Power Devices 191

Section 1 Power Devices 191
1.1 The Dawn of Semiconductor Power Devices 191
1.2 Performance Indicators for Power Devices 192
1.3 Unipolar and Bipolar Devices 192
1.4 Insulated gate bipolar transistor 194
1.5 Unipolar Limit 194
Section 2 Wide Bandgap Semiconductor Power Devices 196
2.1 Wide Bandgap Semiconductor Materials 196
2.2 SiC Vertical MOSFET 196
2.3 SiC Superjunction MOSFET 198
2.4 SiC Bipolar Devices 198
2.5 GaN Vertical MOSFET 199
2.6 Horizontal GaN HEMT 200
Section 3 Summary 202
Chapter 4 Utilization of Data Science 204
Section 1 Current and Future Use of Data Science 204
1.1 Data Science and Power Electronics 204
1.2 AI/ML Application in Power Electronics Circuit Design 204
1.3 AI/ML Application to Magnetic Component Property Prediction and Material Development 205
1.4 ML application to real-time control (inverter control, motor drive, etc.) 206
1.5 Application of AI/ML for Failure Prediction and Anomaly Detection 206
1.6 AI/ML Application to Topology Selection and Parameter Optimization 207
1.7 Future Research Trends and Technical Issues and Prospects 208
Section 2 Application of AI/ML to Power Electronics Circuit Design 209
2.1 Circuit Design Problem Description from AI/ML Perspective 209
2.2 Configuration Example of Optimization Software with AI/ML 209
2.3 Optimum Design Example of High Frequency Converter 210
2.4 AI/ML Design for Inverse Problems 211
Section 3 Machine Learning Modeling 211
3.1 Introduction 211
3.2 Overview of Materials Informatics 212
3.3 Modeling of Magnetic Elements and Iron Loss Analysis 214
3.4 Magnetization Reversal Analysis with Extended Landau Free Energy Model 214
3.5 Application studies of the extended free energy model: examples 222
3.6 Summary and Future Issues 224
Section 4 Utilization of Machine Learning for the Development of Magnetic Materials and Magnetic Elements 224
4.1 Machine Learning for the Development of Passive components Using Soft Magnetic Materials 224
4.2 Case Study of Analysis of Magnetic Materials Using Machine Learning 225
4.3 Case Study of Analysis of Magnetic Elements Using Machine Learning 227
Chapter 5 Technology Roadmap 229
Section 1 Design of Passive components and Its Challenges 229
1.1 Material development based on an integrated discussion of the relationship between magnetic materials and circuit design parameters 229
1.2 Technological Trends in Magnetic Elements (excluding iron-nitrogen) 232
1.3 Capacitor Technology Trends 233
Section 2 Future Issues 237
2.1 Understanding Magnetostriction 237
2.2 Current Status and Future Issues of Mounting Technology 240
2.3 Pioneering Iron-Nitrogen Magnetic Cores 243

2.4 Recycling and Reuse 247
2.5 Rare Materials 252
Section 3 In lieu of a summary 255
3.1 Coordination between circuit system area and passive device area 255
3.2 Developmental Issues in Magnetic Devices 256
3.3 Developmental Issues in Capacitors 258
3.4 Utilization of Data Science 259
3.5 Development into IEEE Collaborative International Technology Roadmap 259

Chapter 0 Introduction

Section 1 Positioning of this roadmap

1.1 Objective.

Keyword: MEXT "Basic Technology R&D Project for Innovative Power Electronics", INNOPEL, decarbonized society, passive device technology roadmap

As part of the MEXT's "Basic Technology Research and Development Project for Innovative Power Electronics" (hereinafter referred to as INNOPEL), we will establish a passive device technology roadmap for innovative power electronics technology that contributes to the realization of a decarbonized society, mainly from an academic perspective.

1.2 Guideline

Keyword: Power electronics, Newell's triangle, Vertical integration technology, Performance limit of passive components, Power devices

Power electronics technology (especially semiconductor power conversion technology) is a technological system aimed at the most efficient and effective conversion of electrical energy into the desired form. As shown in **Figure 0.1.2.1**, Newell's triangle [(1)], this area was defined in 1973 as a technological domain that completely integrates the three domains of electronics (power devices and circuit technology), power (passive components), and control, and has since developed while incorporating many peripheral domains. Since then, it has developed while incorporating many peripheral areas. In other words, it is a vertically integrated technological field of elemental technologies in a wide range of technological fields based on "integration" as a circuit system while taking advantage of the characteristics of the constituent elements, including power devices and passive components. In recent years, while expectations for the development of power electronics technology through research and development of new power devices (SiC, GaN power devices) have been increasing, the performance limitations of passive components have become a technological bottleneck in many power electronics systems. In order to solve this problem, research and development in the three research fields of passive components, power devices, and power electronics circuit systems are being promoted at INNOPEL, and the world's first technology roadmap that provides a bird's-eye view of the direction of research on passive components for power electronics technology will be established, reflecting the research results of the three research fields. We will construct the world's first technology roadmap for passive components for power electronics technology, reflecting the results of this research.

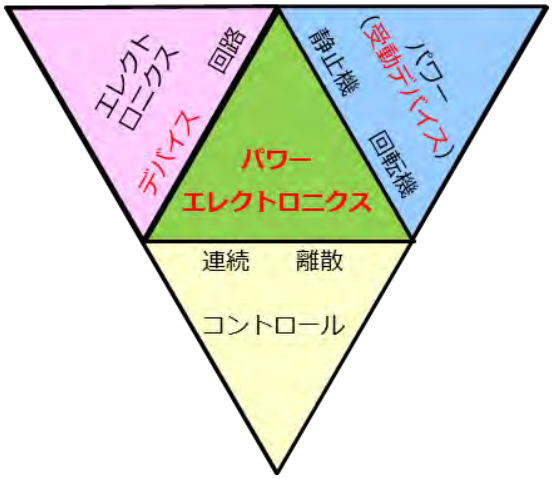


Figure 0.1.2.1 Newell's triangle

Reference

(1) William E. Newell : "Power Electronics -Emerging from Limbo", IEEE Conference record on PESC73, pp.6-12(1973).

1.3 Policy

Keywords: wide range of application fields of power electronics technology, application dependence of passive components, small and medium power capacity power electronics devices, necessity of passive device technology roadmap

As shown in **Figure 0.1.3.1**, power electronics technology is applied to an extremely wide range of industrial fields, including electric power, automobiles and electric railroads, information and communications, home appliances, and robotics. Since the circuit operating conditions (voltage, current, switching frequency, etc.) of power electronic devices vary greatly depending on the field of application, the power devices and passive components used in these devices are also of the appropriate type for the respective operating requirements. **Table 0.1.3.1** provides a rough classification of the types of passive components (magnetic elements and capacitors) used in various power electronic devices and the devices to which they are applied. The most important components of each device are indicated by ◎, ○, and △ marks (blanks indicate applications where they are not generally used). Magnetic elements can be roughly classified into transformers and inductors. For example, in transformers, low-frequency transformers tend to be used more frequently in large-capacity systems, while high-frequency transformers are used more frequently in systems with small to medium capacities or smaller.

While power electronics technology is applied in an extremely wide range of fields, INNOPEL's target for power electronics systems are inverters for automobiles, inverters for driving motors, power supplies for telecommunications, high-performance SSTs, and high-frequency switching power supplies, as devices with small to medium power capacity (capacity: 50 kW or less, switching frequency: 10 kHz to 10 MHz). One of the reasons for this is that there are abundant research examples of a wide variety of magnetic and dielectric materials suitable for power electronics devices in this area. In other words, passive components used in transmission power systems and industrial high power capacity power electronics devices are excluded from the scope of this roadmap because there are few options for magnetic and dielectric materials and research cases are limited. In other words, this passive device technology roadmap is intended to summarize the requirements and basic technologies of passive components required for power electronic devices with small to medium power capacities, as well as to discuss the materials that constitute passive components (magnetic and dielectric materials), the components and design methods of passive components, while taking advantage of INNOPEL's research activities and results. The paper also summarizes the future research and development of passive components, making use of the research and results of INNOPEL, as well as the materials (magnetic and dielectric materials) that compose passive components. The history of research and development of various power devices and wide bandgap devices, which have shown rapid progress in recent years, are also reviewed to help the reader understand the need for a roadmap of passive device technology.

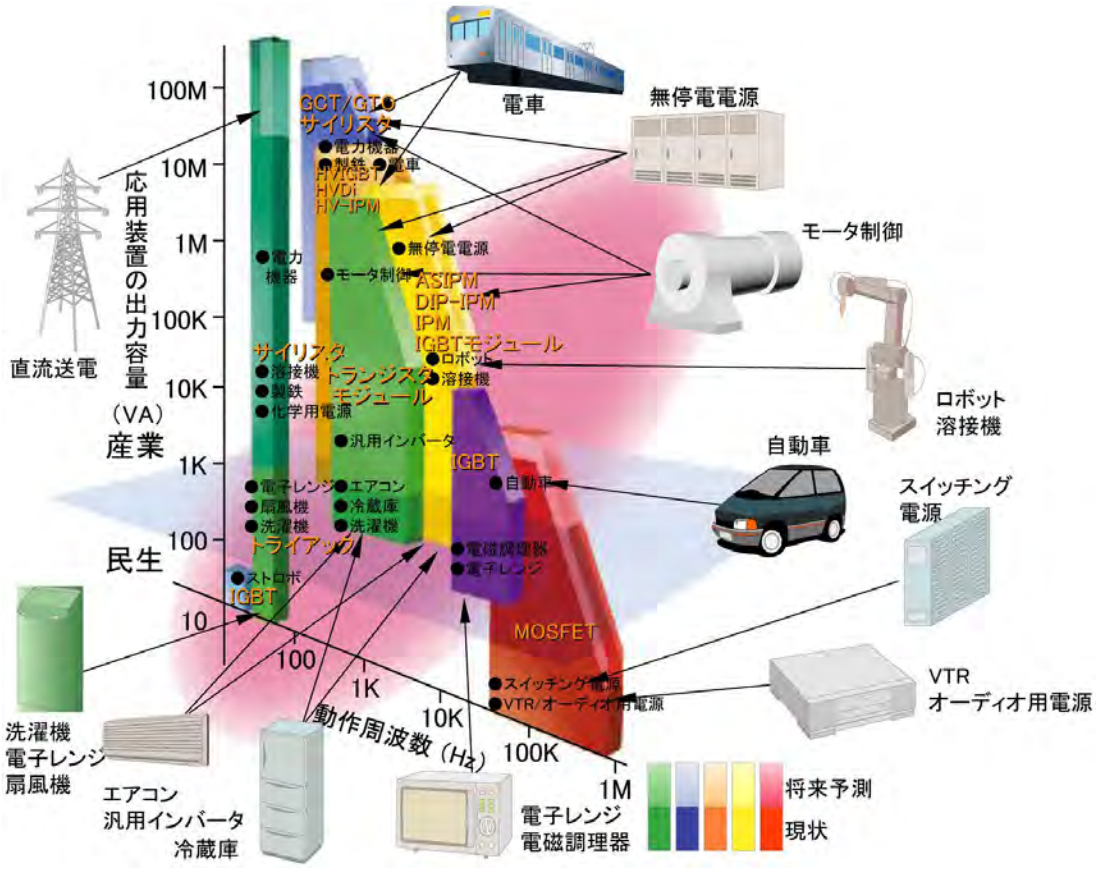


Fig. 0.1.3.1 Application fields of power electronics equipment

Table 0.1.3.1 Applications of power electronics circuit systems and types of passive components used in them

用途	例	磁気素子							コンデンサ					
		変圧器		インダクタ										
		高周波	低周波	交流フィルタ	交流低周波	昇降圧，平滑	共振	EMI	低周波交流	交流フィルタ	直流平滑	共振，ZVS	スナバ	EMI
新・省エネ	大容量 PCS		◎	◎	○			△	○	◎	◎		◎	△
	中小容量 PCS	△		◎	○	○		◎		◎	◎		◎	◎
	大容量 WT		◎	○	○			△	○	◎	◎		◎	
産業用	大容量 UPS		◎	◎	○			○		◎	◎		◎	○
	中小容量 UPS		○	◎	○	○		◎		◎	◎		◎	◎
	中容量 SST	◎		◎	○			◎		◎	◎	○	◎	◎
	大容量 ACDr							△			◎		◎	△
	中小容量 ACDr			△				◎		△	◎		◎	◎
	AF，SVG		△	◎	○			◎		◎	◎		◎	◎
EV用途	主機駆動					◎		△		○	◎		◎	△
	補機	△				◎	△	○			○		○	○
通信電源	中容量 DC/DC	◎				◎	○	◎		◎	◎	◎	◎	◎
	PFC			◎			○	◎		◎	◎		◎	◎
高周波用途	小容量 DC/DC	◎	○			◎	◎	◎			◎	◎		◎
	WPT	○					◎	△			○	◎		△

PCS: power conditioner, WT: wind power generation, UPS: uninterruptible power supply, SST: electronic transformer, ACDr: AC motor drive, AF: active filter, SVG: reactive power compensator, PFC: power factor correction converter, WPT: contactless power supply

1.4 Methodology

Keyword: Passive device technology roadmap study working group, Passive device technology roadmap study working group, Electrical characteristics of magnetic elements and applicable magnetic materials, Electrical characteristics of capacitors and applicable capacitors, INNOPEL's viewpoint

As part of INNOPEL research activities, we organized the "Working Group for Passive Device Technology Roadmap Study" consisting of program participants and external experts, and the "Working Group for Passive Device Technology Roadmap Study" in charge of practical work.

The Passive components Technology Roadmap Study Working Group held a total of four meetings to share awareness of the current technical theory of passive components (transformers, inductors, and capacitors) from the viewpoint of power electronics technology. Researchers mainly in the field of power electronics circuits gave presentations on the topics shown in **Table 0.1.4.1** and exchanged questions and opinions with INNOPEL research participants on the technical issues.

Table 0.1.4.1 Speakers **and** subjects at the Passive Device Technology Roadmap Study Working

	date(s) (e.g. for exhibition)	speaker	Title
1st	April 13, 2023	Kan Akatsu (Yokohama National University)	Design of small, high-efficiency high-frequency transformers suitable for Solid State Transformers
2nd	June 12, 2023	Hiroaki Matsumori (Nagoya Institute of Technology)	Introduction to Inductor Design Methodology
3rd	July 31, 2023	Ryuhei Koyama (Sashizuki Electric Manufacturing Co., Ltd.)	film capacitor
	July 31, 2023	Kazunori Hasegawa (Kyushu Institute of Technology)	Requirements for capacitors from the power electronics circuit side
4th	October 16, 2023	Kazunori Hasegawa (Kyushu Institute of Technology)	Capacitor requirements expected by the circuit side for each application
	October 16, 2023	Toshihisa Shimizu (Tokyo Metropolitan University)	Reflection on the past

In conjunction with the Technology Roadmap Study Working Group meeting, INNOPEL members interviewed the passive device-related requests and issues and exchanged opinions with each other. For example, active discussions were held among the members in the circuit system area on the current status of circuit systems in the field of power electronics and their requirements and issues for passive components, and among the members in the passive device area on the current status of magnetic materials and dielectric materials and their issues. Based on these results, the electrical characteristics of magnetic elements and applicable magnetic materials from the viewpoint of power electronic systems are summarized in **Tables 0.1.4.** 2 and **0.1.4.** 3, and the electrical characteristics of capacitors and applicable capacitors **in Table 0.1.4.4**. In addition, the relevance of the research goals and research topics related to passive components in the research and development conducted under each theme of INNOPEL are summarized in the "Perspective of this Project" section. The "+" mark indicates the research subject and the research team in charge of the research on passive components, and the "-" mark indicates the expected characteristics and performance of the passive components.

Table 0.1.4.2 Electrical characteristics and applicable magnetic materials of transformers used in power electronics equipment

		電気的特長	磁性体	本プロジェクトの視点
変圧器	低周波変圧器	・単相変圧器は数十KVA程度、それ以上は三相変圧器 ・正弦波交流（50/60Hz） ・容量・電圧範囲が極めて広い ・電力効率は99%以上	珪素鋼板	対象外
	インバータ変圧器	・単相変圧器は数十kVA、それ以上は三相変圧器 ・PWMパルス電圧（正弦波交流（50/60Hz）＋PWM周波数） ・容量、電圧範囲が極めて広い ・電力効率は99%以上 ・変圧器漏れインダクタンスを利用する場合あり	珪素鋼板 6.5%珪素鋼板	高周波変圧器で不足する部分について 追加検証
	高周波変圧器	・単相変圧器が主体 ・高周波矩形波交流電圧 ・周波数はパワーデバイスと電力容量に依る （IGBT：数kHz～十数kHz、SiC：十数kHz～数十kHz、 SiパワーMOSFET：数十kHZ～数百kHz） ・数kVA～100kVA（大容量はコア大型化） ・銅損（高周波負荷電流）対応でリッツ線の使用も多い ・偏磁防止のため適切な励磁電流（5～10%程度）	珪素鋼薄帯 アモルファス系 フェライト系 など多様	＋サーバ用電源装置（高橋チーム） ＋高性能SST（和田チーム） ＋超低損失磁性材料（岡本チーム） ・高透磁率 ・高飽和磁束密度（@1.5T） ・小型低損失（@100cc/3.3kW） ・低漏れインダクタンス（@20nH） ・絶縁耐圧（@10～20kV）
	超高周波変圧器	・単相変圧器 ・正弦波または矩形波 ・数百kHz～数MHz ・数十W～1kW ・銅損（高周波負荷電流）対応でリッツ線の使用も多い	Ni-Znフェライト メタルコンポジット カーボニール 空芯トランス	＋MHz共振形電源（佐藤チーム） ＋磁気異方性軟磁性材料（水野チーム） ・損失（鉄損・銅損・他）最小化設計手法 ・既存磁性体の使いこなし （空芯トランスとの比較検討）

Table 0.1.4.3 Electrical characteristics of inductors used in power electronics devices and applicable magnetic materials

		電気的特長	磁性体	本プロジェクトの視点
インダクタ	直流平滑 インダクタ	・単相インダクタ ・リプル電流＋直流電流（磁路ギャップ） ・インダクタンス大（数～数十mH）	珪素鋼板	・直流重畳特性については追加検証
	交流フィルタ インダクタ	・単相あるいは三相インダクタ ・インダクタンス値（%インダクタンス：5～10%） ・PWMリプル電流＋低周波負荷電流による励磁 ・磁界バイアス対応（中・低透磁率、磁路ギャップ）	珪素鋼板 6.5%珪素鋼板 フェライト Fe系粉体 その他	＋ACドライブシステム（高橋チーム） ＋サーバ電源（高橋チーム） ＋高性能SST（和田チーム） ＋超低損失磁性材料（岡本チーム） ・キャリア周波数50kHz～500kHzに対応したAC フィルタ ・高飽和磁束密度（例：1.5T） ・中・低透磁率、磁路ギャップ必要性検討 ・材料選択、構造を含めた最適設計手法 （Area Product法等）
	EMI用 インダクタ	・ディファレンシャルモードインダクタ 低周波＋高周波電流対応、高Bs、磁界バイアス ・コモンモードインダクタ 高周波電流対応 ・150kHzから30MHzまでの周波数帯域に対応 ・複素透磁率の特性にあわせた使用 フェライト系：比透磁率実部（μ'）に依存 アモルファス系：透磁率虚部（μ''）の効果も 活用	Mn-Znフェライト Ni-Znフェライト アモルファス薄帯 カーボニール	各チームでEMIへの取り組み

Table 0.1.4.4 Electrical characteristics of capacitors used in power electronics equipment and applicable capacitors

		電気的特長	適用コンデンサと課題	本プロジェクトの視点
コンデンサ	直流平滑コンデンサ	・電流：PWM周波数に依存したパルス電流＋低周波電流 ・電圧：直流成分＋交流成分（高周波＋低周波） ・静電容量大（数十μF～数千μF/単体） ・低ＥＳＲ、（低ESL）	・電解コンデンサ 長寿命、高耐圧、低ESR ・フィルムコンデンサ 高静電容量、小形、高温度 ・セラミックコンデンサ 静電容量安定、短絡故障保護	＋高耐圧固体電解コンデンサ（幅崎チーム） ・固体電解コンデンサの高耐圧化 ＋高誘電率常誘電体（谷口チーム） ＋ACドライブシステム（高橋チーム） ＋サーバ用電源（高橋チーム） ・低周波リプル電流低減 ＋継続調査 ・電圧/電流リプル耐量 ・温度許容値、外形寸法、寿命推定
	交流フィルタコンデンサ	・電流：PWM周波数に依存したリプル電流＋低周波電流 ・電圧：交流成分（高周波成分＋低周波成分） ・静電容量は中程度（数十μＦ～数百μＦ） ・低ＥＳＲ（電流容量）、低ＥＳＬ（EMIの観点）	・フィルムコンデンサ 低ESR、高エネルギ密度	＋多機能SST（和田チーム） ・フィルムコンデンサの使いこなし ＋高周波スイッチング用途ではセラミックコンデンサの適用も期待。
	スナバコンデンサ	・電流：パルス電流 ・電圧：ほぼ直流（Cs(DC)）、Cs(CL)）、パルス電圧（Cs(ZVS)） ・静電容量小（数百μF～数十μF）、低ＥＳＬ、（低ESR） ・電流容量（ZVSスナバ、充放電スナバ）	・スナバ回路方式に依存 ・フィルムコンデンサ 低ESL、電流容量 ・セラミックコンデンサ 低ESL、短絡故障保護	＋高誘電率常誘電体（谷口チーム） ・静電容量安定化 ＋継続調査 ・実装構造を踏まえたスナバ回路と必要なコンデンサの検討
	ノイズフィルタコンデンサ	・電流：高周波パルス電流＋低周波電流 ・電圧：直流成分あるいは交流成分 ・静電容量小（数ｎＦ～数百ｎＦ） ・極低ＥＳＬ	・フィルムコンデンサ ・セラミックコンデンサ	＋継続調査
	共振コンデンサ	・電流：高周波正弦波電流 ・電圧：高周波正弦波電圧 ・静電容量小（数百nF～数十μF）、低ＥＳＲ、高電流密度 ・静電容量が小さくても高電流密度、高耐圧	・フィルムコンデンサ ・セラミックコンデンサ	＋継続調査

Based on the result of the working group on passive device technology roadmap, the working group on passive device technology roadmap was established to work on the writing of the passive device technology roadmap. The working group reviewed the previous roadmap for passive device technology and discussed the procedure of roadmap preparation, the structure of the roadmap manuscript, and the schedule for writing the roadmap. After that, the draft of the roadmap structure was revised in several working meetings, authors were selected and requested to write the roadmap, and opinions were exchanged on the draft of the roadmap. After that, the manuscript was reviewed by the main members, the authors revised their drafts, and the editing and proofreading of the final manuscript were completed.

1.5 Public Outreach

Keyword: INNOPEL Symposium, IEEJ Industrial Applications Division Meeting, Magnetics Society of Japan Symposium

The progress of the above 1.1 to 1.4 was reported at INNOPEL Symposium 2022 (December 14, 2022) and INNOPEL Symposium 2023 (February 28, 2024), followed by the Organized Session "O1: Roadmap Study of Passive components for Power Electronics" at the 2025 IEEJ Industrial Applications Division Conference (August 20, 2025). The importance of the technology and the usefulness of the roadmap will be widely publicized at an early stage to people in industry, academia, and government, and the importance of the technology and the usefulness of the roadmap will be widely publicized at an early stage to people in industry, academia, and government. The importance of the technology and the usefulness of the roadmap were widely publicized at an early stage, and useful feedback was obtained from the participants, compiled, and reflected in the content.

Section 2 Structure of this Roadmap

2.1 Chapter organization

Keyword: Applications and issues of passive components, Fundamentals and recent research on magnetic and dielectric materials, High-speed SiC/GaN power devices and their impact on passive components, Problem solving by data science, Systematization of passive device technology roadmap linking material development and circuit requirements, Environmental issues

This roadmap consists of five chapters.

Chapter 1 discusses the applications and technical understanding of passive components from the circuit system area. First, typical applications of magnetic elements (transformers and inductors) in power electronic devices, design methods for passive components, and current issues are discussed. Typical applications of capacitors in power electronic devices, their capacitor requirements, and current issues are also discussed. Finally, examples of transformer, inductor, and capacitor designs (benchmarks) developed through INNOPEL research will be presented, and the limitations of the current technology and its solutions will be discussed.

Chapter 2 discusses research on high-performance passive components for power electronic devices from the viewpoint of research and development in the passive element area. Passive components are divided into magnetic elements (transformers and inductors) and capacitors. First, the basic theory of magnetic materials used in power electronics devices, typical structures of magnetic materials (fine particles and thin bands), and their frequency characteristics will be explained. Then, measurement techniques for magnetic materials will be discussed. Typical magnetic materials used in various transformers and inductors and their characteristics are explained with the latest research results. Finally, modeling techniques for magnetic elements will be explained. As for capacitors, the basic characteristics of ceramic capacitors, film capacitors, and electrolytic capacitors used in power electronics devices and the latest research results including INNOPEL research will be introduced.

Chapter 3 presents the history of development, current status, and future prospects of power devices related to passive components for power electronics.

Chapter 4 discusses the current status analysis and future prospects for the utilization of data science to solve passive device problems.

Chapter 5 discusses the technology roadmap. First, the direction of material development based on a comprehensive discussion considering the relationship between circuit design and magnetic material parameters is discussed. In other words, from the viewpoint of whether the performance improvement index of magnetic materials up to now matches the direction of problem solving for transformers and inductors used in power electronics devices, the required performance of magnetic materials is discussed by conducting case studies of several transformers and inductors. As for capacitors, the possibility of new dielectric materials for ceramic capacitors based on the application requirements for power electronics devices, the possibility of higher breakdown voltage of solid electrolytic capacitors for electrolytic capacitors, and the limitations of current technology and expectations for new dielectric materials and films for film capacitors will be discussed. In the case of film capacitors, the limitations of current technology and expectations for new dielectric films are discussed. As future issues, we will discuss the possibility of reducing the loss caused by magnetostriction of magnetic materials and the possibility of nitrogen-iron based magnetic materials, based on the research results of INNOPEL. Furthermore, with a strong awareness of environmental issues, the current status and future issues concerning the recycling and reuse of passive components and rare materials will be discussed.

Chapters 1 through 5 are interconnected and have a coherent structure. The increase in the speed of SiC/GaN power devices , which is discussed in Chapter 3, has brought to light the issues of passive components and increased the need for new materials and structures, and provides the basis for understanding the overall background ofthis roadmap.

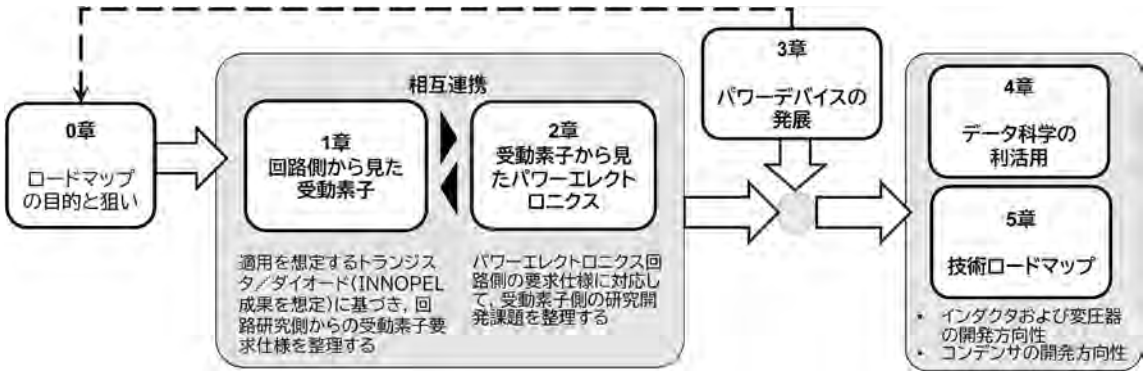


Figure 0.2.1.1 Relationship between chapters

[Toshihisa Shimizu]

2.2 Interchapter Relationships

Keywords: interdependence of physical properties, design, and loss in magnetic elements, Steinmetz formula, DC bias characteristics (DC superposition characteristics), difference in viewpoints between circuit technology and materials research, multi-objective optimization

In this roadmap, similar themes are discussed in several chapters. This is because circuit engineers and materials researchers focus on different aspects and discuss the same phenomenon from different standpoints. In particular, the discussion of magnetic elements is an area where design requirements, material properties, measurements, and modeling are interrelated and evolving, and therefore it is sometimes difficult to understand the discussion only from the structure of the chapters. Therefore, in this section, the relationships among chapters on the main topics related to magnetic elements are organized to clarify the logical flow of the discussion.

2.2.1 Magnetic elements and their relationship to physical properties, design, and losses

In the development of passive components, it is important to achieve an optimum balance of several performance factors such as miniaturization, loss characteristics, reliability, thermal margin, and cost, in response to the different requirements of each application. This optimization applies to both magnetic elements and capacitors. In the case of magnetic elements, material properties (permeability μ, saturation flux density B_s, coercive force H_c, etc.), circuit design (maximum operating flux density B_{max}, AC current I_{ac}, DC current I_{dc}, inductance L, *etc.*), and losses are interdependent and constrained in the design process. Among the losses, the iron loss P_{cv} , which is caused by the material, is determined by the magnetic permeability μ, operating flux density B, magnetic field H, switching frequency f_{sw}, *etc.* under the design conditions. **Figure 0.2.2.1** shows the above relationship conceptually.

From the circuit design point of view, the required electrical specifications are first determined, and then the appropriate magnetic materials, core shape, winding conditions, etc. are selected to satisfy these specifications. This flow corresponds to the design guidelines presented in Chapter 1. On the other hand, from the viewpoint of materials research, the frequency dependence of magnetic permeability, saturation flux density, loss mechanism, and processing constraints determine the performance range that can be designed and the limits of miniaturization and high efficiency. This is consistent with the discussion of material properties in Chapter 2.

These two perspectives approach the same design problem from different standpoints, but share the same design space to be addressed. That is, while design requirements direct material selection and device design, material properties determine the range of conditions that can be selected for design and the lower limit of achievable loss performance. It is reasonable to view passive device development as a multi-objective optimization problem based on this interdependence. This roadmap assumes this bidirectional nature, and each chapter integrates materials, design, loss evaluation, modeling, and future technology trends.

In addition to iron loss, copper loss is also a loss factor in magnetic elements. In addition to the DC resistance R_{dc} of the conductor, copper loss depends on the AC resistance R_{ac}, which is increased by skin effect, proximity effect, winding structure, and magnetic field distribution. Therefore, copper loss is more strongly affected by conductor design, layer composition, operating current waveform, and frequency conditions than by material properties. In this roadmap, the basic organization of copper loss and its relationship to materials and structure is presented in Chapter 2, and the subsequent chapters only touch on it indirectly in relation to higher frequencies and design requirements. It should be noted that the depth of discussion differs from that of iron loss.

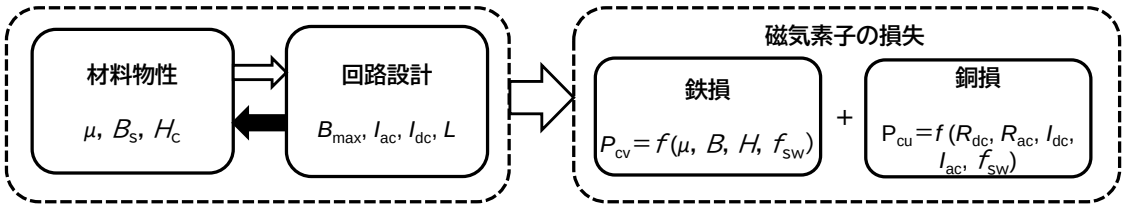


Figure 0.2.2.1 Relationship between physical properties, design, and loss in magnetic elements

2.2.2 Positioning of the Steinmetz formula

The Steinmetz equation is the classical core loss model and is the common ground referred to from different perspectives throughout this roadmap. Its treatment is developed as a framework for understanding, evaluation, design, and comparison, with the role changing from chapter to chapter. This is illustrated in **Figure 0.2.2.2.**

In Chapter 1, the Steinmetz equation is introduced as a loss model for sinusoidal excitation and is positioned as a basic equation for understanding magnetic material properties and loss behavior. Based on actual operating conditions, the extended Steinmetz equation (iGSE) corresponding to square wave and PWM waveforms is also presented, showing how the loss model has developed in response to application requirements.

In Chapter 2, the Steinmetz equation is treated as an organizing axis for loss separation (hysteresis loss, eddy current loss, excess loss,

etc.), and the physical meaning and application limits of the equation are organized. This chapter clarifies that while the Steinmetz equation is a valid approximation, it is subject to errors depending on conditions such as frequency, waveform, and material.

Chapter 3 does not deal with the equation itself, but discusses the increase in loss in regions where the Steinmetz equation can exceed the range of application, such as high dv/dt and non-sinusoidal excitation, and suggests the limits of application in terms of material development and system requirements.

In Chapter 4, the Steinmetz equation is treated as a standard for comparing loss estimation methods from data science and machine learning. The possibility that models using measured data can complement or replace the Steinmetz formula is presented, and the Steinmetz formula is positioned as a reference measure for performance evaluation.

In Chapter 5, the Steinmetz equation is used not as an object of loss analysis but as a common measure to establish design decisions such as material comparison, evaluation of application suitability, and consideration of room for miniaturization. It is characterized by the fact that it enables quantitative comparison of material performance and functions as a basis for R&D direction and design decision-making.

The Steinmetz formula is used in this roadmap as "basic formula → loss understanding → application limits → comparison with alternative methods → design decision scale".

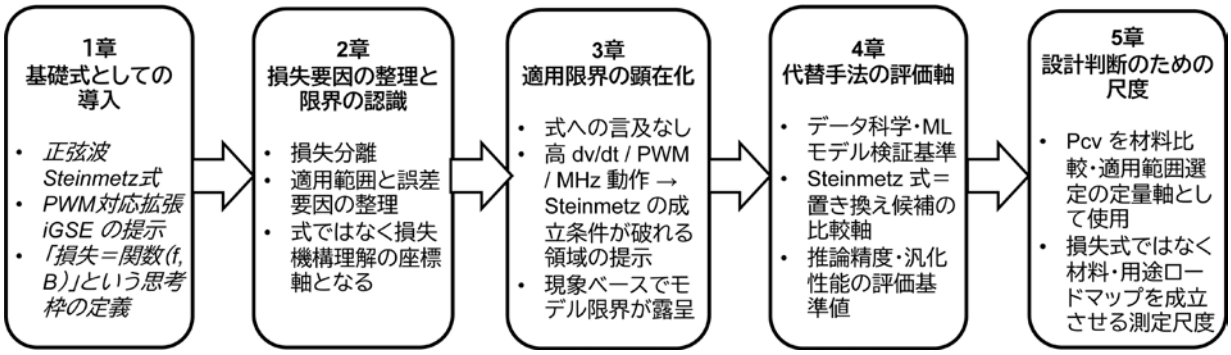


Figure 0.2.2.2 Positioning of the Steinmetz equation in the chapters

The chapters are organized in a step-by-step manner and serve as a common language for magnetic core losses.

2.2.3 Arrangement on the influence of DC bias (DC superposition characteristics)

Magnetic elements are strongly affected by DC bias, resulting in inductance reduction, loss change, and saturation constraint. These phenomena are treated in a four-step flow: Phenomenon Presentation (Chapter 1), Cause Elucidation (Chapter 2), Statistical Integration (Chapter 2), and Future Directions (Chapter 5). This is shown in **Figure 0.2.2.3**.

In Chapter 1, it is shown that a decrease in effective permeability and a change in iron loss occur as DC current increases, and that the manner in which these changes occur differs greatly from material to material. The characteristics and issues of concentrated and dispersed gaps are also discussed. These are summarized as phenomenological problems faced by designers.

In Chapter 2, the causes of the above differences are first discussed from the viewpoint of material properties based on the measured characteristics of *B-H* curves and magnetic permeability. In other words, the decrease in permeability and increase or decrease in iron loss due to DC bias are discussed for each material from the viewpoint of the characteristics of the shape of the *B-H* curve and the size of the magnetic polarization, assuming the magnetization process by magnetic wall movement. The effect of the gap is explained from the viewpoint of concentration and dispersion of magnetic resistance, regardless of the material. In this way, the causal structure of the physical property origin is systematically organized for the design issues presented in Chapter 1.

In Chapter 2, the DC superposition characteristics are further classified in an integrated manner using multivariate data. The first principal component PC1 strongly contributes to the bias field dependence of effective permeability, asymmetry of the *B-H* curve, and bias field dependence of iron loss, and functions as an axis representing "DC bias sensitivity. The second principal component PC2 reflects the "type" of iron loss, such as monotonically decreasing, monotonically increasing, or having a minimum value in relation to the bias magnetic field strength, and quantitatively distinguishes the "type in relation to bias magnetic field strength" that differs for each material. A unified scale for inter-material comparison of DC superposition characteristics is thus proposed.

In Chapter 5, DC superposition characteristics are positioned as an essential item for future passive device design and material development, and the stability of effective permeability and loss under DC bias conditions is an essential indicator for next-generation

power electronics devices and systems that are oriented toward higher currents and speeds, emphasizing the importance of incorporating the knowledge of physical origins and statistical classification presented in Chapters 1-2. The importance of incorporating the knowledge of physical properties origin and statistical classification into the design process is emphasized. It is also suggested that the definitions and measurement methods of effective permeability and iron loss as material evaluation indices should be considered for future modeling.

[Masahiro Yamaguchi]

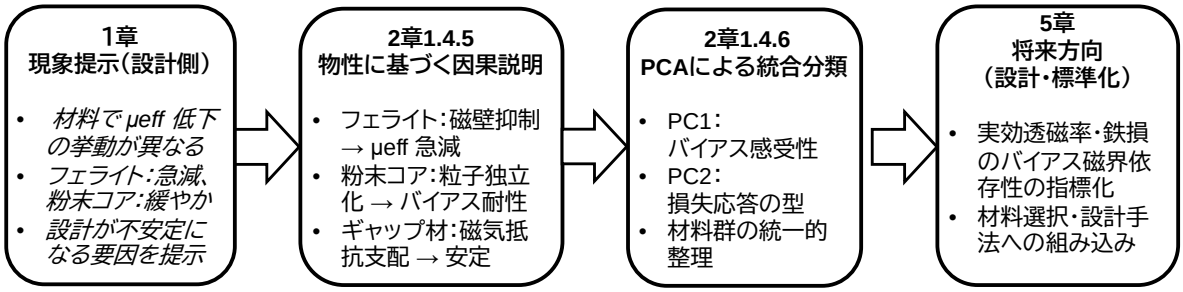


Figure 0.2.2.3 Effect of DC bias (DC superimposed characteristics)

Chapter 1 Passive device viewed from circuit side

Section 1 How to use passive components used in power electronics circuits

Keyword: Transformer, Inductor, Iron loss, Copper loss, Inverter, Converter, Chopper circuit

In power electronic circuits, power conversion is performed using power semiconductors as switching elements to control voltage and current. Transformers and inductors are indispensable passive components in realizing such power conversion [(1)].

Transformers and inductors basically consist of wires wound around magnetic materials, and it is difficult to tell the difference between them from the outside. However, the functions required of both are different as shown below, and their design methods are also completely different. This section describes the roles of transformers and inductors and a simple design method.

A transformer is an element that converts electric power into magnetic energy for transmission, and is responsible for voltage level conversion and electrical isolation between circuits. In particular, isolated DC-DC converters, for example, use a high-frequency switching voltage to convert power as magnetic flux and transmit it to the secondary side through an iron core (magnetic material) [(2)].

Inductors, on the other hand, are elements that temporarily store energy, smooth current, and eliminate switching noise, and are incorporated into circuits as elements of filters, resonant circuits, and current control. They play an important role in mitigating the current ripple and transient response associated with switching operations and in obtaining the desired voltage and current waveforms. Furthermore, in situations where DC current flows, the DC superposition characteristics of the inductor and the saturation characteristics of the magnetic material must be fully considered.

Thus, transformers and inductors are designed based on different purposes and operating principles, and are important elements that directly affect the performance, efficiency, and safety of power electronic circuits. In this section, the roles of these elements and basic matters in their design methods are explained.

1.1.1 Role of Transformers and Inductors

(1) (Power) transformer

Transformers are used primarily for isolation and transformation applications in power electronic circuits. **Figure 1.1.1.1** shows a typical transformer structure. A transformer consists of an iron core with primary winding turns N_1 and secondary windings N_2. For insulation, the primary and secondary windings of the transformer are coupled by magnetic flux through the iron core, resulting in an electrical to magnetic to electrical energy conversion, which makes electrical insulation possible. As for the transformer function, the relationship between the primary and secondary windings N_1, N_2 and the primary and secondary voltages v_1, v_2 is

$$\frac{v_2}{v_1} = \frac{N_2}{N_1} \tag{1.1.1.1}$$

Therefore, the secondary voltage can be boosted or stepped down to the desired level by appropriately setting the turn ratio of the primary and secondary windings.

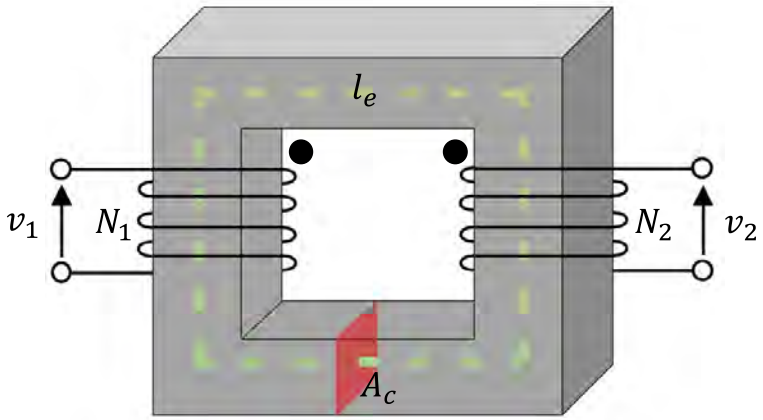


Figure 1.1.1.1 Structure of a transformer

Next, as an example of a transformer used in a power electronics circuit, consider the DC-DC converter containing a transformer and inductor **shown in Figure 1.1.** 2. The B-H curve corresponding to the equivalent circuit, excitation waveform, and excitation waveform of the transformer is shown in **Figure 1.1.3**. The equivalent circuit is based on an ideal transformer and is generally expressed using the resistance, leakage inductance, and excitation inductance of the winding. As a characteristic of the excitation waveform, the current flowing in the excitation inductance of the transformer (excitation current) is extremely small compared to the load current, so the primary winding side current is almost equal to the secondary winding side current (load current). As a result, the influence of the magnetizing force due to the load current can be ignored, and the magnetic flux density in the iron core is mainly determined by the voltage applied to the primary side. When a positive-negative symmetrical excitation voltage is applied, no DC magnetization occurs, so the B-H curve is drawn symmetrically around the origin, and the transformer design is mainly determined by the excitation voltage. In the field of power electronics, the partial B-H curve generated when the magnetization reverses within the range where the iron core does not reach saturation is called a minor loop. When designing a transformer for power electronics circuits, the iron core is first selected, and the number of turns required is set so that the iron core does not reach magnetic saturation with respect to the excitation voltage waveform.

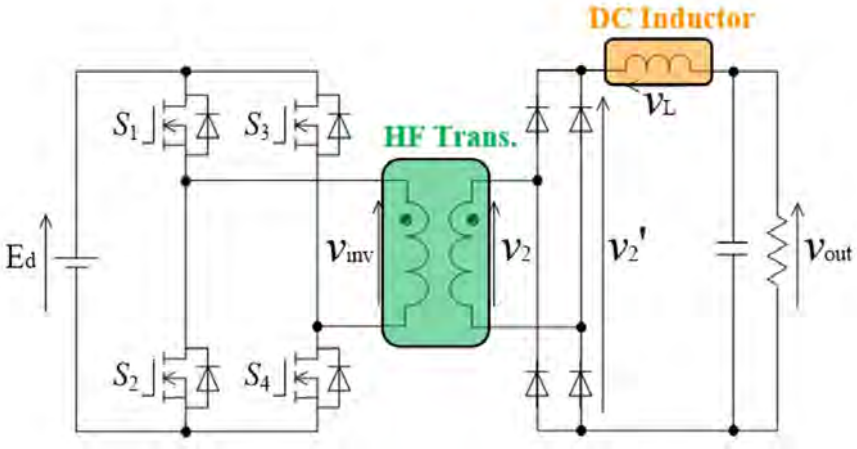


Figure 1.1.2 Example of a DC-DC converter including transformer and inductor

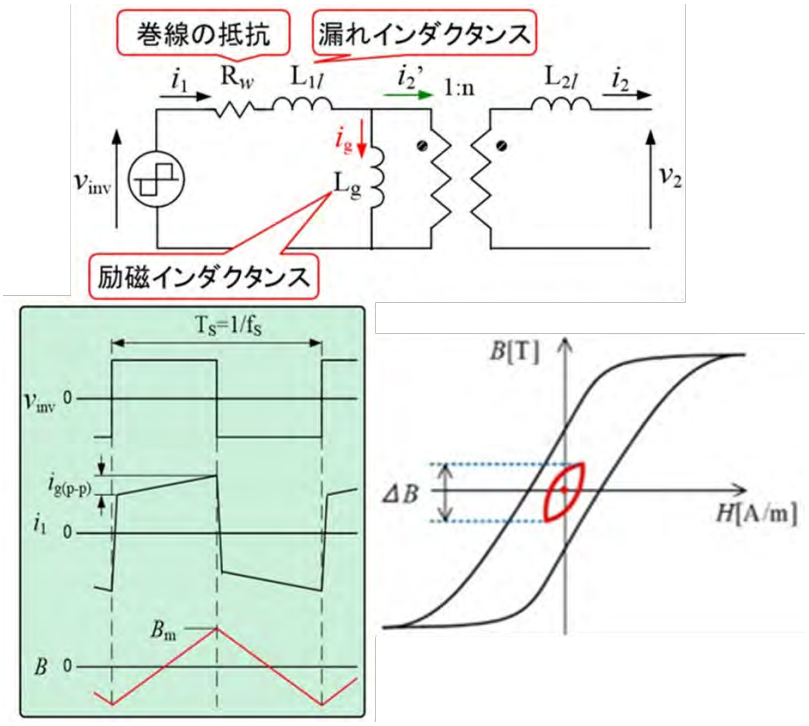


Figure 1.1.3 Transformer equivalent circuit, excitation waveform and B-H curve

Once the iron core used in the transformer is determined, the number of turns of the primary winding when an arbitrary primary winding voltage corresponding to a typical square wave or PWM (Pulse Width Modulation) waveform is applied as the excitation voltage $v_1(t)$ in a power electronics circuit N_1 can be determined by following the procedure below.

First, the magnetic flux density of the iron core when an arbitrary primary winding voltage $v_1(t)$ is applied is derived from the following.

$$B = \frac{1}{N_1 A_c} \int v_1(t)\, dt \tag{1.1.1.2}$$

where the flux density ripple ΔB when operating at any primary winding voltage $v_1(t)$ for any time t_1 between $t_2 (t_1 < t_2)$

$$\Delta B = \frac{1}{N_1 A_c} \int_{t_1}^{t_2} v_1(t) dt \tag{1.1.1.3}$$

will be.

Since the B-H curve in a transformer is drawn around the origin as shown in **Figure 1.1.1.** 3, the relationship that must be satisfied between the flux density ripple ΔB and the saturation flux density B_{sat} of the iron core used is

$$\frac{1}{2}\Delta B < B_{sat} \tag{1.1.1.4}$$

This means that a modification of Eq. In other words, by modifying equation (1.1.1.3), we can derive the number of turns of the primary winding N_1 for the selected iron core.

$$N_1 > \frac{1}{2B_{sat} A_c} \int_{t_1}^{t_2} v_1(t) dt \tag{1.1.1.5}$$

However, in order to design a transformer that can be determined by the above excitation voltage, the excitation current should be kept approximately 5 to 10% of the rated current. This is to allow a certain margin for the excitation current so that the iron core will not be demagnetized or one-saturated even if a minute DC component is generated in the current flowing in the transformer due to effects such as dead time of the switching element of the converter (i.e., to keep the center of the B-H curve near the origin).

Assuming that the transformer is an ideal transformer with no magnetic flux leakage, the excitation current i_g can be derived from the following equation using the excitation inductance L_g.

$$i_g = \frac{l_e}{\mu_0 \mu_r A_c N_1^2} \int v_1(t)\, dt = \frac{1}{L_g} \int v_1(t) \tag{1.1.1.6}$$

μ_0 is the permeability of the vacuum, μ_r is the specific permeability of the iron core, A_c is the effective cross-sectional area of the iron core, and l_e is the effective magnetic path length of the iron core. The larger the excitation inductance L_g, the smaller the excitation current.

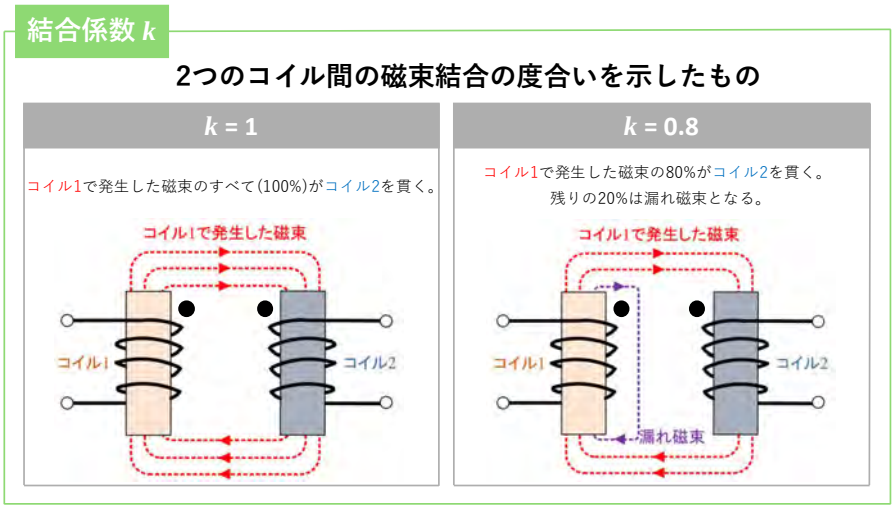


Figure 1.1.1.4 Difference in flux coupling between coils depending on coupling coefficient k

Silicon steel sheets and amorphous materials with high saturation magnetic flux density B_{sat} are often used for low-frequency operation corresponding to the commercial frequencies of 50/60 Hz, while ferrite with low saturation magnetic flux density and low loss in high-frequency operation corresponding to the switching frequencies of power electronics devices (several kHz to several MHz) is often selected for high-frequency operation. In high-frequency operation, which corresponds to the switching frequency of power electronics devices (several kHz to several MHz), the integral value ($\int_{t_1}^{t_2} v_1(t)dt$) of the excitation voltage t_1 at the excitation voltage t_2 is reduced, so ferrite is sometimes selected because of its low saturation magnetic flux density B_{sat} and low loss in high-frequency operation. Basically, high-frequency operation contributes to the miniaturization of transformers, but actual operation generates heat due to losses, so it is necessary to consider heat dissipation in conjunction with miniaturization. Therefore, it is necessary to consider the trade-off between miniaturization and losses (heat generation).

Here, not all magnetic flux is completely shared between the transformer windings, and some flux leaks out. The inductance generated by such uncoupled magnetic flux components is called leakage inductance.

The coupling coefficient k is a quantitative indicator of the degree of coupling of the windings and is defined by the following equation using the self-inductance L_1 of the primary winding, the self-inductance L_2 of the secondary winding, and the mutual inductance M.

$$k = \frac{M}{\sqrt{L_1 L_2}}, (0 \le k \le 1) \tag{1.1.1.7}$$

However, $L_1 = \frac{\mu_0 \mu_r A_c}{l_e} {N_1}^2 L_2 = \frac{\mu_0 \mu_r A_c}{l_e} {N_2}^2$

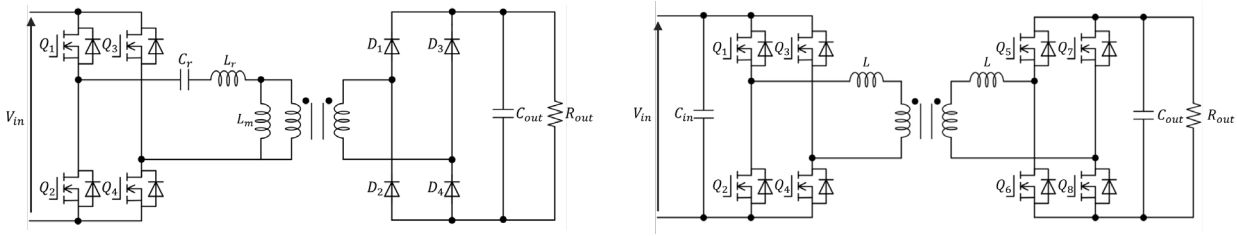
Figure 1.1.1.4 shows the difference in flux coupling between coils depending on the coupling coefficient k. In an ideal transformer, magnetic flux does not leak out, i.e., coupling coefficient k = 1. In reality, however, the coupling coefficient k is usually less than 1 due to the winding arrangement and the shape of the iron core.

Leakage inductance has tended to be avoided in transformers that are driven at commercial frequencies for power, as it is a factor that deteriorates transient response. However, in power electronic circuits, there are many examples where leakage inductance is intentionally incorporated into the design.

A typical application is the circuit shown in **Figure 1.1.1.5** below.

(a) LLC resonant converter: Soft switching ZVS (Zero Voltage Switching) and ZCS (Zero Current Switching) are realized by utilizing the leakage inductance as a resonant inductor.

(b) DAB (Dual Active Bridge) converter: The leakage inductance controls power transmission between the primary and secondary, contributing to current smoothing and timing control of energy transfer.



(a) LLC Resonant Converter (b) DAB Converter

Figure 1.1.1.5 Circuit diagram of each converter

In the design of transformers for power electronic circuits, design techniques are required to secure the desired leakage inductance by adjusting the winding structure and insulation distance. Since the target values of the coupling coefficient should be "high" or "low" depending on the circuit system, it is important to optimize the design according to the purpose.k

In designing transformers, loss reduction is an important factor in improving transformer performance. Transformer losses include "hysteresis loss, eddy current loss (iron loss)" and "loss due to winding resistance (copper loss)," and these must be reduced so that the transformer operating temperature is appropriate. For this purpose, it is necessary to reduce these losses by using various methods, such as selecting appropriate magnetic materials, using low-resistance conductors, and optimizing the winding structure, depending on each power electronics circuit.

Finally, it should be noted that insulation breakdown voltage must also be considered for use in actual power electronics equipment. In particular, for high-voltage applications, the design must satisfy the dielectric strength requirements by selecting insulation materials for the windings and ensuring sufficient distance between the windings.

(2) Inductor

Inductors are required to have the ability to store energy and smooth current by limiting current through inductance. For proper circuit operation, the inductance value of the inductor must be appropriately selected. On the other hand, the minimum inductor design requirements from the circuit side are only the required inductance value and the maximum current that can flow. However, like transformers, inductors can be designed by combining magnetic materials and windings, and because of the wide variety of combinations, inductors with the desired characteristics may not be available from component manufacturers. In such cases, the power electronics circuit designer is responsible for the design of magnetic materials and windings. This paper briefly describes the design method of inductors.

The design of inductors used in AC filters and boost/boost/down converters will be briefly discussed.

First, once the conditions of the power electronics circuit to be designed are determined, the operating frequency, current capacity, and allowable power loss of the inductor are generally determined, which naturally narrows down the magnetic materials to be used. For example, silicon steel sheets and amorphous materials are selected for low-frequency applications, while ferrite materials and sendust are selected for high-frequency applications. Detailed characteristics of magnetic materials will be described later, but the choice of magnetic material also affects the loss (heat generation) and size of the inductor.

Considering the inductance L of an inductor with a toroidal-shaped iron core as shown in **Figure 1.1.1.6**, the inductance when the winding is N once is shown by the following equation.

$$L = \frac{\mu_0 \mu_r A_c}{l_e} N^2 \tag{1.1.1.8}$$

where μ_0 is the permeability of the vacuum, μ_r is the specific permeability of the iron core, A_c is the effective cross-sectional area of the iron core, and l_e is the effective magnetic path length of the iron core.

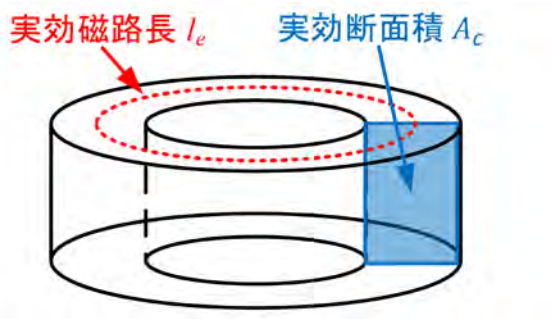


Figure 1.1.1.6 Effective cross-sectional area A_c and effective magnetic path length l_e in a toroidal core

In this way, by combining magnetic materials and windings, the necessary inductance conditions can be searched for. The coefficient $\frac{\mu_0 \mu_r A_c}{l_e}$ in Equation （1.1.1.8）corresponds to the value A_L of the core constant, so the inductance value can be derived by finding the effective cross-sectional area A_c and effective magnetic path length l_e for the magnetic circuit of the magnetic flux produced by the winding, even for iron cores of various shapes such as U-cores and E-cores. The inductance value can be derived by determining the effective cross-sectional area and effective magnetic path length of the target shape.

The above is the basic concept of inductance of inductors in general. However, in inductors used in power electronics circuits, DC current (bias current) often flows superimposed in addition to the ripple component of AC current. For example, in the DC-DC converter including the transformer and inductor shown in **Figure 1.1.1.2** above, the B-H curve (minor loop) corresponding to the equivalent circuit, excitation waveform, and excitation waveform of the inductor L_g is shown in **Figure 1.1.1.7**. The DC current is superimposed and flows in addition to the ripple component of the AC current. As a result, the B-H curve (minor loop) occurs at a position away from the origin. The minor loop is said to be formed near the operating point determined by the DC bias, but in actual power electronic circuits, the position of the minor loop is affected by the magnetization history and remanent magnetization caused by current control (feedback control) and switching operations, so the position of the minor loop changes dynamically and is not constant. Therefore, in power electronic circuits, the exact position of the minor loop on the B-H plane cannot be strictly defined and is generally not well known.

As the bias current continues to be applied, the slope of the minor loop becomes slower and the inductance value decreases due to the decrease in effective permeability. At the same time, one side of the minor loop approaches the saturation magnetic flux density region, making the iron core susceptible to one-sided saturation. When using inductors under these conditions, it is necessary to consider the characteristic of the inductance value decreasing with increasing DC current (DC superposition characteristic). As shown in **Figure 1.1.1.8**, the DC superposition characteristic is a characteristic in which the permeability of the magnetic material decreases as a DC current (bias current) flows through the inductor, and the inductance value and specific permeability change in accordance with the current as a result.

In transformers, as with inductors, it is important to reduce losses. Designs must minimize hysteresis loss, eddy current loss (iron loss), and loss due to winding resistance (copper loss), and various methods must be used to reduce loss, such as selecting appropriate magnetic materials, using low-resistance conductors, and optimizing the winding structure.

Finally, size and cost are also important design constraints. In order to meet the requirements for circuit miniaturization and cost reduction, inductors should be minimized in size and inexpensive materials and manufacturing processes should be selected. However, it is important to achieve a balanced design so that performance is not compromised by prioritizing size and cost. By comprehensively considering these factors and optimizing the design, an inductor with high efficiency and high reliability can be realized.

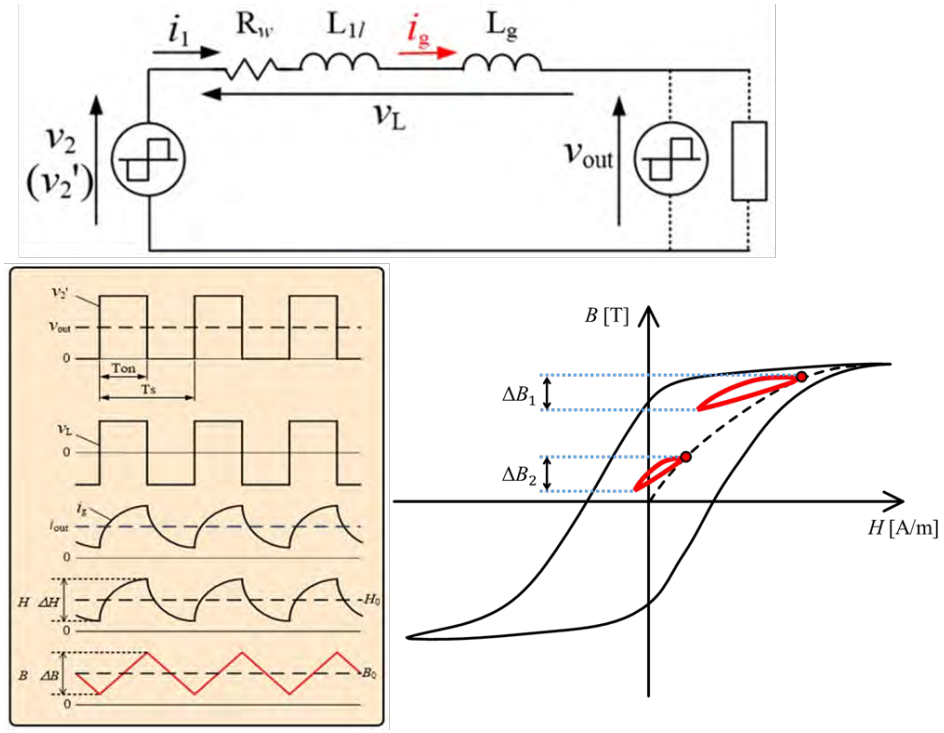


Fig. 1.1.7 Equivalent circuit, excitation waveform, and B-H curve of an inductor

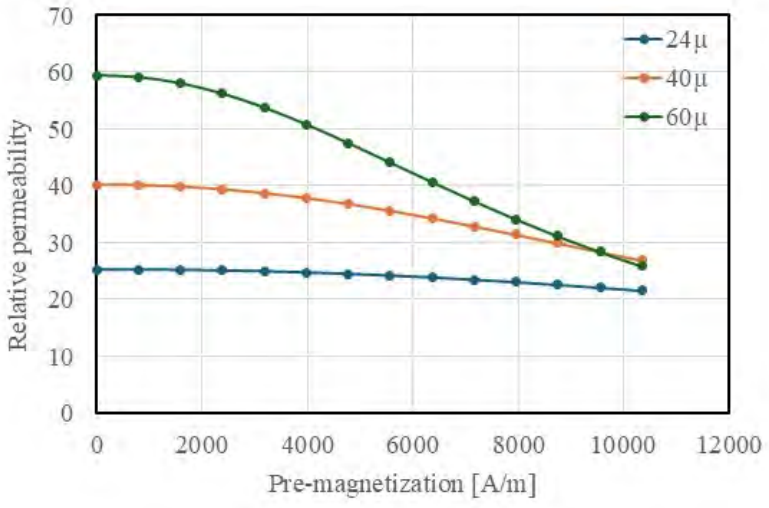


Figure 1.1.8 DC superposition characteristics of specific permeability (dust core)

1.1.2 Structure of transformer and inductor (internal iron type, external iron type)

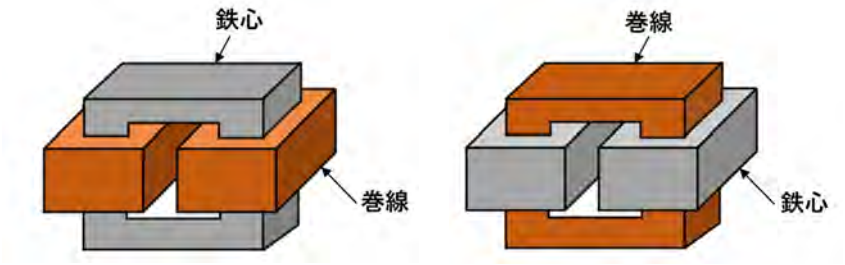
Transformers and inductors used in power electronic circuits consist of an iron core and windings, and their structure has a significant impact on electrical characteristics and operation. In particular, based on the arrangement of the iron core and windings, these devices can be broadly classified into "core-type" and "shell-type," as shown in **Figure 1.1.1.9**. **Table 1.1.1.1** shows the details of each structure.

The inner iron type has a structure in which the windings are located inside the iron core, i.e., in the central column or legs, and the windings surround the iron core. This structure is often used in power transformers and high-current inductors because of its high accessibility to the windings and easy insulation and cooling. On the other hand, leakage flux is relatively high and the coupling coefficient tends to vary depending on the structure.

In the outer iron type, the winding is placed outside the iron core, and the iron core surrounds the winding. The high magnetic flux confinement and low magnetic flux leakage provide excellent coupling coefficient, which is advantageous in noise suppression and high-

frequency operation. However, the structure tends to be complex, and ingenuity is required in the manufacturing and cooling of the windings.

Thus, the inner-iron type and outer-iron type each have their own characteristics and should be selected appropriately according to the purpose and operating conditions of the circuit.



(a) Core-type (b) Shell-type

Fig. 1.1.1.9 Structure of transformer and inductor

Table 1.1.1: Transformer and inductor construction details

(data) item	**Core-type**	**Shell-type**
Winding position	Winding wires are placed in the central column and legs of the iron core	Iron core surrounds the winding
bond coefficient	Medium (varies by design)	Highly coupled (low flux leakage)
Insulation and cooling properties	Easy to secure	Winding is encased in an iron core, requiring ingenuity in cooling
EMI countermeasures	Leakage flux is easily released to the outside	Closed magnetic flux, advantageous for EMI filter design
Ease of mounting and maintenance	Simple structure and easy maintenance	Complicated structure and difficult to manufacture windings
field of application	Power transformers, high current inductors, LLC resonant converters	High-density transformers, high-frequency applications

1.1.3 Principle of generation of iron loss and copper loss

Losses that occur when transformers and inductors are excited can be broadly divided into iron loss and copper loss, as shown in **Figure 1.1.1.10**. Iron loss is divided into hysteresis loss, eddy current loss, excess loss, and fringing loss. Copper loss is the loss that occurs in the winding, and iron loss is the loss that occurs in the magnetic material. Copper loss is divided into DC copper loss and AC copper loss, and AC copper loss is divided into skin effect, proximity effect, and fringing loss, which are factors that increase the equivalent resistance of the loss. The principle of loss generation is described below (fringing loss refers to the iron loss and copper loss caused by the magnetic flux leaking from the vicinity of the gap (fringing flux) and crossing the magnetic material and the winding. See 1.2.4 for details.)

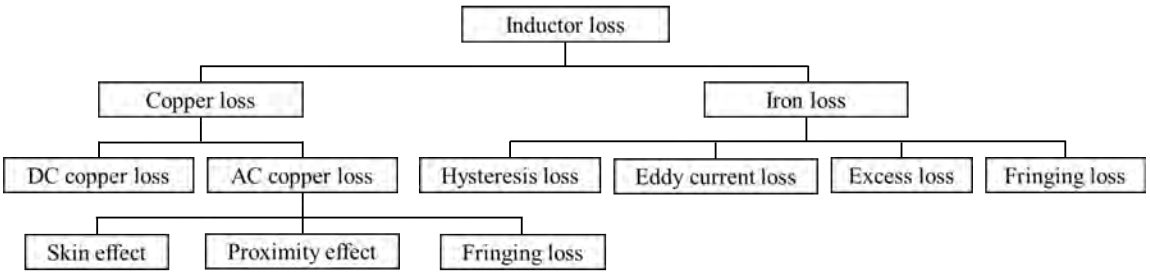


Fig. 1.1.1.10 Classification of inductor losses (including transformers)

(1) copper loss

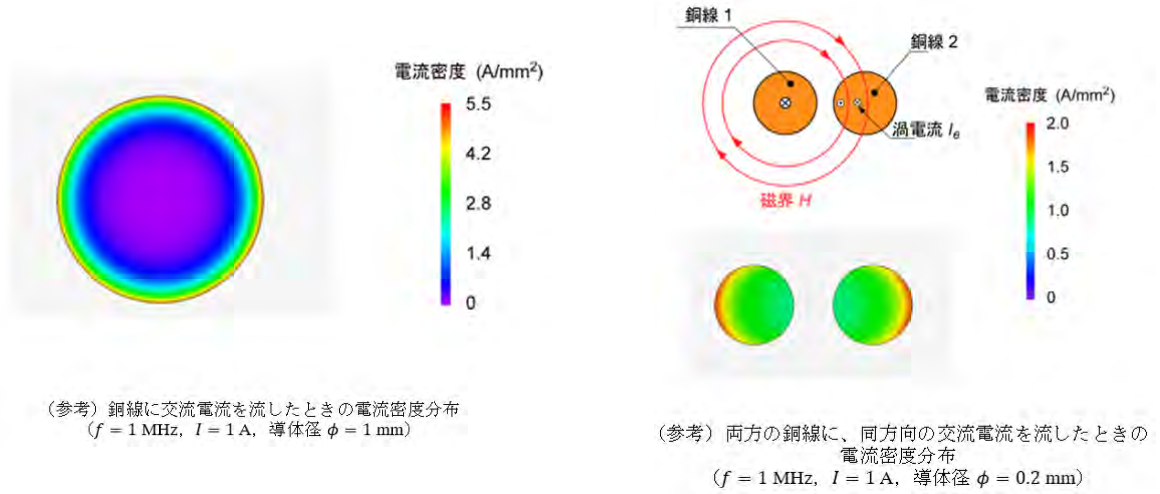
When considering the copper loss of inductors used in power converters with relatively high switching frequency, not only the DC copper loss due to the simple DC resistance of the winding, but also the AC copper loss due to the effects of skin effect and proximity effect cannot

be ignored. As shown in **Figure 1.1.1.11** (a), the skin effect is a phenomenon in which the current path concentrates on the copper wire surface (skin depth δ [m]) when AC current flows through the copper wire. As shown in Equation (1.1.1.9), the higher the frequency, the more the current is concentrated on the surface and the greater the electrical resistance of the copper wire.

$$\delta = \sqrt{\frac{2}{\omega\mu\sigma}} \tag{1.1.1.9}$$

where ω is the angular frequency and σ is the conductivity.

On the other hand, as shown in **Figure 1.1.1.11** (b), the proximity effect occurs when multiple copper wires are located very close together. The magnetic field formed by each adjacent copper wire induces eddy currents, and the current in the copper wire is concentrated in a narrow area that is in contact with the adjacent copper wire. Similar to the skin effect, the electrical resistance of the copper wire increases because the area where the current flows in the copper wire is restricted. The fringing loss is a breakdown of the AC copper loss, in which the magnetic flux leaking from the magnetic material (fringing flux) interlocks with the winding, resulting in Joule heating of the winding in the interlaced area. This loss is particularly noticeable when there is a gap in the magnetic material, and is described in detail in Section 1.2.4 below.



（参考）銅線に交流電流を流したときの電流密度分布
（$f = 1$ MHz，$I = 1$ A，導体径 $\phi = 1$ mm）

（参考）両方の銅線に、同方向の交流電流を流したときの
電流密度分布
（$f = 1$ MHz，$I = 1$ A，導体径 $\phi = 0.2$ mm）

(a) skin effect (b) proximity effect

Figure 1.1.1.11: Epidermal and proximity effects

If the conductor is a rectangular wire of the height h and width b shown in **Figure 1.1.1.12**, the skin effect and proximity effect can be approximated by the equations.

In this case, the copper loss P_S per unit length due to the skin effect can be expressed as follows [3]

$$P_S = \frac{\hat{I}^2}{4b\sigma\delta}\frac{sinh\,\nu + sin\,\nu}{cosh\,\nu - cos\,\nu} \tag{1.1.1.10}$$

where $\hat{I}$ is the peak current value. In addition, the value of

$$\nu = \frac{h}{\delta} \tag{1.1.1.11}$$

and is the ratio of height to epidermal depth.

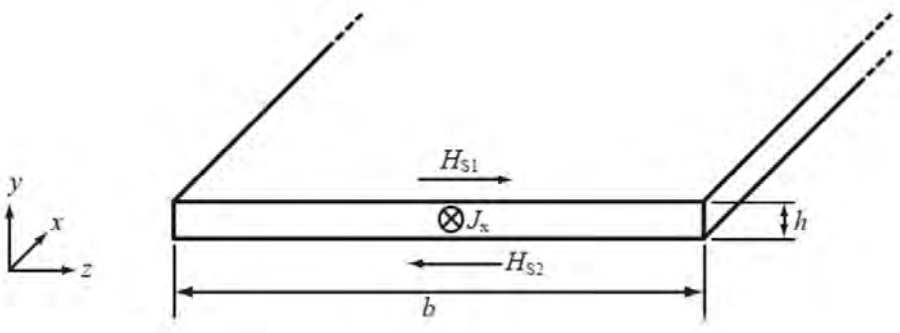


Figure 1.1.1.12: Cross-sectional diagram of a flat wire with current density in the x-axis direction

As shown in **Figure 1.1.1.13,** it is known that the copper loss P_P per unit length due to the proximity effect when an external magnetic field in the z-axis direction is applied can be calculated using Equation (1.1.1.12) [3].

$$P_P = \frac{b}{\sigma\delta}\frac{\sinh\nu - \sin\nu}{\cosh\nu + \cos\nu}\widehat{H_e}^2 \tag{1.1.1.12}$$

However, $\widehat{H_e}$ is the peak value of the complex magnetic field.

For a detailed derivation, see reference [3].

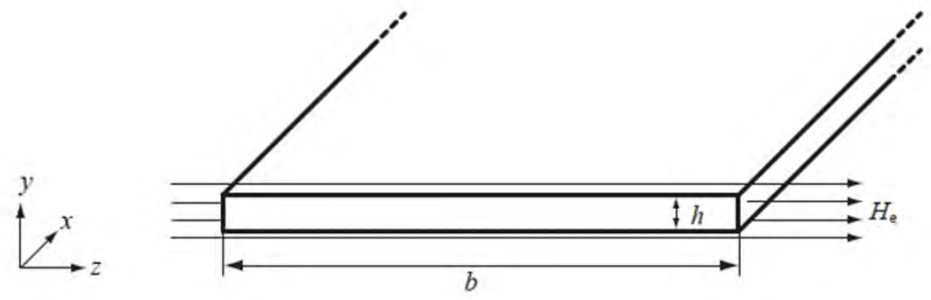


Figure 1.1.1.13: Cross-sectional diagram of a flat wire when an external magnetic field in the z-axis direction is applied

(2) iron loss

The magnetic materials of transformers and inductors are repeatedly subjected to AC magnetic fields, which cause energy losses within the magnetic materials. The three main losses are hysteresis loss, eddy current loss, and abnormal eddy current loss, which together are called iron loss.

Hysteresis loss is the loss that occurs when an AC magnetic field is applied to a magnetic material and the magnetic field strength *H* changes with a delay relative to the magnetic flux density *B*, resulting in a hysteresis loop in the B-H relationship. The hysteresis loop and the change in the magnetic domain are shown in **Figure 1.1.1.14**. The area of the loop represents the amount of energy consumed by internal friction due to magnetic wall movement and spin rotation, which is lost with each cycle. Therefore, the hysteresis loss increases in proportion to the applied frequency.

On the other hand, eddy current loss is Joule loss caused by eddy currents (eddy closed-circuit currents) induced inside magnetic materials by time-varying magnetic flux. As shown in **Figure 1.1.1.15**, when a magnetic material is conductive, an electric current flows inside the material in response to the fluctuating magnetic flux, which causes heat to be generated. Eddy current losses are proportional to the square of the magnetic flux density, the square of the frequency, and the square of the material thickness, and are particularly noticeable during high-frequency operation. For this reason, the use of a laminated iron core consisting of insulated thin iron plates and materials with high electrical resistance (ferrite, etc.) is an effective means of suppressing eddy current losses.

Anomalous eddy current losses are losses due to small eddy currents generated by the movement of magnetic walls at relatively low power frequencies. When an external magnetic field is applied to the magnetic core, the magnetic wall moves so that the magnetic domain is aligned with the external magnetic field, and the magnetic domain expands or contracts. This movement of the magnetic wall magnetizes the magnetic core. Losses occur due to the minute eddy currents generated during this movement of the magnetic wall, which causes abnormal eddy current losses.

Since these losses directly affect the efficiency and thermal design of the circuit, both hysteresis loss and eddy current loss must be well balanced in the design of magnetic materials through material selection and iron core geometry. **Figure 1.1.1.15** shows how eddy currents are suppressed by the lamination structure. The breakdown of AC copper loss also includes fringing loss, which is almost the same as the

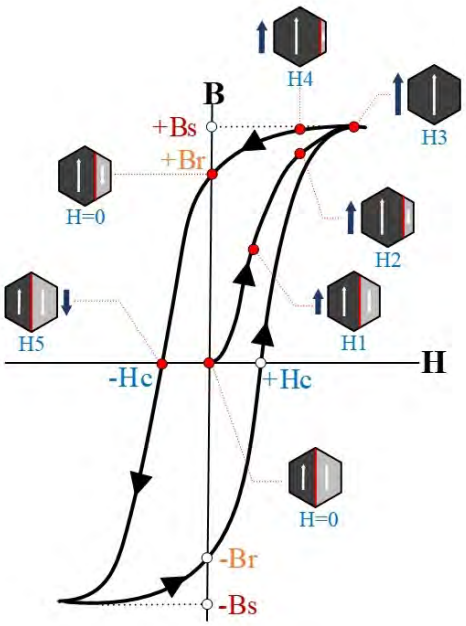


Figure 1.1.14. Hysteresis loops and magnetic domain changes

copper loss, and is a phenomenon in which the magnetic flux leaking from the magnetic material is chained to the magnetic material part, causing the loss. Especially in the case of magnetic materials such as silicon steel sheets and amorphous materials with low resistivity, the AC copper loss is the result of the magnetic flux leakage from the magnetic material.

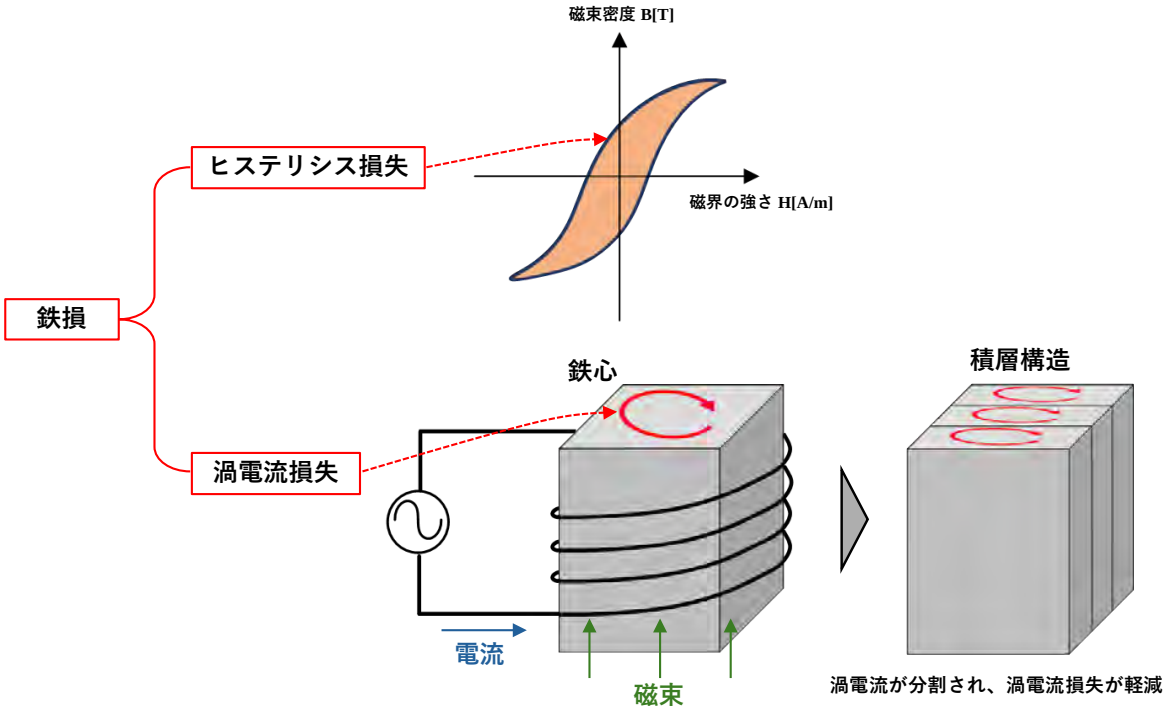


Fig. 1.1.15 Major Factors of Iron Loss **and** Examples of Eddy Current Suppression Techniques Using Laminated Structures

This is especially noticeable in sheet materials. This loss is especially noticeable when there is a gap in the magnetic material, and is described in detail in Section 1.2.4 below.

fBWhen designing transformers and inductors, it is common for power electronics engineers to utilize loss data provided by material manufacturers as a convenient way to estimate iron loss. In many cases, these data are presented as iron loss data per unit volume, including frequency, magnetic flux density, and temperature coefficient. To simplify the treatment of these data, they are often expressed approximately in the form of the Steinmetz equation [4]. This is widely used as a model for predicting iron loss under sinusoidal excitation conditions.

$$P_{cv} = kf^{\alpha}\hat{B}^{\beta} \tag{1.1.1.13}$$

where P is the iron loss per unit volume, $\hat{B}$ is the peak value of magnetic flux density, and f is the excitation frequency. The coefficients for α, β, k, and are Steinmetz's coefficients.

In some cases, the Steinmetz coefficient is listed in the data sheet, but if not, the Steinmetz coefficient, α, β, k is extracted from the iron loss data by curve fitting.

The iron loss that can be calculated with high accuracy using the Steinmetz equation is limited to the low-frequency iron loss that occurs due to the low-frequency component of the output current in transformers with sinusoidal excitation and filter inductors used in single-phase PWM inverters and three-phase PWM inverters. Steinmetz's equation is subject to errors of 20% or more in iron loss calculations for inductors used in many power converters, including PWM inverters, for the following reasons

1) The iron loss value for sinusoidal excitation is shown, but the iron loss for square wave excitation such as PWM waveforms is not taken into account.

2) Since the effect of the magnetic field bias is not taken into account, the calculation error of the iron loss drawn when the B-H curve is centered at a point other than the origin cannot be ignored.

To cope with such non-sinusoidal excitation conditions, extended models of the Steinmetz equation such as the improved Steinmetz equation (iGSE) have been proposed[5] The iGSE is shown in Equation (1.1.1.14). The iGSE can convert iron loss values for sinusoidal excitation into iron loss values for square wave excitation using the conversion equations for the Steinmetz coefficient α, β, k in Equation (1.1.1.13), and the Steinmetz coefficient in Equation (1.1.1.15) [3], [6], [7].

$$P_{cv} = \frac{1}{T_{sw}} \int_0^{T_{sw}} k_i \left| \frac{dB}{dt} \right|^{\alpha} \Delta B^{\beta-\alpha}\, dt \qquad (1.1.1.14)$$

$$k_i = \frac{k}{(2\pi)^{\alpha-1} \int_0^{2\pi} |\cos\theta|^{\alpha} 2^{\beta-\alpha}\, d\theta} \qquad (1.1.1.15)$$

However, α, β and k are Steinmetz's coefficients.

1.1.4 Methods of measuring iron loss (principles of the Epstein and two-coil methods)

This paper describes the Epstein method and the two-coil method, which are the basic methods for measuring iron loss. For the latest methods, please refer to 2.1.3.

(1) Epstein and two-coil method

The Epstein method is an iron loss measurement method for silicon steel sheets (electromagnetic steel sheets) recommended in the international standards IEC 60404-2 and JIS C 2550. The test configuration consists of electromagnetic steel plate veneers assembled into a well-shaped Epstein frame and a device as shown in **Figure 1.1.1.16** [8][9]. The formation of a well girder requires at least 12 veneers (at least 4 veneers on each side4), and incorporating these veneers into the well girder constitutes a closed magnetic path. The iron loss measurement using the primary and secondary windings (hereafter referred to as the two-coil method) is described in the next section, but it can directly measure the iron loss by ignoring the copper loss in terms of equivalent circuit.

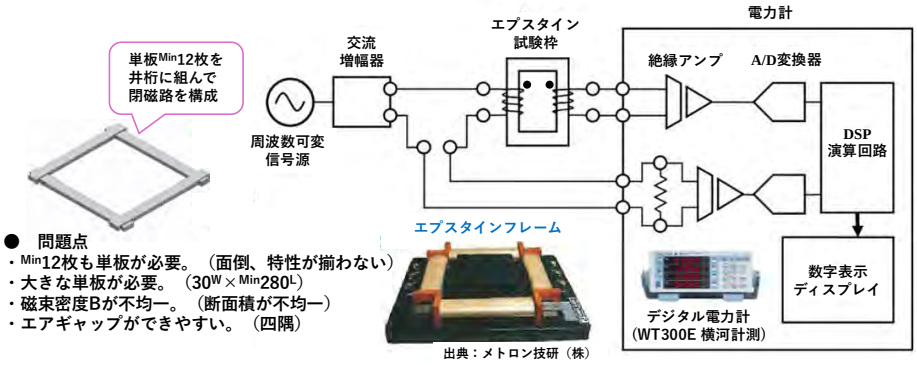


Fig. 1.1.1.16 Iron loss measurement using Epstein frame (some figures added to Fig. 19 in Ref. [9])

However, it is extremely difficult to evaluate the iron loss characteristics of a single veneer with a high degree of accuracy because it is necessary to prepare 12 or more veneers of exactly the same characteristics and shape, because of individual differences in veneer production, and because the magnetic flux density distribution inside the magnetic body differs between the four corners and each side of the well shape since the veneers are assembled into a well girder. In recent years, methods to improve the accuracy of iron loss measurement have been considered, such as using silicon steel sheets cut into a ring shape instead of the well girders of the Epstein method, or using a toroidal shape for powder materials.

(2) Principle of iron loss measurement by 2-coil method

The two-coil method is a method of measuring iron loss from the product of the voltage of the secondary winding and the current of the primary winding for excitation, where the inductor is wound with a secondary winding for voltage detection. When the inductor voltage is detected from the secondary winding, the iron loss can be measured directly, excluding the effects of leakage flux and copper loss [10]-[14]. The principle of this method is shown below.

The equivalent circuit of an inductor using the two-coil method can be considered in the same way as the equivalent circuit of a transformer because the primary and secondary windings are used for the inductor. 1 is the leakage inductance of the primary winding, $R_{winding2}$ is the copper loss of the secondary winding, L_{leak2} is the leakage inductance of the secondary winding, M is the mutual inductance, and L_1 and L_2 are the effective inductances of the primary and secondary, respectively.

In the two-coil method, the voltage detected in the secondary winding is captured by a measuring instrument such as a power meter or oscilloscope via a voltage detection element. For example, since the oscilloscope has an input impedance of 1 MΩ, the currents flowing in L_{leak2} and $R_{winding2}$ can be considered sufficiently small, and the voltage drop in L_{leak2} and $R_{winding2}$ can be ignored. Therefore, as **Figure 1.1.1.18** shows, the voltage detected in the secondary winding can be regarded as the voltage of equivalent resistance $R_{Iron\ loss,\ which}$ corresponds to iron loss. Therefore, the two-coil method can directly measure iron loss from the current in the primary winding and the voltage in the secondary

winding. **Figure 1.1.1.19** shows an example of a two-coil inductor composed of a toroidal core.

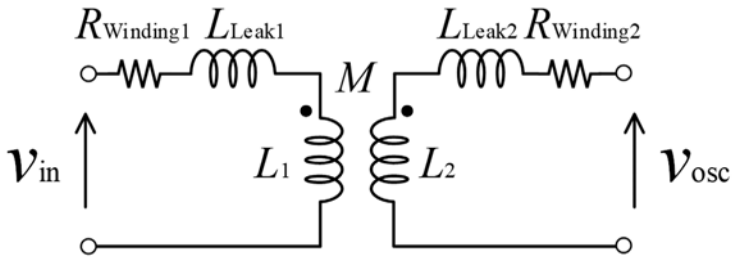


Figure 1.1.17. Inductor equivalent circuit **based on the** two-coil method

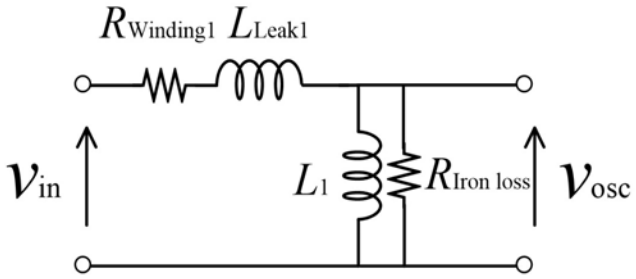


Figure 1.1.18. Inductor equivalent circuit (L-type) **based on the** two-coil method

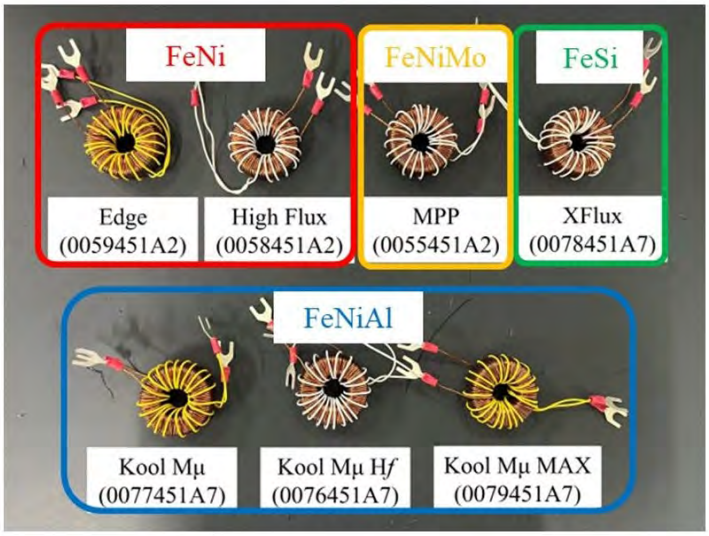


Figure 1.1.19. Example of two coils attached to an inductor consisting of a toroidal core

However, when the excitation frequency is MHz-class, it is necessary to consider the effects of stray capacitance such as capacitance generated between the inductor windings and the decrease in the input impedance of the oscilloscope [15].

References

(1) W. G. Hurley and W. H. Wölfle, "Transformers and inductors for power electronics: theory, design and applications," 4th ed. Hoboken, NJ, USA: Wiley, pp. 16, 2013

(2) N. Mohan, T. M. Undeland, and W. P. Robbins, "Power Electronics: Converters, Applications, and Design," 3rd ed. Hoboken, NJ. USA: Wiley, 2003.

(3) J. Muhlethaler "MODELING AND MULTI-OBJECTIVE OPTIMIZATION OF INDUCTIVE POWER COMPONENTS," PhD thesis, ETH Zurich, 2012.

(4) C. P. Steinmetz, "On the law of hysteresis," in Proceedings of the IEEE, Vol. 72, No. 2, pp. 197-221, Feb. 1984, doi: 10.1109/ PROC.1984.

(5) J Li, T. Abdallah and C. R. Sullivan, "Improved calculation of core loss with nonsinusoidal waveforms," Conference Record of the 36th IAS Annual Meeting (Cat. No. 01CH37248), Chicago, IL, USA, 2001, pp. 2203-2210 vol.4, doi: 10.1109 /IAS.2001.955931.

(6) H. Matsumori, T. Shimizu, X. Wang and F. Blaabjerg, "A Practical Core Loss Model for Filter Inductors of Power Electronic Converters ," in IEEE Journal of Emerging and Selected Topics in Power Electronics, Vol. 6, No. 1, pp. 29-39, March 2018, doi: 10.1109/JESTPE.2017. 2761127.

(7) A. Krings and J. Soulard, "Overview and comparison of iron loss models for electrical machines," in Proc. 5th Int. Conf. Exhibit. Ecol. Vehicles Renew. Energies (EVER), Monte-Carlo, Monaco, Mar. 2010, pp. 1-8.

(8) IEC 60404-2:2008, Magnetic materials - Part 2: Methods of measurement of the magnetic properties of electrical steel strip and sheet by IEC 60404-2:2008, Magnetic materials - Part 2: Methods of measurement of the magnetic properties of electrical steel strip and sheet by means of an Epstein frame, 2008.

(9) JIS C 2550-2:2013, Magnetic measurement methods for electromagnetic steel sheets-Part 2: Magnetic property measurement method using Epstein tester, 2013.
(10) Iwasaki Tsushinki Corporation, BH Analyzer, HP
(11) Yokogawa Measuring Corporation: "Principles and Standards of Iron Loss Measurement," TechEyesOnline, No. Reference-ElectricalSteelSheet-02, pp. 1-10, 2023
(12) H. Matsumori, T. Shimizu, K. Takano and H. Ishii, "Evaluation of Iron Loss of AC Filter Inductor Used in Three-Phase PWM Inverters Based on an Iron Loss Analyzer," in IEEE Transactions on Power Electronics, Vol. 31, No. 4, pp. 3080-3095, April 2016, doi: 10.1109/TPEL.2015. 2453055.
(13) J. Wang, N. Rasekh, X. Yuan and K. J. Dagan, "An Analytical Method for Fast Calculation of Inductor Operating Space for High-Frequency Core Loss Estimation in Two-Level and Three-Level PWM Converters," in IEEE Transactions on Industry Applications, Vol. 57, No. 1, pp. 650-663, Jan.-Feb. 2021. Jan.-Feb. 2021, doi: 10.1109/TIA.2020.3037879
(14) J. Wang, K. J. Dagan, X. Yuan, W. Wang and P. H. Mellor, "A Practical Approach for Core Loss Estimation of a High-Current Gapped Inductor in PWM Converters With a User-Friendly Loss Map," in IEEE *Transactions on Power Electronics*, Vol. 34, No. 6, pp. 5697-5710, June 2019, doi: 10. 1109/TPEL.2018.2867264
(10) J. Wang, K. J. Dagan, X. Yuan, W. Wang and P. H. Mellor, "A Practical Approach for Core Loss Estimation of a High-Current Gapped Inductor in PWM Converters With a User-Friendly Loss Map," in IEEE *Transactions on Power Electronics*, Vol. 34, No. 6, pp. 5697-5710, June 2019, doi: 10. 1109/TPEL.2018.2867264
(15) M. Mu, *High Frequency Magnetic Core Loss Study*, Ph.D. dissertation, Dept. Electr. Eng., Virginia Polytechnic Institute and State Univ. Blacksburg, VA, USA, 2013.

1.2 Gap

Keyword: Gap, Inductance, Fringing flux, Fringing loss

In the design of transformers and inductors used in power electronics circuits, it is a common practice to intentionally provide gaps (voids) in the iron core. This is mainly to prevent magnetic saturation and stabilize the inductance value [(1)(2)].

When the magnetic flux density exceeds a certain level, the iron core undergoes magnetic saturation, resulting in a sudden decrease in magnetic permeability. When the iron core saturates, the inductance value drops significantly, resulting in a rapid increase in current and other serious effects on the stable operation of the magnetic circuit. Therefore, by inserting a gap in the magnetic circuit, the magnetic resistance of the entire magnetic circuit increases, and even if the same current flows as before the gap insertion, the magnetic flux density is suppressed, making magnetic saturation less likely to occur. In other words, the existence of a gap serves to ensure the magnetic margin of the iron core.

In addition, because the gap makes part of the magnetic circuit air or non-magnetic material, the overall inductance is decoupled from the nonlinearity of the iron core material, resulting in small changes in the inductance value in response to current fluctuations. As a result, relatively linear characteristics can be maintained regardless of the operating point, such as low or high load, improving the predictability and stability of circuit design. Furthermore, since designers of power electronics circuits cannot go into the internal structure of magnetic materials (internal magnetic composition), both the saturation magnetic flux density and inductance value can be controlled by adjusting the gap length in addition to the selection of magnetic materials.

Even when an overcurrent flows, an inductor with a gap has the advantage that it is less likely to saturate and its inductance value does not decrease rapidly, thus making it easier to control excessive current increases. This is also effective from the viewpoint of current limiting functions and protection circuits.

On the other hand, a new phenomenon that arises when a gap is provided is the fringing flux. As described below, this is a phenomenon in which magnetic flux leaks out of the iron core at the end face of the gap, and the magnetic flux density is non-uniformly distributed near the gap. The fringing magnetic flux increases the actual gap cross-sectional area, which may cause a slight error in the inductance value. For the same reason, the iron loss is also non-uniform, so the accurate design of these devices requires correction by using finite element method (FEM) software. In addition, the leakage flux induces eddy currents in the surrounding conductors, which may lead to increased losses and generation of electromagnetic noise EMI (Electro Magnetic Interference). Especially in applications involving high-frequency operation, it is important to take measures against fringing magnetic flux, such as shielding the magnetic field at the gap and devising the winding arrangement.

Furthermore, if the gap is open to the outside, the fringing magnetic flux may give a strong magnetic field to the surrounding windings, causing localized heat generation and increased copper loss. Thus, the design of inductors with gaps requires multifaceted consideration of magnetic circuits, thermal design, noise suppression, etc., and is an area where the designer's knowledge and experience are truly reflected.

In the following sections, we will discuss in detail the concept of inductance value at gap insertion considering the effect of fringing flux, fringing loss, etc.

1.2.1 Concept of inductance value at air gap insertion

In this paper, among gaps, those with air gaps are specifically called air gaps, and in the discussion of inductance and fringing losses, these air gaps will be the subject of discussion.

The inductance value *L at* the time of air gap insertion is shown in Equations (1.1.2.1) and (1.1.2.2).

$$L = \frac{N^2}{R_m} \tag{1.1.2.1}$$

$$R_m = R_c + R_g = \frac{l_c}{\mu_0 \mu_r A_c} + \frac{l_g}{\mu_0 A_g} \quad (1.\ 1.2.2)$$

where N is the number of turns, R_m is the total magnetic resistance, R_c is the magnetic resistance of the iron core, R_g is the magnetic resistance of the air gap, μ_0 is the permeability of the vacuum, μ_r is the specific permeability of the iron core, A_c is the effective cross-sectional area of the iron core, l_c is the effective magnetic path length of the iron core, A_g is the effective cross-sectional area of the air gap, l_g is the effective magnetic path length of the air gap.

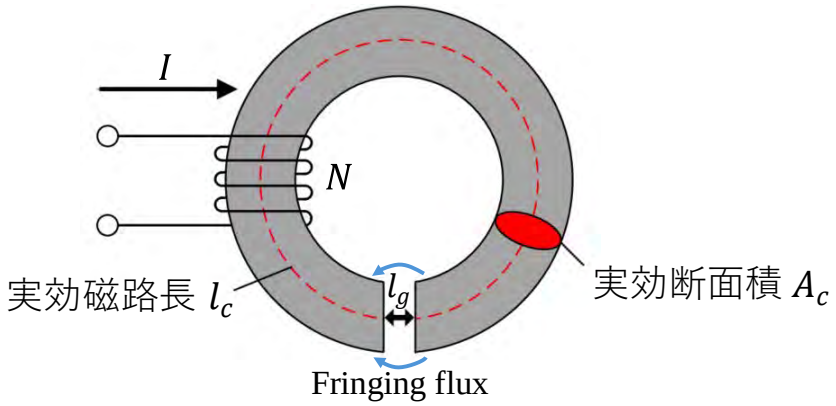


Figure 1.1.2.1 Toroidal core with air gap

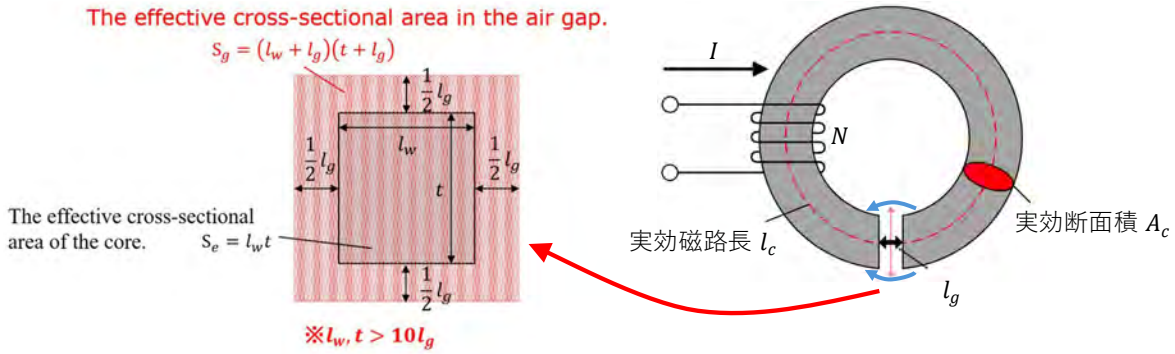


Figure 1.1.2.2 Effective cross-sectional area of air gap section

Figure 1.1.2.1 shows a schematic of a toroidal core with an air gap.

In addition, as described later in detail in 1.2.4, the magnetic flux swells in the air gap area, as shown in **Figure 1.1.2.2.** That is, the effective cross-sectional area of the air gap is larger than that of the iron core. This is due to the effect of suppressing the sudden increase in magnetic resistance that occurs when magnetic flux passes from the iron core to the air gap section. In reference [(2)], the following equation is introduced as the effective cross-sectional area of the air gap

$$A_g = (l_w + l_g)(t + l_g) \quad (1.1.2.3)$$

where l_w is the width of the iron core and t is the thickness of the iron core. Reference [(2)] states that equation (1.1.2.3) is valid for $w < 10l_g$ and $t < 10l_g$. Equation (1.1.2.3) has the advantage of simplicity in calculation because it uses only known parameters. However, the effective cross-sectional area of the air gap section varies depending on the permeability of the iron core, the shape of the effective cross-sectional area of the iron core, and the gap length, and even under the above conditions, equation (1. 1.2.3) may not hold.

Therefore, reference [(3)] introduces a method L for estimating A_g. Specifically, the equation (1.1.2.4) is used to calculate A_g

$$A_g = \frac{l_g}{\mu_0 \left(L - \frac{l_c}{\mu_0 \mu_{r,i} A_c} \right)} \quad (\ 1.1.2.4)$$

where $\mu_{r,i}$ is the initial specific permeability. Equation (1.1.2.4) is obtained by solving equations （1.1.2.1) and (1.1.2.2) for A_g. The initial specific permeability $\mu_{r,i}$ is read from the data sheet of the magnetic material.

1.2.2 Change in apparent B-H curve during gap insertion

Gapped inductors effectively suppress saturation of magnetic materials by means of a gap introduced in the magnetic circuit. This gap suppresses the rapid increase in magnetic flux density even when the magnetic field strength exceeds a certain limit, and stable operation under high magnetic field strength is expected. In addition, the existence of the gap reduces the nonlinearity of the magnetic properties and keeps the relationship between the magnetic field strength and the magnetic flux density more linear, thereby improving the operational stability of the magnetic element. Furthermore, the control of saturation can be optimized by adjusting the gap design, allowing for flexibility in meeting various applications and design requirements. Gapped inductors thus play an important role in the development of highly reliable, high-performance magnetic elements.

Inserting a gap increases the magnetoresistance and decreases the real permeability [(2)]. As a result, the slope of the B-H curve becomes smaller, and different curves are drawn before and after the gap is inserted. **Figure 1.1.2.3** shows a comparison of the B-H curves of an inductor with and without a gap.

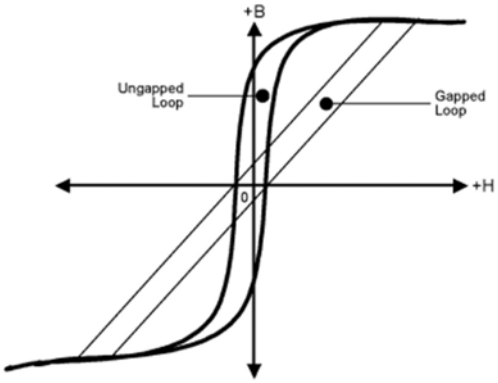


Figure 1.1.2.3 Variation of B-H curve due to gap insertion

1.2.3 Magnetic flux density distribution at air gap insertion

When an air gap is inserted in the iron core, the magnetic flux density distribution in the magnetic circuit deviates from the ideal uniform state and local non-uniformity is generated. **Figure 1.1.2.4** shows the magnetic flux density distribution of the UU core analyzed by FEM. Magnetic materials have high permeability, and magnetic flux preferentially passes through the iron core. However, since the magnetic resistance is extremely large at the air gap, the magnetic flux becomes an energy bottleneck when it passes across the air gap. As a result, magnetic flux is locally concentrated in the iron core region before and after the air gap, resulting in a high magnetic flux density B. On the other hand, the magnetic flux density decreases in the iron core after passing through the air gap, resulting in an asymmetric and non-uniform distribution as a whole.

Such a local increase in magnetic flux density also has a direct effect on the iron loss distribution [(3)]. Both hysteresis loss and eddy current loss, which are iron losses, depend on the magnitude of the magnetic flux density and its rate of change, so the loss increases locally in areas where the magnetic flux is concentrated, resulting in uneven heat generation. This also results in a non-uniform temperature distribution, which increases the risk of overheating in some magnetic materials.

The iron loss characteristics shown in the data sheets of commercially available magnetic materials usually assume that the magnetic flux density inside the iron core is uniform. The evaluation is made under the condition that the magnetic flux is evenly distributed as in a toroidal shape at the time of measurement, and the magnetic flux concentration and distribution bias due to the air gap are not included. In other words, if the magnetic flux density is not uniform inside the iron core, the spatial average and local peak values of B will not be clear, and the calculation results may deviate significantly. Therefore, for inductors with air gaps and complex core geometries, it is essential to evaluate the spatial loss distribution using FEM or other methods and to make corrections based on actual measurements. It is also necessary to design the air gap position and length appropriately.

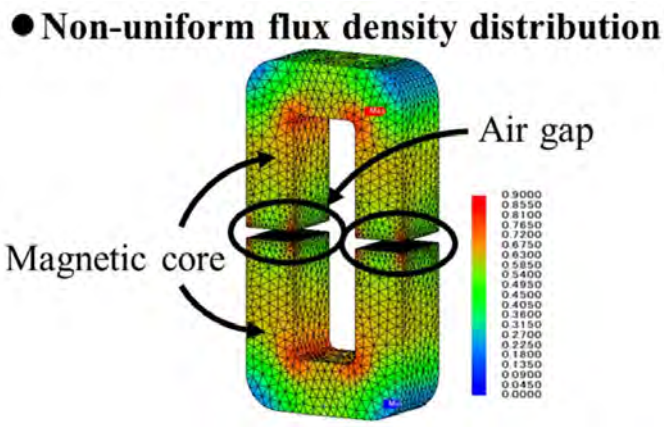


Figure 1.1.2.4 Uneven magnetic flux density distribution

1.2.4 Losses due to flux leakage from the air gap (fringing losses)

When an inductor has an air gap, as shown in **Figure 1.1.2.5**, the magnetic flux expands at the air gap and spreads to the surrounding area. In this case, Joule losses (fringing losses) due to eddy currents are generated when the magnetic flux leaking from the air gap (fringing flux), indicated by the blue line, crosses the inductor winding and the magnetic core of the multilayer structure [(4)]. As shown in **Figure 1.1.2.6** (a), the closer the inductor winding is to the air gap, the more the fringing loss increases. This is due to the increase in the amount of fringing flux crossing to the inductor winding. **Figure 1.1.2.6** (b) shows the heat generated by an inductor with an air gap photographed with a thermal camera. The inductor used has an air gap of 13 mm, so there is a distance of 5 mm between the magnetic material and the winding, but even with this structure, heat generation due to fringing losses caused by the air gap can be observed in the center of the winding [(5)]. The main measure to suppress the fringing losses in the inductor winding is to place the inductor winding away from the air gap. However, how far away the windings should be from the air gap is a matter of experience and has not been quantified. The main measure to suppress fringing losses on the iron core surface is the use of a pressed iron core (see Chapter 2, Section 1.2.2). In a pressed iron core, the magnetic powder is insulator-coated and compression-molded. Therefore, the air gap becomes a finely dispersed structure instead of a concentrated one as in a UU core, eliminating fringing flux, increasing electrical resistance, and reducing eddy currents.

Fig. 1.1.2.7 briefly introduces the methods for reducing fringing losses in windings and magnetic materials [(6)-(9)]. To reduce the fringing losses in the windings, the windings should be located away from the points where the magnetic flux leaks. Therefore, the position of the air gap and the structure of the winding should be devised to reduce the loss. On the other hand, for the fringing loss that occurs in magnetic materials, the loss can be reduced by machining the cross section of the magnetic material according to the path of the fringing magnetic flux, so that the magnetic flux flow is no longer interlinked with the surface of the magnetic material sheet.

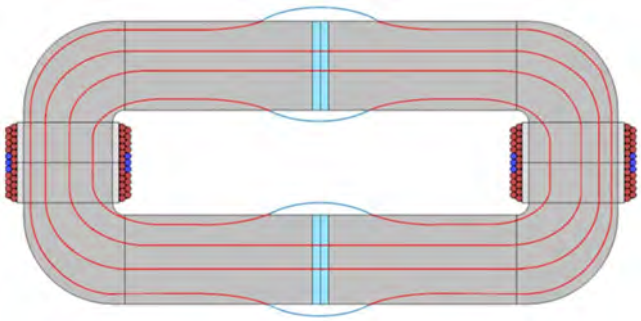
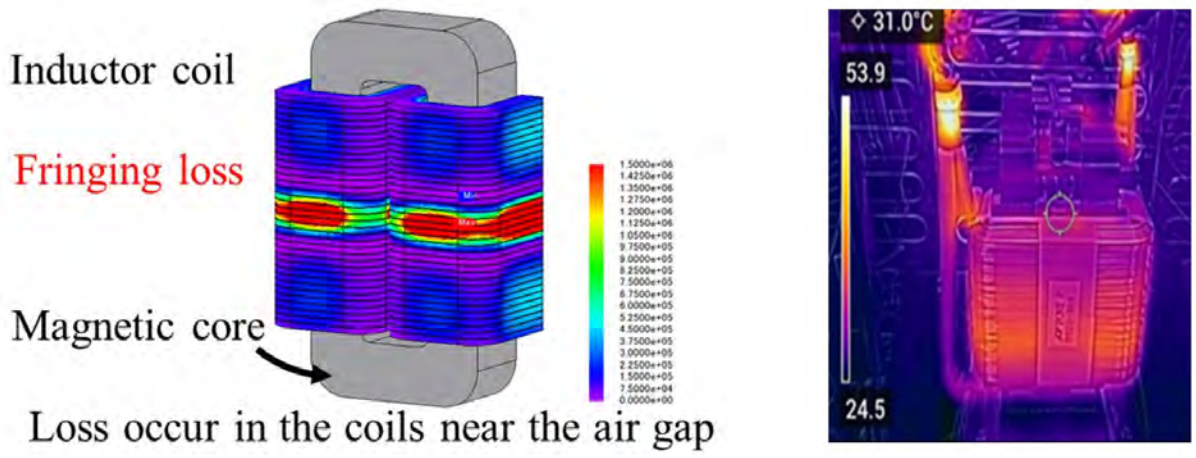
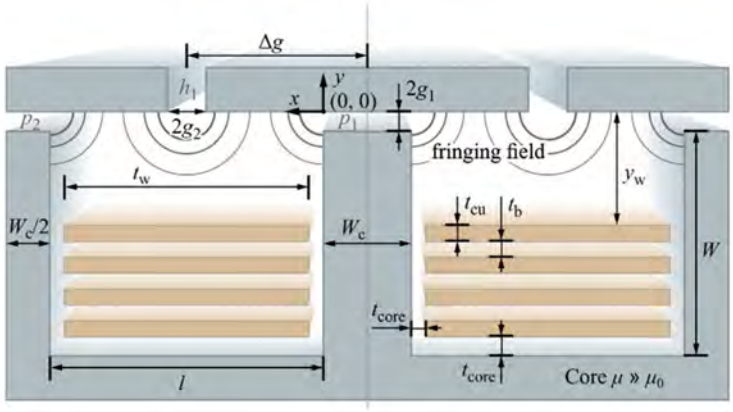


Figure 1.1.2.5 Fringing magnetic flux

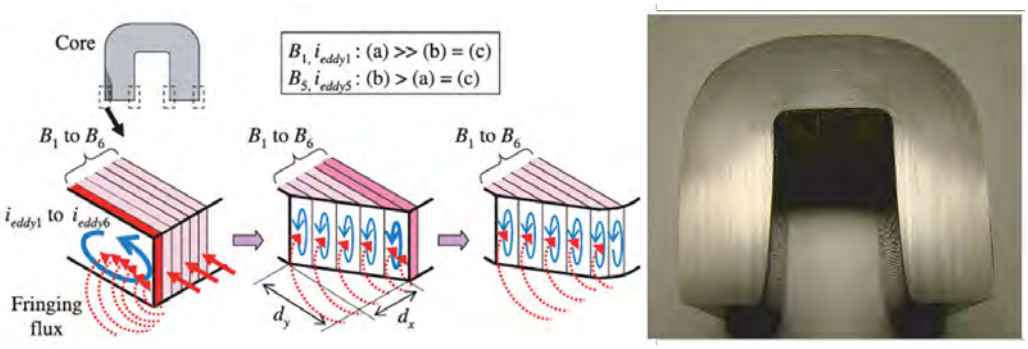


(a) Simulated locations of fringing loss (b) Inductor heating due to fringing magnetic flux

Figure 1.1.2.6 Losses due to fringing flux



(a) Methods for reducing fringing losses in windings, Reprinted from [8], © 2021 IEEE



(b) Methods to reduce fringing losses in magnetic materials [7]

Fig. 1.1.2.7 Examples of methods to reduce fringing losses in windings and magnetic materials

[Hiroaki Matsumori]

References

(1) N. Mohan, T. M. Undeland, and W. P. Robbins , *Power Electronics: Converters, Applications, and Design*, 3rd ed. Hoboken, NJ, USA: Wiley, 2003.

(2) W. G. Hurley and W. H. Wölfle, "Transformers and inductors for power electronics: theory, design and applications," 4th ed. Wiley, 2013.

(3) Akihiro Miwa, Toshihisa Shimizu, Koji Takano, and Hitoshi Ishii, "Low Loss Design of Inductors for Buck Chopper Circuits Considering DC Magnetic Field Bias Characteristics of Iron Loss," IEEJ Transactions on D (Industrial Applications Division Journal), Vol. 137, No. 5, pp. 385-394, May 2017. doi:10.1541/ieejias.137.385.

(4) H. Sato and T. Shimizu, "Study on an accurate iron loss calculation method considering the non-uniformity of the magnetic flux density, " *2015 IEEE Energy Conversion Congress and Exposition (ECCE)*, Montreal, QC, Canada, 2015, pp. 3032-3039, doi: 10.1109/ECCE.2015. 7310084.

(5) H. T. Le, H. Matsumori, K. Takano and K. Wada, "DC inductor loss measurement used in DC/DC converters under high DC current conditions. " 2023 IEEE Energy Conversion Congress and Exposition (ECCE), Nashville, TN, USA, 2023, pp. 5592-5596, doi: 10.1109/ECCE53617.2023. 10362351.

(6) R. S. Yang, A. J. Hanson, B. A. Reese, C. R. Sullivan and D. J. Perreault, "A Low-Loss Inductor Structure and Design Guidelines for High- Frequency Applications," in *IEEE Transactions on Power Electronics*, Vol. 34, No. 10, pp. 9993-10005, Oct. 2019, doi: 10.1109/TPEL.2019. 2892397.
(7) T. Tera, H. Taki, and T. Shimizu, "Loss Reduction of Laminated Core Inductor used in On-board Chargers for EVs," *IEEJ Journal of Industry Applications*, Vol. 4, No. 5, pp. 626-633, 2015, doi: 10.1541/ieejjia.4.626.
(8) S. Mukherjee, Y. Gao, and D. Maksimović, "Reduction of AC Winding Losses Due to Fringing-Field Effects in High-Frequency Inductors With Orthogonal Air Gaps," *IEEE Transactions on Power Electronics*, Vol. 36, No. 1, pp. 815-828, Jan. 2021, doi: 10.1109/TPEL.2020.3002507.
(9) R. S. Kasikowski and B. Wiecek, "Fringing-Effect Losses in Inductors by Thermal Modeling and Thermographic Measurements," in IEEE Transactions on Power Electronics, Vol. 36, No. 9, pp. 9772-9786, Sept. 2021, doi: 10.1109/TPEL.2021.3058961.

1.3 Insulation performance of transformer, ratio of iron loss to copper loss, inter-winding capacitance

Keyword: Iron loss, Copper loss, Proximity effect, Interleaved winding, Parasitic capacitance, Partial discharge test

1.3.1 Ratio of iron loss to copper loss

In the design of transformers, including high-frequency transformers, it is common to make the magnetic permeability of the iron core

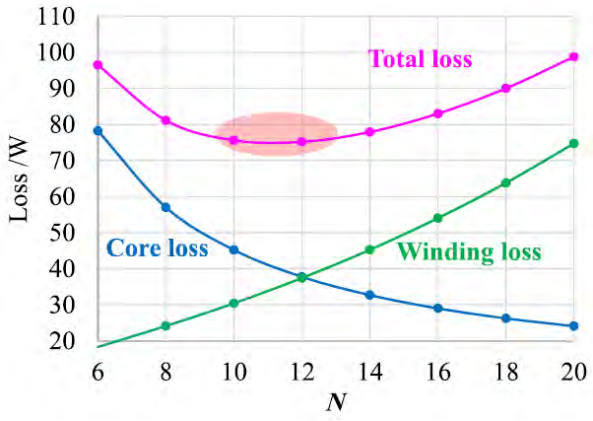


Fig. 1.1.3.1 Example of iron loss, copper loss, and their sum for each

high enough and the gap as small as possible so that the excitation inductance is large enough. The excitation current will be very small. The turn ratio is determined by the required voltage transformation ratio, but the choice of the number of turns can be treated as a parameter for adjusting the magnetic flux density in the iron core within the range where the excitation inductance is sufficiently large (e.g., 5% or less of the load current).

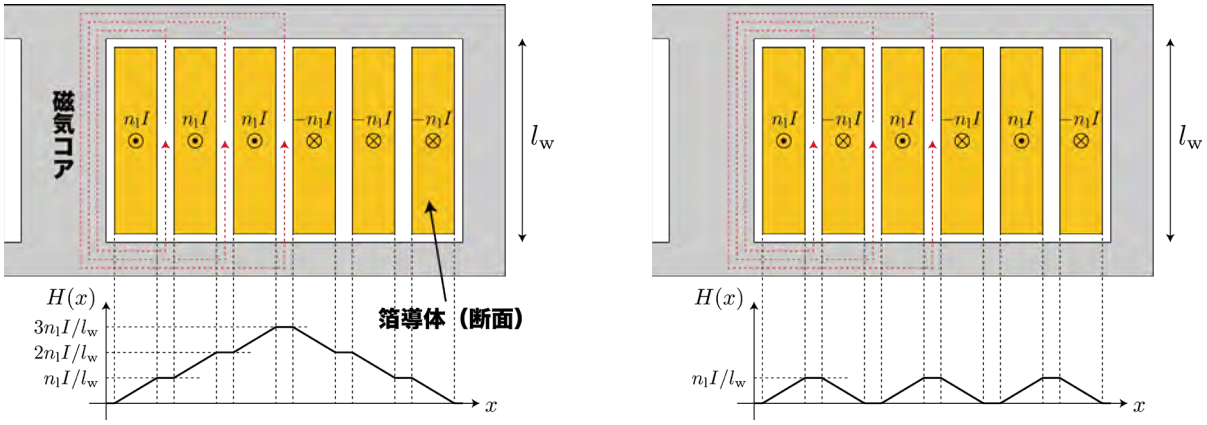
The magnetic flux Φ in the iron core is determined by the waveform of the voltage v applied to the winding (time integration of the voltage) and the number of turns N.

$$\Phi = \frac{1}{N}\int v\,dt \tag{1.1.3.1}$$

The magnetic flux density B is divided by the cross-sectional area A_C of the iron core. Since the magnetic flux density is this divided by the cross-sectional area of the iron core

$$B = \frac{\Phi}{A_C} \tag{1.1.3.2}$$

The same input voltage waveform with a smaller number of turns results in a larger iron loss. When the number of turns is reduced for the same input voltage waveform, the iron loss increases because the magnetic flux density in the iron core increases when the same iron core cross-sectional area is used. Alternatively, the iron core cross-sectional area must be increased to prevent saturation, and the iron loss of the entire iron core increases even if the iron loss per volume does not increase. On the other hand, a small number of turns shortens the winding length and reduces the copper loss. Conversely, increasing the number of turns lowers the magnetic flux density of the iron core, which reduces iron loss, but increases copper loss. As described above, the trends of increase and decrease of iron loss and copper loss are opposite with respect to the number of turns, so there is a number of turns that minimizes the total loss, which is the sum of iron loss and copper loss. For example, in the design of a high-frequency transformer under certain conditions, it is reported in reference (1) that a plot of iron loss, copper loss, and their sum for each number of turns is shown in **Figure 1.1.3.1**.



(a) When the primary and secondary windings are each wound intensively

(b) Interleaved winding, where the primary and secondary windings are wound alternately

Figure 1.1.3.2 Magnetic field created by transformer winding currents

In the design of rotating machines and commercial frequency transformers, this concept is expressed in terms of electrical and magnetic loading, and there are various design theories on how to distribute the loading to minimize loss or volume. In the design of high-frequency transformers, there have been some efforts to apply such transformer design theories [(2)], but at present they are not well established in the design of high-frequency transformers.

Thus, in transformers, it is possible to use iron core materials that match the material characteristics by controlling the magnetic flux density of the iron core. However, this is limited to cases where the magnetic permeability of the iron core material is high enough to ensure sufficient excitation inductance even when the number of turns is reduced. In the design of transformers with relatively low current and high voltage, there may be restrictions such as the need to secure a sufficient number of turns to ensure a sufficiently high excitation inductance.

1.3.2 Proximity Effects and How to Reduce Them

Like inductors, transformers also experience an increase in copper loss due to skin and proximity effects for high-frequency currents. Countermeasures such as the use of Litz wires are also effective. However, since the direction of the magnetomotive force is opposite in the primary and secondary windings of a transformer, it is possible to reduce the magnetic field in the winding by interleaving the windings, thereby suppressing the increase in copper loss due to the proximity effect.

Figure 1.1.3.2 schematically shows the strength *H* of the magnetic field created by the winding current in a transformer. The current flowing in one layer is nlI, and the same number of layers can also be considered. When the primary and secondary windings are wound intensively as shown in **Figure 1.1.3.2** (a), the magnetic field created by the current flowing in both windings becomes stronger on the side of the primary winding closest to the secondary winding and on the side of the secondary winding closest to the primary winding. When the current is high frequency, the high frequency magnetic field induces eddy currents in the windings, resulting in the proximity effect that causes losses. In this winding arrangement, the effect is significant because the magnetic field becomes strong at some points as described above. On the other hand, in the case of interleaved winding, where the primary and secondary windings are wound alternately as shown in **Figure 1.1.3.2** (b), the currents in the primary and secondary windings are in opposite directions, so the generated magnetic field is canceled and is not strong in any arrangement. This means that the influence of the proximity effect is relatively small. However, because insulation materials must be placed between all adjacent layers of primary and secondary windings to ensure insulation between the primary and secondary windings, the volume becomes large or mounting is difficult in applications where high insulation capability is required. Another disadvantage is the increase in coupling capacitance between the primary and secondary windings. Large coupling capacitance increases conducted noise and radiated noise, as described below.

1.3.3 Effects of primary and secondary inter-winding capacitance and inter-winding line capacitance

Transformers have parasitic capacitances in various places, although the capacitances are small. In power electronics, high-frequency and high-speed drives are being developed, so although the capacitance is small, it can have a large impact.

Parasitic capacitance exists between all turns of the primary and secondary windings. By approximating the capacitance between the turns

belonging to the primary winding and the turns belonging to the secondary winding together, it can be represented by *the* equivalent capacitance C_c connected between the points at the beginning and the end of the primary and secondary windings. This parasitic capacitance between the primary and secondary windings affects the high-frequency AC insulation performance. When fast switching, i.e., high dv/dt, occurs in the parasitic capacitance between the primary and secondary windings, a leakage current flows between the primary and secondary sides of the transformer due to the change in potential difference between the windings. This current often takes a path of large loops or earth, which is different from that assumed in the design, leading to an increase in conducted and radiated noise.

Figure 1.1.3.3 shows an example of a converter connected to an AC system and including a high-frequency transformer for isolation: the power devices on the primary and secondary sides and the switching on the secondary side cause the voltage at both ends of the capacitance C_c between the primary and secondary windings to change in a step-like manner. This causes a current to flow between the primary and secondary. This current becomes common mode noise, for example, when it flows through the earth between a grounded point on the secondary side and a grounded point of the AC low voltage distribution network (e.g., a pole transformer).

On the other hand, there are also parasitic capacitances between turns in each of the primary and secondary windings. Although parasitic

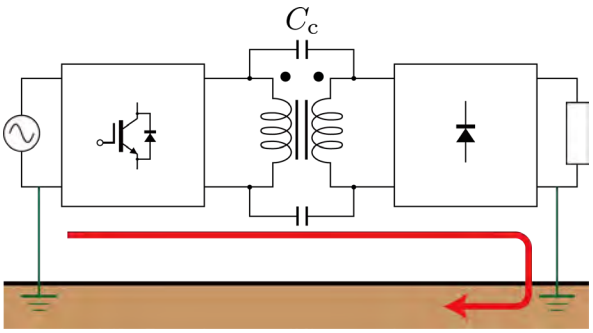


Figure 1.1.3.3 Leakage current due to capacitance between primary and secondary windings

capacitances exist between all turns, they can be represented by a parasitic capacitance C_p, which is connected between the two points at the beginning and end of the winding, i.e., equivalently connected in parallel to each winding of the transformer. The equivalent capacitance connected in parallel to the windings lowers the self-resonant frequency, thus limiting operation at high frequencies. In addition, in many power electronics applications, it is common to apply a square wave voltage to the windings in a voltage transformation circuit, which increases the power dissipation in the power device, which can also be a problem.

Figure 1.1.3.4 shows how the parasitic capacitance C_p in parallel with the transformer winding causes losses. The charged charge is short-circuited through the device to be turned on. At this time, the electrostatic energy ($1/2\ C_p\ V_{dc}^2$) stored by the charge of C_p is all lost due to the small resistance of the device being shorted. When C_p is charged, the charge current is charged in a step-like manner through the power device that is turned on, and in this case, loss occurs in the power device that is turned on, and energy equal to approximately $1/2\ C_p\ V_{dc}^2$ is lost. In addition, this leads to ringing during switching. However, under conditions of zero-voltage turn-on of power devices- for example, in heavy-load operation of DAB (Dual Active Bridge) converters - the voltage at both ends of the device is zero before the device is turned on, i.e., C_p has completed discharge and no stepwise charging of C_p occurs, so there is no loss due to parasitic capacitance.

Losses in power devices due to the parasitic capacitance C_p of transformers are often so small that they can be ignored, but since these losses are proportional to the square of the voltage, they may not be negligible compared to the switching losses of the power device itself in high-voltage transformers that exceed 1000 V. Transformers for high-voltage converters are designed to reduce the C_p by using a honeycomb winding to reduce the facing area between turns, dividing the winding into several blocks and placing a distance between them, and other winding structure innovations.

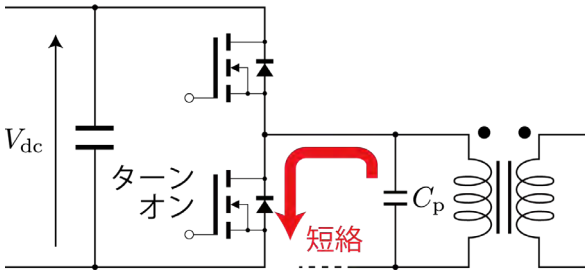


Figure 1.1.3.4 Increased losses in power devices due to parasitic capacitance between windings

1.3.4 Insulation performance

In power system applications, which have been gaining in popularity in recent years, the required (DC) insulation performance can affect the transformer's size and losses. For example, high-frequency transformers used in SSTs (Solid-State Transformers) connected to high-voltage distribution networks are often considered in the so-called ISOP (Input Series Output Parallel) configuration, in which the primary side (high-voltage side) is connected to a series-connected transformer circuit and the secondary side (low-voltage side) to a parallel-connected transformer circuit. The secondary side is close to the ground potential, but the terminal conversion circuit of the series-connected conversion circuits on the primary side is connected to the potential of the high-voltage distribution network, so the voltage between the primary and secondary windings of the transformer is approximately the voltage of the high-voltage distribution network. This isolation is necessary to ensure user safety and must be achieved with extremely high reliability. Withstand voltages of about three times the nominal voltage of the high-voltage distribution network are required. For commercial frequency transformers, isolation of several tens of kV is a natural requirement for pole transformers and distribution transformers, but for high frequency transformers, research has only recently been focused on SSTs connected to the high voltage distribution network.

In commercial frequency transformers for power distribution, there are two types of transformers for maintaining insulation: those that use insulating oil and dry molded transformers; in SSTs, the use of insulating oil is not anticipated, so reinforcing insulation with epoxy or other potting materials is an option [(3)]. Typical insulation materials have a dielectric strength of about 20 kV/mm, while the dielectric strength in air is 3.0 kV/mm. In the electric field distribution determined by the geometry and winding arrangement, the design should be such that the electric field strength in the insulating material and in the air outside does not exceed the specified values, respectively. When using these solid insulating materials, degradation due to partial discharge caused by the presence of voids is a factor that characterizes the insulation performance, and it is common to evaluate the insulation performance by partial discharge tests.

[Takanori Isobe]

References

(1) S. Zhao, Q. Li, F. C. Lee and B. Li, "High-Frequency Transformer Design for Modular Power Conversion From Medium-Voltage AC to 400 VDC ", IEEE Transactions on Power Electronics, Vol. 33, No. 9, pp. 7545-7557 (2018).

(2) Reiji Watase and Shigeo Masukawa : "Position Design Method for Single-Phase High-Frequency Transformers Using Differentially Incremental Proportional Method," 31st IEEJ National Convention, 4-035 (2019).

(3) Z. Li, E. Hsieh, Q. Li and F. C. Lee, "High-Frequency Transformer Design with Medium-Voltage Insulation for Resonant Converter in Solid- State Transformer," IEEE Transactions on Power Electronics, Vol. 38, No. 8, pp. 9917-9932 (2023).

1.4 Review of magnetic materials used in transformers and inductors

Keyword: Magnetic materials, excitation of power converters, suitable materials for power converters, iron loss in sinusoidal and square wave, DC bias

1.4.1 Magnetic materials used in transformers and inductors

Figure 1.1.4.1 shows the relationship between saturation magnetic flux density and specific permeability μ_i for various magnetic materials [(1)]. It can be seen that the value of specific permeability μ_i increases as the saturation flux density decreases. In the evaluation of iron loss for different magnetic materials such as Co-based amorphous, sendust, and high-purity iron powder, it has been reported that the iron loss tends to decrease as the magnetic flux density during operation decreases. Therefore, iron loss can be reduced by using appropriate magnetic materials based on the maximum magnetic flux density to be excited in the inductor [(2)-(5)].

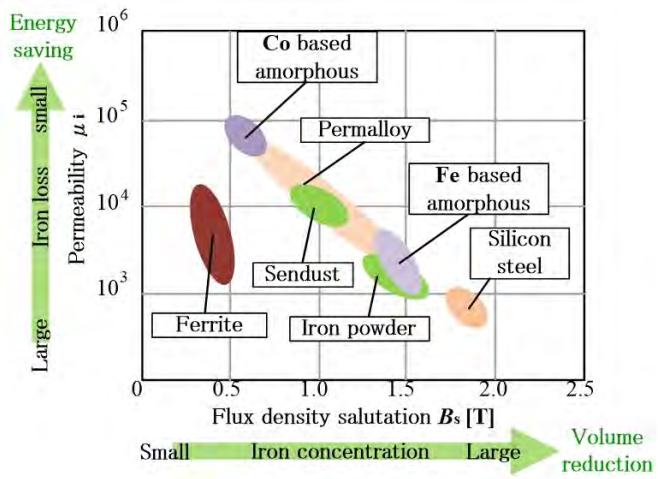


Figure 1.1.4.1 Properties of various magnetic materials

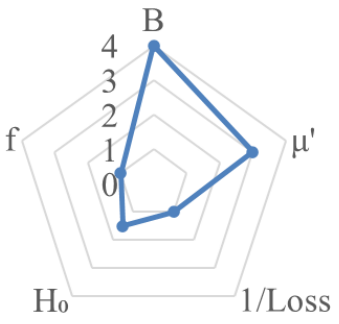
Next, transformers and suitable magnetic materials for each application are discussed. Transformer specifications are broadly classified according to constraints such as power capacity, excitation frequency, and withstand voltage between windings. **Figure 1.1.4.2** shows a radar chart of the characteristics of various magnetic materials. The axis of each radar chart consists of five items that are important for the characteristics of magnetic materials for power electronics: saturation magnetic flux density, specific permeability, loss, DC bias, and frequency of application. The levels of specific evaluation indices are shown in **Table 1.1.4.1**. Note that the axis of loss is indicated by taking the reciprocal of the value, so that the outward spread of the loss in the radar chart indicates a smaller loss and better material performance.

Comparison using this radar chart enables us to understand the relative strengths and weaknesses of each magnetic material in terms of their characteristics, and to easily determine which magnetic material should be selected for various circuit topologies and applications. In the following, typical magnetic materials used in power electronics equipment are classified using a radar chart. Then, magnetic materials suitable for transformers and inductors for each application will be introduced.

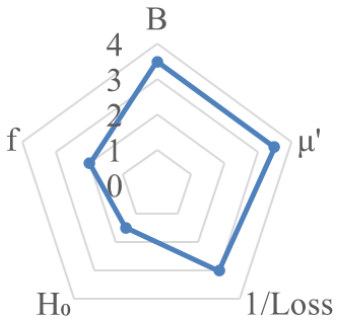
Table 1.1.4.1 Inductor material evaluation index for radar chart

	飽和磁束密度 B [T]	比透磁率 μ'	損失 [1/(kW/m³)]	DCバイアス Ho [A/m]	周波数 f [kHz]
1	0.50 未満	1～100	1/150 未満	100未満	1 未満
2	0.50～0.80	101～1000	1/150~1/76	100~500	1~10
3	0.81~1.2	1001～5000	1/75~1/10	501~1000	11~200
4	1.21 以上	5001 以上	1/10 以上	1001 以上	200 以上

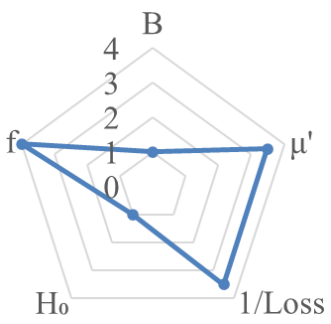
*Losses in figures and tables are approximate calculations based on data sheets with a flux density ripple of 100 mT and an excitation frequency of 10 kHz.



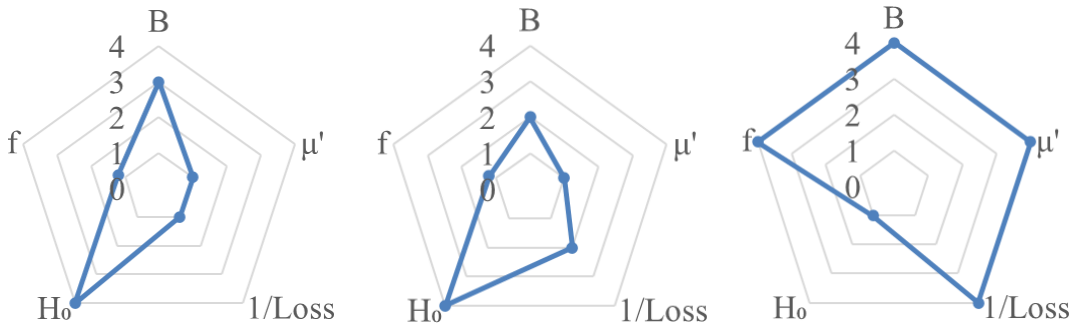
(a) Fe-Si
(Nippon Metal Co., Ltd.: "Guide to Ultra-Thin Silicon Steel Sheet Products, FS Series" [7])



(b) amorphous
(Niterra Materials: "General catalog of Amorphous Magnetic Parts,") MT Series" [1])



(c) Ferrite (Mn-Zn)
(Magnetic: "FERRITE CORES 0_41405TC" [8])



(d) Fe-Si dust (Magnetics: "XFlux Cores Manufacturer, 0078050A7" [9])

(e) sendust (Magnetics: "Kool Mu HF Cores Manufacturer, 0077533A7" [10])

(f) nanocrystal (Hitachi Metals, Ltd: Finemet Catalogue," FT-3K50T F Series" [6])

Figure 1.1.4.2 Radar chart showing the properties of various magnetic materials

Fe-Si (silicon steel sheet), shown in **Figure 1.1.4.2** (a), is a magnetic material with a large saturation magnetic flux density and high specific magnetic permeability. On the other hand, it is characterized by relatively high loss in the high-frequency range.

The amorphous material shown in **Figure 1.1.4.2** (b) has a slightly lower saturation magnetic flux density than silicon steel sheet, but has lower iron loss and is suitable for high-frequency applications.

The ferrite (Mn-Zn) shown in **Figure 1.1.4.2** (c) is a material with both high specific permeability and low loss characteristics. Although it has a low saturation magnetic flux density, it is characterized by its excellent magnetic properties in the high-frequency range.

The Fe-Si dust shown in **Figure 1.1.4.2** (d) has a dispersive magnetic path structure unique to powder iron cores and a relatively large saturation magnetic flux density. In addition, while it has excellent DC superposition characteristics, the magnetic properties are relatively stable with respect to frequency, although the specific permeability is small.

The sendust shown in **Figure 1.1.4.2** (e) is a Fe-Si-Al alloy powder material and exhibits low loss characteristics, although its saturation magnetic flux density is lower than that of Fe-Si dust. Another advantage is that the temperature dependence of the magnetic properties is small.

The nanocrystal shown in **Figure 1.1.4.2** (f) is a material with both extremely high specific magnetic permeability and low loss characteristics. The fine crystal grains suppress magnetic wall migration and exhibit excellent magnetic properties over a wide frequency range.

Next, transformers and suitable magnetic materials for each application are discussed. Transformer specifications can be broadly classified into four types depending on the frequency used.

(1) Commercial frequency transformer:

The main excitation is sinusoidal 50/60 Hz AC, but when used for voltage matching of equipment, a high withstand voltage across the windings is required.

Single-phase transformers are for tens of kVA, and three-phase transformers for more than tens of kVA.

In the case of large capacitance, the winding window frame area of the iron core becomes large because of the larger circuit current.

The excitation current is generally 5 to 10% of the rated current.

In the case of multiple inverters, a multi-winding transformer is required.

Power efficiency must be 98.5% or higher.

In light of the above, silicon steel sheets are generally used as the magnetic material.

(2) Inverter transformer:

In PWM inverters and multilevel inverters, a PWM switching frequency component is superimposed in addition to the sinusoidal AC excitation voltage.

When used for voltage matching, a high inter-winding withstand voltage is required. However, if non-insulation is acceptable, a high inter-winding withstand voltage is not required for a single-winding transformer configuration.

In the case of large capacitance, the winding window frame area of the iron core becomes large because of the larger circuit current.

To prevent unbalanced magnetization due to the DC current component of the PWM inverter, the excitation current is set to be approximately 5 to 10% of the rated current.

In some cases, the leakage inductance of the transformer is used to provide the function of a filter inductor.
Based on the above, 3% silicon steel sheet is the most common magnetic material, which reduces the saturation magnetic flux density by about 10%, but 6.5% silicon steel sheet with low loss may also be used.

(3) High frequency transformer:

The power devices are excited by a high-frequency square wave AC voltage. The excitation frequency depends on the power device used and its power capacity: generally several kHz to several dozen kHz for IGBTs, several dozen kHz to several dozen kHz for SiC, and several dozen kHZ to several MHz for Si power MOSFETs.
In the case of large capacitance, the winding window frame area of the iron core becomes large because the circuit current becomes large.
Because the winding current increases the copper loss in the primary and secondary windings at high frequencies, especially above several tens of kHz, litz wire is often used.
The excitation current is generally 5 to 10% of the rated current.
In light of the above, a wide variety of magnetic materials are used depending on the operating frequency. For frequencies up to 10 kHz, silicon steel sheets (0.1 mm to 0.05 mm) and amorphous thin strips are used; for frequencies above 10 kHz, highly permeable ferrites and highly permeable alloy powders (nanocrystalline materials) are also used.

(4) Very high frequency transformer:

In the frequency band above about 10 MHz, an air-core transformer configuration may be used without using magnetic materials.

Next, inductors and suitable magnetic materials for each application are discussed. Inductor specifications are broadly classified into those for DC smoothing and those for AC filtering.

(1) Inductors for DC smoothing:

The current flow currents include DC currents and high-frequency AC currents that depend on the switching frequency.
The DC current component varies depending on the load current of the device.
In view of the above, a wide variety of magnetic materials are used depending on the operating frequency. Up to several tens of kHz, silicon steel sheets (0.1 mm to 0.05 mm) and amorphous thin strips are used, and above several tens of kHz, high permeability ferrite and alloy powders (FE-Si dust, sendust) made of low permeability ferrite are used. When using high permeability magnetic materials, it is necessary to provide a magnetic path gap to prevent magnetic saturation. In the case of high current, a magnetic path gap may be provided even with low permeability magnetic materials.

(2) Inductors for AC filters:

The (low-frequency) AC wave output currents of PWM inverters and multilevel inverters and the high-frequency AC currents that depend on the switching frequency are included.
The low-frequency AC current component varies depending on the load condition.
As with inductors for DC smoothing, a magnetic path gap must be provided for high-current applications even if low permeability magnetic materials are used.
In view of the above, a wide variety of magnetic materials are used depending on the operating frequency. Up to several tens of kHz, silicon steel sheets (0.1 mm to 0.05 mm) and thin amorphous strips are used, while high permeability ferrite and low permeability alloy powders are used above several tens of kHz.

(3) Inductors for common mode (CM choke):

CM chokes are often used in combination with Y capacitors to form LC low-pass filters. In general, safety standards for leakage currents into the ground system strictly limit the capacitance value of Y capacitors that can be used to the order of nF. Therefore, a CM choke is required to have a large inductance of several mH to several tens of mH to meet the required common-mode (CM) noise attenuation. If a large number of turns of winding is applied to the iron core to increase the inductance, the stray capacitance between the windings increases, and the impedance of the CM choke drops in the high-frequency region. Therefore, in order to achieve a large inductance with as few turns as possible, the magnetic material of the CM choke is required to have a high specific permeability of several thousand to several tens of thousands, and nanocrystals and ferrites (Mn-Zn) are widely used. In a configuration that uses a Y-capacitor, most of the CM noise is returned through the Y-capacitor in the system. Therefore, high saturation flux density and low iron loss characteristics are not important for the magnetic material of CM chokes, except for large-capacity applications of several tens of kW or more.

On the other hand, in motor drive systems powered by three-phase PWM inverters, a CM choke is sometimes connected between the inverter and the motor to reduce damage to the motor windings *due to* high *dv/dt*. In this application, the CM voltage (average of the output phase voltages) generated by the inverter is applied almost directly to both ends of the CM choke, depending on the CM choke design. Under these conditions, the CM choke is excited by a large signal, so the magnetic material of the CM choke must have not only high permeability

but also high saturation magnetic flux density and low iron loss characteristics.

1.4.2 Difference in iron loss between sinusoidal voltage excitation and square wave voltage excitation

Power electronics designers usually design magnetic components based on data sheets provided by magnetic material manufacturers. However, the iron loss values provided by magnetic material manufacturers often differ from the actual power converter operation. This is due to differences in the excitation waveforms of magnetic components. The data sheet assumes sinusoidal voltage excitation as shown **in Figure 1.1.4.3**, whereas the excitation waveform of the transformer in the DC-DC converter shown in **Figure 1.1.4.4** is square wave voltage.

Bf = 120 mT, = 20 kHz, and the measured iron losses when a sinusoidal voltage is applied and when a rectangular wave voltage is applied without DC bias are shown in **Table 1.1.4.2**. In all iron cores, the loss with sinusoidal excitation exceeds the loss with rectangular wave excitation. In Kool Mμ MAX (Fe-Si-Al), the maximum loss difference for sinusoidal excitation was 0.68 J/m^3 (64.9 %). From the above, the iron loss value varies with the difference in the excitation waveform of the magnetic components.

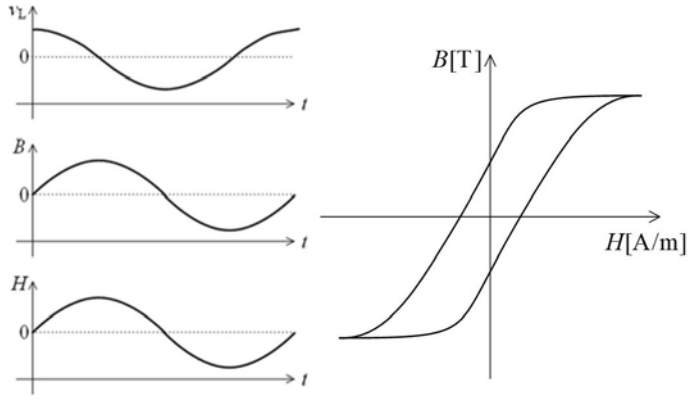


Figure 1.1.4.3 Sinusoidal voltage excitation waveform and B-H curve
(Iron loss data sheet)

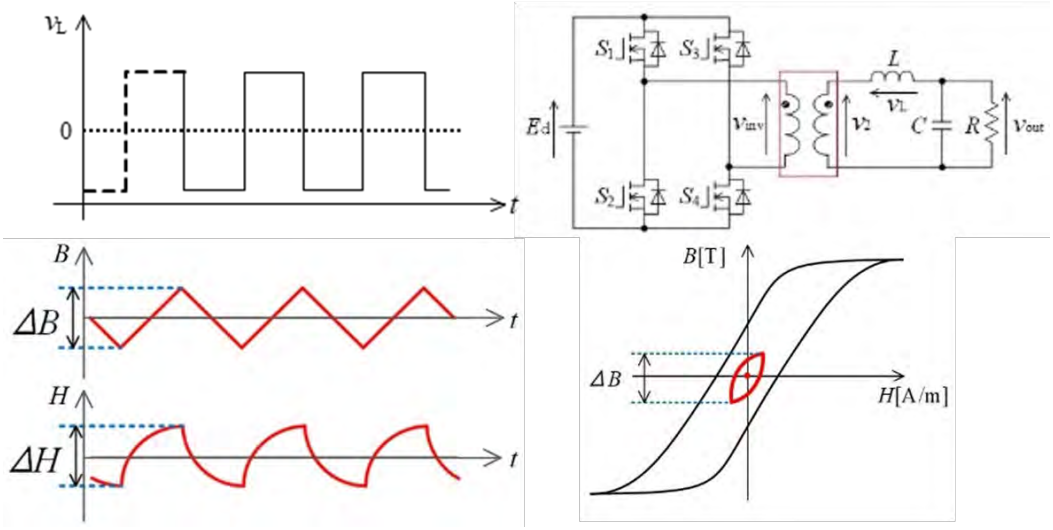


Figure 1.1.4.4 Square wave voltage excitation waveform and B-H curve without DC bias
(Excitation waveform of a transformer in a power converter)

Table 1.1.4.2 Iron loss comparison for sinusoidal and square wave voltage excitation without DC bias ($\boldsymbol{\Delta B = 120\ mT,\ f = 20\ kHz}$)

Core name	Kool Mμ®	Kool $^{Mμ®}$ MAX	Kool $^{Mμ®}$ Hf	XFlux®.	High Flux	Edge™.	MPP
Alloy composition	Fe-Si-Al	Fe-Si-Al	Fe-Si-Al	Fe-Si	Fe-Ni	Fe-Ni	Fe-Ni-Mo

Iron loss [J/m3] Iron loss	Sinusoidal voltage excitation	0.83	1.04	0.59	3.44	1.22	0.70	0.75
	Rectangular voltage excitation	0.33	0.36	0.32	3.01	1.12	0.52	0.61
Difference [%].		60.3	64.9	45.7	12.5	8.30	26.2	17.7

*Magnetic cores in the table are purchased from Magnetics, Inc. under Spang & Company.

1.4.3 Example of iron loss when DC bias is added to square wave voltage excitation

The excitation voltage waveform of an inductor in a DC-DC converter, as shown in **Figure 1.1.4.5**, is a square wave, as in the transformer described in the previous section. However, the difference is that in the inductor, the magnetic flux density and field strength waveforms include a DC bias component. As shown in **Figures 1.1.4.5 and 1.1.4.6**, it is known that the value of the DC bias component changes the position at which the B-H curve (minor loop) is generated, and the iron loss value changes accordingly.

Figure 1.1.4.7 shows the measured iron loss characteristics in square wave voltage excitation with DC bias. For example, the iron loss of Xflux® (Fe-Si) monotonically increases, while that of Kool Mμ (Fe-Si-Al) decreases by 0.30 J/m^3 (12.6%) when the magnetic field bias H_0 is increased from 4000 A/m to 5000 A/m. From the measurement results, it can be confirmed that there are differences in the iron loss characteristics for each magnetic material in response to changes in DC bias. These results suggest that the behavior of iron loss differs from the characteristics described in the datasheet depending on the operating conditions of the power converter.

[Hiroaki Matsumori]

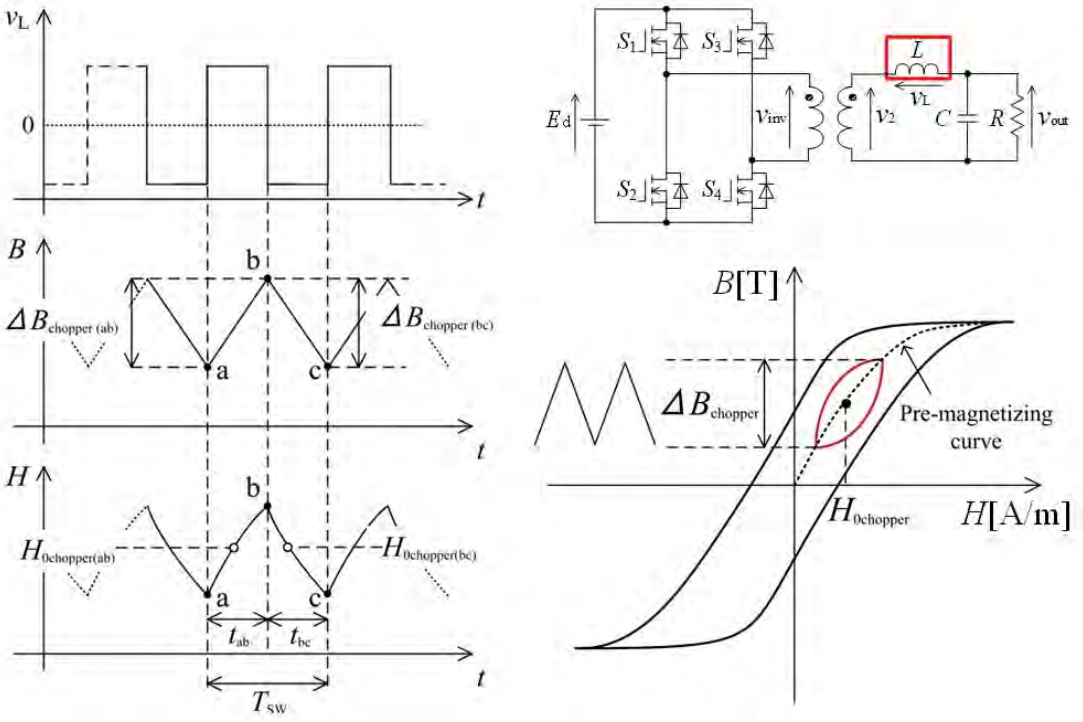


Figure 1.1.4.5 Square wave voltage excitation waveform with DC bias and B-H curve
(Excitation of an inductor in a power converter)

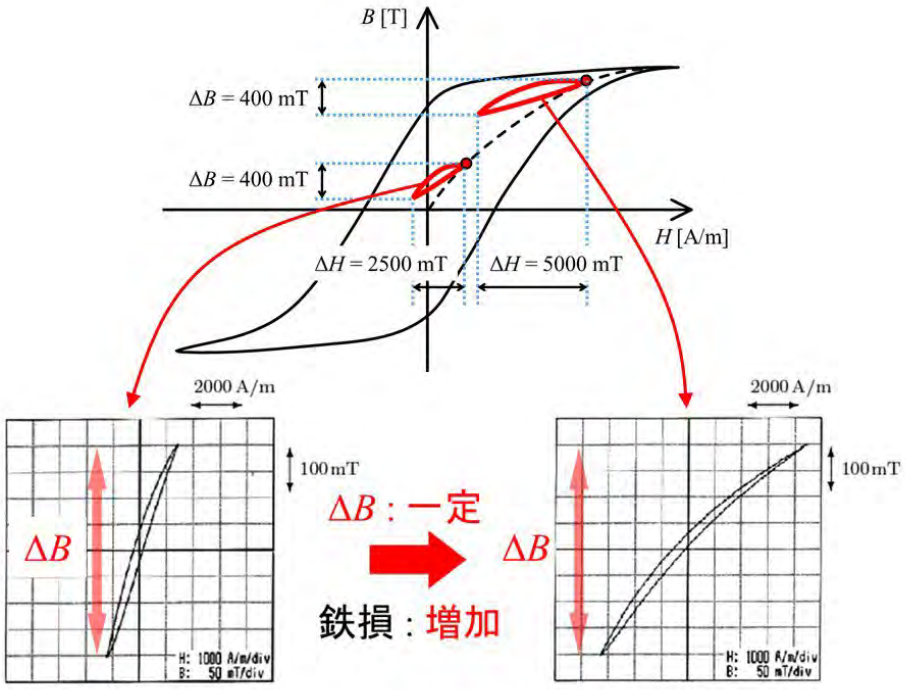


Fig. 1.1.4.6 Location of occurrence of B-H curve and iron loss values due to DC bias

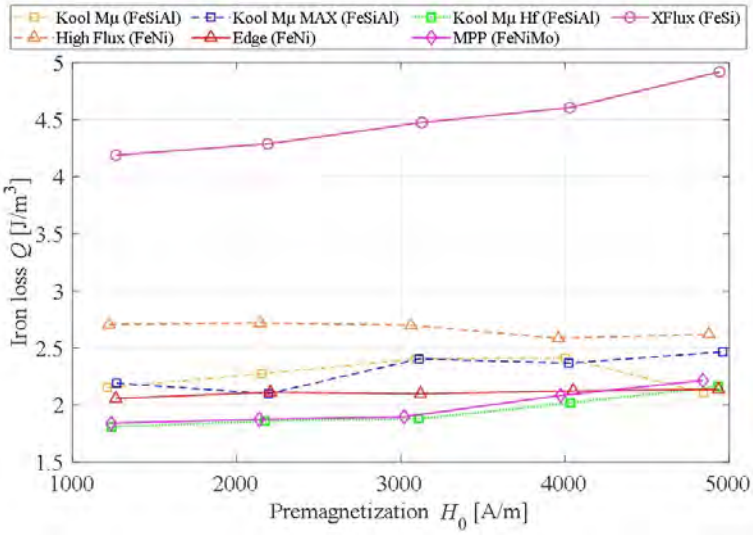


Fig. 1.1.4.7 Iron loss characteristics in square wave voltage excitation with DC bias（$\boldsymbol{\Delta B = 120\ mT,\ f = 20\ kHz}$ ）

References

(1) Niterra Materials: "General catalog of Amorphous Magnetic Parts", available online(2025/10/05).

(2) G. Calderon-Lopez, Y. Wang and A. J. Forsyth, "Mitigation of Gap Losses in Nanocrystalline Tape-Wound Cores," in IEEE Transactions on Power Electronics, Vol. 34, No. 5, pp. 4656-4664, May 2019, doi: 10.1109/TPEL.2018.2863665.

(3) A. J. Hanson, J. A. Belk, S. Lim, C. R. Sullivan and D. J. Perreault, "Measurements and Performance Factor Comparisons of Magnetic Materials at High Frequency," in IEEE Transactions on Power Electronics, Vol. 31, No. 11, pp. 7909-7925, Nov. 2016, doi: 10.1109/TPEL.2015.2514084 .

(4) T. Yamaguchi and H.Matsumori , "Proper magnetic materials selection method for AC power inductors under high-frequency rectangular voltage," AIP Advances, Vol. 14, No. 1, pp. 015132, Jan. 2024. doi: 10.1063/9.0000740.

(5) M. S. Rylko, B. J. Lyons, J. G. Hayes and M. G. Egan, "Revised Magnetics Performance Factors and Experimental Comparison of High-Flux Materials for High-Current DC-DC Inductors," in IEEE Transactions on Power Electronics, Vol. 26, No. 8, pp. 2112-2126, Aug. 2011, doi: 10.1109/TPEL.2010.2103573.

(6) Hitachi Metals, Ltd.: "Finemet Catalogue," 2015.

(7) Nippon Metal Corporation: "Guide to Ultra-Thin Silicon Steel Sheet Products," 2015.

(8) Magnetics: "FERRITE CORES", available online (2025/10/05).

(9) Magnetics: "XFlux Cores Manufacturer," available online (2025/10/05).

(10) Magnetics: "Kool Mu HF Cores Manufacturer," available online (2025/10/05).

1.5 High flux density materials and low-loss magnetic elements

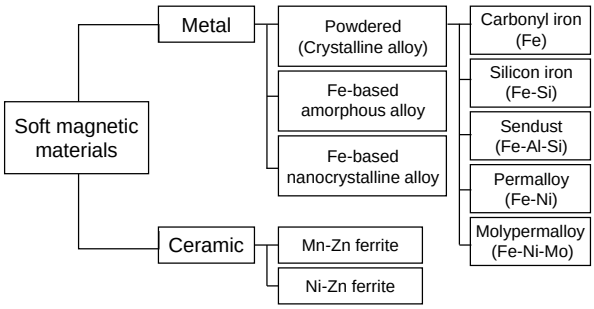
Keyword: Magnetic flux density, magnetic element loss (copper loss/iron loss), magnetic element volume

1.5.1 Compact and lightweight magnetic elements using high magnetic flux density materials

Figure 1.1.5.1 shows typical soft magnetic materials used for magnetic elements in power conversion circuits. There are two main types of soft magnetic materials: metallic materials consisting mainly of iron combined with silicon and nickel, and ceramic-derived ferrite materials consisting mainly of iron oxide combined with manganese, zinc, nickel, and other elements. There are three types of metallic materials: crystalline alloys, amorphous alloys, and nanocrystalline alloys obtained by heat treatment of amorphous alloys above their crystallization temperature. Crystalline alloys are also called "compacted materials" because they are made by applying an insulating coating to the surface of magnetic powder and then compressing and forming it into a bulk iron core. The relationship between iron loss/frequency and frequency exhibited by metallic materials and ferrite is plotted in **Figure 1.1.5.2**. Iron loss can be broadly classified into three categories: hysteresis loss, eddy current loss, and residual loss, which is the sum of losses other than these two. Hysteresis loss is expressed as the area of the hysteresis loop in the *B*-*H* curve multiplied by frequency, which corresponds to the vertical axis intercept (constant) in **Figure 1.1.5.2**. Eddy current loss proportional to the square of the frequency is dominant at higher frequencies in the pressed materials. Nanocrystalline alloys and amorphous alloys with smaller grain size can suppress eddy current loss. On the other hand, ferrite has a higher electrical resistivity than pressed materials, so eddy current losses are small at high frequencies. However, the residual loss caused by the oxide (insulator) is dominant in the high frequency band.

The relationship between saturation magnetic flux density B_s, operating frequency, and iron loss for various soft magnetic materials is shown in **Figure 1.1.5. 3**[(1)]. From **Figure 1.1.5.3** (a), the operating frequency range of magnetic elements using various soft magnetic materials roughly corresponds to the aforementioned frequency characteristics of iron loss. Metallic materials with an iron loss of around 1 T are generally applied for operation in the tens to hundreds of kHz band, while ferrite with relatively small eddy current loss is used in the higher frequency band. However, ferrite is only about 0. 5 T, and an air gap must be provided in the iron core for application to high-voltage and high-current circuits. **Figure 1.1.5.3** (b) plots the relationship between iron loss and various soft magnetic materials for the same excitation frequency and magnetic flux density B_s amplitude, showing that there is a trade-off between high B_s and low iron loss for the major existing soft magnetic materials.

If high B_s materials can be applied to inductors, the desired inductance can be achieved without magnetic saturation even in DC



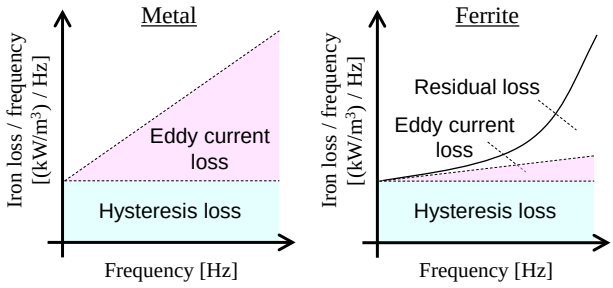
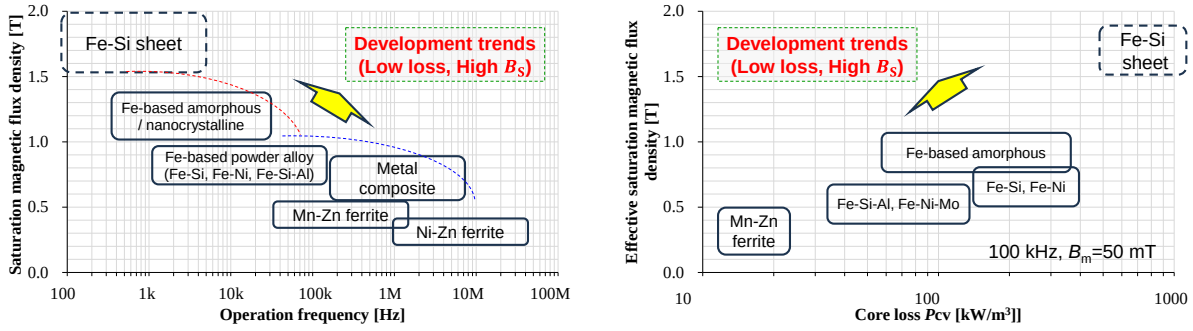


Figure 1.1.5.1 Major soft magnetic materials used in power conversion circuits **Figure 1.1.5.2** Frequency characteristics of iron loss exhibited by metallic materials and ferrite



(a) Relationship between saturation magnetic flux density and operating frequency (b) Relationship between saturation magnetic flux density and iron loss

Fig. 1.1.5.3 Development Trend of Soft Magnetic Materials (High Saturation Flux Density, Low Loss)[(1)]

superposition and large-amplitude current operation. In the case of transformers, higher materials not only lead to higher voltage operation and fewer turns, but also to gapless transformer design. In other words, if soft magnetic materials with higher inductance and lower high-frequency loss than existing ferrite or pressed materials are realized, it will be possible to design smaller and lighter inductors and transformers with large volume and mass in the circuit.

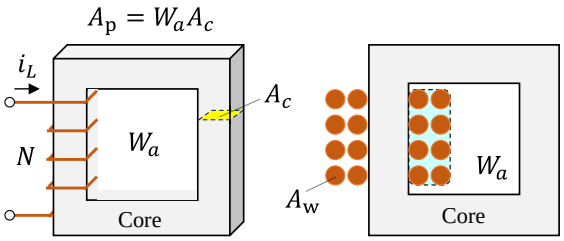


Fig. 1.1.5.4 Cross-sectional area of iron core, window area, and area occupied by windings

Next, the area product method, one of the magnetic element design methods that includes the selection of high B_s core material and structure, is explained, and the effect of the application of high materials and high-frequency switching operation on the miniaturization and weight reduction of magnetic elements is considered. For simplicity, an inductor with sinusoidal excitation is used here as an example (**Fig. 1.1.5.4**). Assuming that the maximum flux linkage, ϕ_m, the number of turns N, the cross-sectional area of the iron core, A_c, and the maximum flux density, $B_m (< B_s)$, the relationship between them is expressed as follows

$$\phi_m = NA_c B_m \tag{1.1.5.1}$$

On the other hand, if inductance L and maximum inductor current I_{L_max} are assumed, ϕ_m can also be expressed using L, I_{L_max} as follows.

$$\phi_m = LI_{L_max} \tag{1.1.5.2}$$

From Equations (1.1.5.1) and (1.1.5.2), B_m is expressed as follows.

$$B_m = \frac{LI_{L_max}}{NA_c} \tag{1.1.5.3}$$

Let the conductor cross-sectional area A_w be I_{L_max} and using the current density J_m amplitude

$$A_w = \frac{I_{L_max}}{J_m} \tag{1.1.5.4}$$

W_a can be expressed as If we consider the winding on the iron core NA_w with window area W_a, we can define the ratio k_u of the conductor area to the core area as follows

$$k_u \equiv \frac{NA_w}{W_a} \tag{1.1.5.5}$$

k_u is called window utilization factor (occupancy factor). It is usually used to be about 0.3 to 0.7, depending on the winding insulation coating and bobbin dimensions. From Eqs. (1.1.5.4) and (1.1.5.5), N can be seen that

$$N = \frac{k_u W_a}{A_w} = \frac{k_u W_a J_m}{I_{L_max}} \tag{1.1.5.6}$$

It can also be expressed as From the relationships in Eqs. (1.1.5.1), (1.1.5.2), and (1.1.5.6), we have

$$LI_{L_max} = NA_c B_m = \frac{k_u W_a A_c J_m B_m}{I_{L_max}} \tag{1.1.5.7}$$

W_m is valid. The stored energy W_m of the inductor can be expressed as

$$W_m = \frac{1}{2} LI_{L_max}{}^2 = \frac{1}{2} k_u W_a A_c J_m B_m \tag{1.1.5.8 }$$

The product of the window area W_a and the cross sectional area A_c of the iron core, expressed in Eq. (1.1.5.8), can be defined as an area A_p product as follows

$$A_{\mathrm{p}} \equiv W_{\mathrm{a}}A_{\mathrm{c}} = \frac{LI_{\mathrm{L_max}}{}^{2}}{k_{\mathrm{u}}J_{\mathrm{m}}B_{\mathrm{m}}} = \frac{2W_{\mathrm{m}}}{k_{\mathrm{u}}J_{\mathrm{m}}B_{\mathrm{m}}} \tag{1.1.5.9}$$

If the effective value of the voltage $V_{\mathrm{L_rms}}$ applied to the inductor is the effective value $I_{\mathrm{L_rms}}$ of the current flowing through the inductor, the apparent power of the inductor P_{Q} is expressed as follows

$$P_{\mathrm{Q}} = V_{\mathrm{L_rms}}I_{\mathrm{L_rms}} = \left(\frac{V_{\mathrm{L_max}}}{\sqrt{2}}\right)\left(\frac{I_{\mathrm{L_max}}}{\sqrt{2}}\right) = fW_{\mathrm{m}} \tag{1.1.5.10}$$

where $V_{\mathrm{L_max}}$ is the maximum value of the inductor voltage and f is the excitation frequency. Therefore, A_{p} can be expressed as

$$A_{\mathrm{p}} = \frac{2W_{\mathrm{m}}}{k_{\mathrm{u}}J_{\mathrm{m}}B_{\mathrm{m}}} = \frac{2P_{\mathrm{Q}}}{k_{\mathrm{u}}J_{\mathrm{m}}B_{\mathrm{m}}f} \tag{1.1.5.11}$$

From the above, it can be seen that the area A_{p} product expresses the relationship between the iron core dimension parameters and the electrical and magnetic parameters of the inductor [(2)-(4)]. The window area W_{a} corresponds to the current capacity (winding current density), and the core cross-sectional area A_{c} corresponds to the magnetic flux density inside the core. In designing a magnetic element, first calculate the A_{p} value that can be determined from the desired conditions, and then select an iron core that is greater than or equal to this calculated A_{p} value [(4)]. The relationship in Equation (1.1.5.11) also indicates that the larger the maximum flux density B_{m} and excitation frequency f, the smaller the A_{p} value. In other words, this can be considered as one of the reasons why it is expected that " applying an even higher B_{s} soft magnetic material and increasing the operating flux density amplitude (ΔB) and switching frequency will lead to the realization of a smaller magnetic element.

The volume of the magnetic element (Volume) and the area product A_{p} can also be related by performing dimensional analysis as follows [(3)]. Let the coefficients k_1, k_2 be dimensionless quantities and the dimension of length be denoted by X (m), then Volume is k_1X^3 (m^3) and A_{p} is k_2X^4 (m^4). So $X^4 = \frac{A_{\mathrm{p}}}{k_2}$ can be written as $X = \left(\frac{A_{\mathrm{p}}}{k_2}\right)^{0.25}$.

Therefore, it can be expressed as Volume $= k_1\left(\frac{A_{\mathrm{p}}}{k_2}\right)^{0.75} = \frac{k_1}{(k_2)^{0.75}}\left(A_{\mathrm{p}}\right)^{0.75} \equiv k_{\mathrm{v}}\left(A_{\mathrm{p}}\right)^{0.75}$. The coefficient k_{v} is a constant uniquely determined by the iron core geometry, and the volume of the magnetic element is related to A_{p} raised to ther power of 0.75. From the above, A_{p} is widely used as a design index for magnetic element size [(5)-(7)].

1.5.2 Difference between superiority of material loss characteristics and superiority of magnetic element loss characteristics

Comparison of superiority or inferiority of iron loss characteristics of individual materials is generally discussed based on the frequency characteristics of iron loss when the maximum magnetic flux density (magnetic flux density amplitude) is kept constant under sinusoidal excitation conditions in which a DC bias magnetic field is not included. In this case, iron loss increases as the operating flux density and excitation frequency increase, and the superiority of material loss characteristics is evaluated by the size of iron loss expressed in terms of volume ratio (kW/m^3) and mass ratio (W/kg). On the other hand, magnetic elements used in power conversion circuits are generally square wave voltage excitation (triangular wave current excitation). In the case of inductors, since direct current is superimposed, the operating point on the *B*-*H* plane is different from that of the evaluation of the iron loss characteristics of the material itself. In other words, when comparing the superiority or inferiority of loss characteristics as a magnetic element, it is important to understand the operating flux density amplitude, excitation frequency, and iron loss characteristics for DC superposition under square wave voltage excitation conditions. Taking the inductor of a chopper circuit as an example, if the inductance is the same, the magnitude of the current ripple is halved when the switching frequency is doubled. Assuming a certain amplitude of inductor current ripple, the higher the switching frequency, the smaller the inductance required. In this way, from the viewpoint of power electronics circuit design, the process starts with the desired circuit operating conditions such as operating voltage and current, conversion power, and switching frequency, etc. Then, for magnetic elements such as inductors and high-frequency transformers, allowable loss, volume, temperature, etc. are set as design conditions (constraint conditions). The process generally involves determining the iron core material, core shape, and winding conditions that satisfy these conditions. In other words, it is difficult to simply compare the loss of magnetic elements made of different iron core materials, and material selection and design must take into account many factors, including winding loss (copper loss), thermal design (balance between heat generation due to loss and heat dissipation/cooling

performance), shape, workability, and cost.

In the following, we consider the relationship between the operating flux density amplitude and the losses produced by the magnetic elements [(2)-(4)]. The DC resistance $R_{\mathrm{w_dc}}$ of a winding is proportional to the conductor length l_{w} and inversely proportional to the conductor cross-sectional area A_{w}, as expressed in Equation (1.1.5.12).

$$R_{\mathrm{w_dc}} = \rho_{(\mathrm{Cu})} \frac{l_{\mathrm{w}}}{A_{\mathrm{w}}} \tag{1.1.5.12}$$

However, $\rho_{(\mathrm{Cu})}$ represents the resistivity of copper. If the winding length l_{MLT} per turn is taken as the winding length per turn, the winding length per N turn can be written as $l_{\mathrm{w}} = N l_{\mathrm{MLT}}$. The conductor cross-sectional area A_{w} can also be expressed as $A_{\mathrm{w}} = \frac{k_{\mathrm{u}} W_{\mathrm{a}}}{N}$ from equation (1.1.5.6). Therefore, $R_{\mathrm{w_dc}}$ can be expressed as in equation (1.1.5.13).

$$R_{\mathrm{w_dc}} = \rho_{(\mathrm{Cu})} \frac{N l_{\mathrm{MLT}}}{A_{\mathrm{w}}} = \rho_{(\mathrm{Cu})} \frac{l_{\mathrm{MLT}}}{k_{\mathrm{u}} W_{\mathrm{a}}} N^2 \tag{1.1.5.13}$$

Also, from equations (1.1.5.1) and (1.1.5.2), we have N

$$N = A_{\mathrm{c}} \frac{L I_{\mathrm{L_max}}}{B_{\mathrm{m}}} \tag{1.1.5.14}$$

then the DC copper loss $P_{\mathrm{w_dc}}$ can be expressed as in equation (1.1.5.15).

$$P_{\mathrm{w_dc}} = R_{\mathrm{w_dc}} {I_{\mathrm{L_rms}}}^2 = R_{\mathrm{w_dc}} \left(\frac{I_{\mathrm{L_max}}}{\sqrt{2}}\right)^2 = \frac{\rho_{(\mathrm{Cu})} l_{\mathrm{MLT}}}{2 k_{\mathrm{u}} W_{\mathrm{a}}} N^2 {I_{\mathrm{L_max}}}^2 = \frac{\rho_{(\mathrm{Cu})} l_{\mathrm{MLT}}}{2 k_{\mathrm{u}} W_{\mathrm{a}}} \left(\frac{L}{A_{\mathrm{c}} B_{\mathrm{m}}}\right)^2 {I_{\mathrm{L_max}}}^4 \tag{1.1.5.15}$$

Focusing on the relationship between the operating flux density and copper loss in equation (1.1.5.15), we see that $P_{\mathrm{w_dc}}$ is inversely proportional to ${B_{\mathrm{m}}}^2$.In other words, the larger the operating flux density amplitude (ΔB) is, the smaller the copper loss becomes.

Next, consider the AC resistance of the winding: the model equation for the AC resistance of a winding derived by Dowell takes a form that includes not only the skin effect but also the proximity effect [(4)(8)]. When a winding of a circular-section conductor of diameter d is wound in multiple layers in a solenoidal fashion, the AC resistance $R_{\mathrm{w_ac}}$ of the winding can be expressed as follows.

$$R_{\mathrm{w_ac}} = R_{\mathrm{w_dc}} A \left[\frac{e^{2A} - e^{-2A} + 2\sin(2A)}{e^{2A} + e^{-2A} - 2\cos(2A)} + \frac{2({n_{\mathrm{layer}}}^2 - 1)}{3} \frac{e^{A} - e^{-A} - 2\sin(A)}{e^{A} + e^{-A} + 2\cos(A)}\right] \tag{1.1.5.16}$$

$$A = \left(\frac{\pi}{4}\right)^{\frac{3}{4}} \frac{d}{\delta_{\mathrm{w}}} \sqrt{\eta} = \left(\frac{\pi}{4}\right)^{\frac{3}{4}} d \sqrt{\eta \frac{\pi \mu_0 f}{\rho_{(\mathrm{Cu})}}} \tag{1.1.5.17}$$

n_{layer} is the number of layers of the winding, $\delta_{\mathrm{w}} = \sqrt{\frac{\rho_{(\mathrm{Cu})}}{\pi \mu_0 f}}$ is the number of layers of the winding, is the depth of the winding skin, μ_0 is the permeability of the vacuum, and f is the excitation frequency. The winding spacing coefficient η is called the spacing coefficient or spacing factor, and is usually about the same as $\eta = 0.8$ [(5)]. As an example, a single-layer solenoid with winding diameter d and winding pitch p spacing is represented by $\eta = \frac{d}{p}$. As explained in Section 1.1.3, the copper loss, which accounts for $R_{\mathrm{w_ac}}$ that increases with higher f due to the skin effect and the proximity effect, is larger than in Equation (1.1.5.15).

On the other hand, the iron loss P_{cv} per unit volume of the iron core in sinusoidal excitation is expressed by the Steinmetz equation.

$$P_{\mathrm{cv}} = k f^{\alpha} {B_{\mathrm{m}}}^{\beta} \tag{1.1.5.18}$$

k, α, β is the Steinmetz coefficient. Let us consider the expression of iron loss using an inductor as an example. Inductance L is expressed

$L = A_{\mathrm{L}}N^2$ in terms of the number of turns N and permeance A_{L}. Assuming an iron core of toroidal shape, $A_{\mathrm{L}} = \dfrac{\mu_0\mu_{\mathrm{r}}A_{\mathrm{c}}}{l_{\mathrm{c}}}$ (μ_{r}: specific permeability of the iron core material), it can be expressed as $N = \sqrt{\dfrac{L}{A_L}} = \sqrt{\dfrac{l_{\mathrm{c}}L}{\mu_0\mu_{\mathrm{r}}A_{\mathrm{c}}}}$. From equation (1.1.5.3), B_{m} can be expressed as

$$B_{\mathrm{m}} = \frac{LI_{\mathrm{L_max}}}{NA_{\mathrm{c}}} = \frac{LI_{\mathrm{L_max}}}{A_{\mathrm{c}}}\sqrt{\frac{\mu_0\mu_{\mathrm{r}}A_{\mathrm{c}}}{l_{\mathrm{c}}L}} = I_{\mathrm{L_max}}\sqrt{\frac{\mu_0\mu_{\mathrm{r}}L}{l_{\mathrm{c}}A_{\mathrm{c}}}} = I_{\mathrm{L_max}}\sqrt{\frac{\mu_0\mu_{\mathrm{r}}L}{V_{\mathrm{c}}}} \tag{1.1.5.19}$$

where V_{c} is the volume of the iron core. Therefore, the iron loss P_{c} can be expressed from equations (1.1.5.18) and (1.1.5.19) as

$$P_{\mathrm{c}} = P_{\mathrm{cv}}V_{\mathrm{c}} = k_{\mathrm{c}}f^{\alpha}\left(I_{\mathrm{L_max}}\sqrt{\frac{\mu_0\mu_r L}{V_{\mathrm{c}}}}\right)^{\beta}V_{\mathrm{c}} = k_{\mathrm{c}}f^{\alpha}\left(I_{\mathrm{L_max}}\sqrt{\mu_0\mu_r L}\right)^{\beta}V_{\mathrm{c}}{}^{1-\frac{\beta}{2}} \tag{1.1.5.20}$$

The extended generalized Steinmetz equation (improved Generalized Steinmetz Equation) corresponding to square wave voltage excitation is expressed as follows

$$P_{\mathrm{cv}} = \frac{1}{T}\int_0^T k_i\left|\frac{\mathrm{d}B}{\mathrm{d}t}\right|^{\alpha}|\Delta B(t)|^{\beta-\alpha}\mathrm{d}t \tag{1.1.5.21}$$

$$k_i = \frac{k}{(2\pi)^{\alpha-1}\int_0^{2\pi}|\cos\theta|^{\alpha}2^{\beta-\alpha}\mathrm{d}\theta} \tag{1.1.5.22}$$

T is the switching cycle and θ is the phase of one switching cycle (0 to 2π). From these iron loss model equations, the higher the excitation frequency f and the larger the maximum flux density B_{m} (amplitude ΔB), the higher the iron loss. Also, the higher f under the constant iron loss constraint, the settable B_{m} becomes the smaller.

The total loss of an inductor P_{total} is expressed as the sum of the copper loss and the iron loss. For simplicity, assuming that the copper loss and iron loss per unit volume are expressed by Equations (1.1.5.15) and (1.1.5.18), respectively, P_{total} can be expressed as follows

$$P_{\mathrm{total}} = P_{\mathrm{w_dc}} + P_{\mathrm{cv}}V_{\mathrm{c}} = \frac{\rho_{(\mathrm{Cu})}l_{\mathrm{MLT}}L^2}{2k_{\mathrm{u}}W_{\mathrm{a}}A_{\mathrm{c}}{}^2B_{\mathrm{m}}{}^2}I_{\mathrm{L_max}}{}^4 + V_{\mathrm{c}}kf^{\alpha}B_{\mathrm{m}}{}^{\beta} \tag{1.1.5.23}$$

By differentiating this P_{total} by B_{m} the first derivative, the magnetic flux density $B_{\mathrm{m_opt}}$ with the minimum P_{total} can be expressed as

$$\frac{\mathrm{d}P_{\mathrm{total}}}{\mathrm{d}B_{\mathrm{m}}} = \frac{\mathrm{d}P_{\mathrm{w_dc}}}{\mathrm{d}B_{\mathrm{m}}} + \frac{\mathrm{d}P_{\mathrm{c}}}{\mathrm{d}B_{\mathrm{m}}} = -\frac{\rho_{(\mathrm{Cu})}l_{\mathrm{MLT}}L^2}{k_{\mathrm{u}}W_{\mathrm{a}}A_{\mathrm{c}}{}^2B_{\mathrm{m}}{}^3}I_{\mathrm{L_max}}{}^4 + \beta V_{\mathrm{c}}k_{\mathrm{c}}f^{\alpha}B_{\mathrm{m}}{}^{\beta-1} \tag{1.1.5.24}$$

$$\frac{\mathrm{d}P_{\mathrm{total}}}{\mathrm{d}B_{\mathrm{m}}} = 0 \;\Leftrightarrow\; B_{\mathrm{m_opt}} = \left(\frac{\rho_{(\mathrm{Cu})}l_{\mathrm{MLT}}L^2I_{\mathrm{L_max}}{}^4}{\beta k_{\mathrm{c}}k_{\mathrm{u}}W_{\mathrm{a}}A_{\mathrm{c}}{}^2V_{\mathrm{c}}f^{\alpha}}\right)^{\frac{1}{\beta+2}} \tag{1.1.5.25}$$

As described above, when considering circuit operation by increasing the maximum magnetic flux density and magnetic flux density amplitude, a reduction in copper loss can be expected, but at the same time an increase in iron loss will result. In addition, the higher the switching frequency, the higher the copper and iron losses become. If it is necessary to secure a window area from the viewpoints of current density, insulation, and heat dissipation of the winding, it will be contrary to the realization of miniaturization of the magnetic element. The optimum operating point of the magnetic flux density at which the total loss of the magnetic element is minimized is when $\dfrac{\mathrm{d}P_{\mathrm{w_dc}}}{\mathrm{d}B_{\mathrm{m}}} = -\dfrac{\mathrm{d}P_{\mathrm{c}}}{\mathrm{d}B_{\mathrm{m}}}$ from the relationship in Equation (1.1.5.24). As shown in **Figure 1.1.5.4**, the maximum flux density and number of turns are generally determined by the index "copper loss = iron loss".

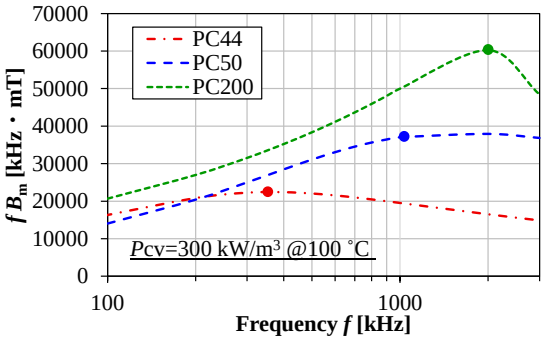


Figure 1.1.5.5 Performance Factor of Mn-Zn ferrite [9]

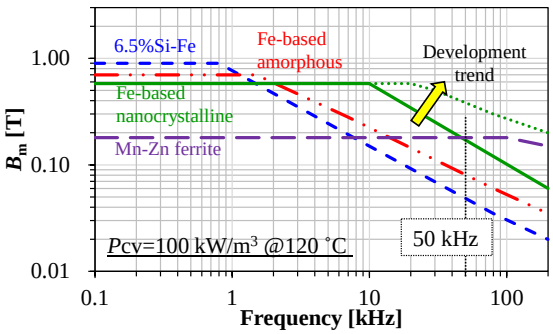


Figure 1.1.5.6 Performance Factor of Mn-Zn ferrite that can operate under the same iron loss conditions

Maximum flux density and operating circumference of various soft magnetic materials

Wave number relationship [1]

1.5.3 Material selection index in the study of miniaturization of magnetic elements (whether the transformer can be smaller than ferrite when the loss conditions are the same)

Based on the previous section, this section describes an example of a study report focusing on the relationship between the maximum magnetic flux density and operating frequency assuming the same operating temperature and iron loss in order to compare the superiority and inferiority of magnetic element characteristics made of different materials. From the relationship in Equation (1.1.5.18), the iron loss P_{cv} per unit volume of the iron core in sinusoidal excitation can be expressed as follows

$$P_{cv} = kf^{\alpha}{B_m}^{\beta} = k(fB_m)^{\beta}f^{\alpha-\beta} \tag{1.1.5.26}$$

Transforming equation (1.1.5.26), the product of f and B_m is expressed as

$$fB_m = \left(\frac{P_{cv}}{k}\right)^{\frac{1}{\beta}} f^{\left(1-\frac{\alpha}{\beta}\right)} \tag{1.1.5.27}$$

The results of plotting the relationship between fB_m and f three types of Mn-Zn ferrite with known Steinmetz coefficients k, α, β and the same operating temperature (100 ℃) with a constant P_{cv} (300 kW/m^3) are shown in **Figure 1.1.5.5** [9]. This result indicates that the transformer core size can be optimized at the operating frequency where the maximum fB_m value of the Performance Factor can be obtained fB_m when considering the application of each material to the transformer core. It is reported that the performance factor is a useful index in the selection of magnetic element materials and the minimum design study of the iron core size.

Next, an example is given to compare the characteristics of different soft magnetic materials: silicon steel sheet, iron-based amorphous alloys, iron-based nanocrystalline alloys, and Mn-Zn ferrite. Assuming the same operating temperature (120 ˚C) and the same iron loss (100 kW/m3), the relationship between the maximum magnetic flux density and operating frequency is **shown in Figure 1.1.5.** 6**,** where the maximum magnetic flux density is the magnetic flux density that B_S is 50 % of the operating frequency [1]. From this result, it is possible to compare how much magnetic flux density each material can operate at over what operating frequency range, based on a certain iron loss. For operating frequencies below 1 kHz, cores made of silicon steel sheet or iron-based amorphous alloys can operate at higher flux densities than those made of iron-based nanocrystalline alloys or ferrite. However, as the operating frequency increases, their magnetic flux density becomes limited assuming the same iron loss, and for operating frequencies between a few kHz and 50 kHz, iron-based nanocrystalline alloys can be operated at higher magnetic flux density. On the other hand, in the operating frequency range above 50 kHz, Mn-Zn ferrite can be operated at a higher flux density than Fe-based nanocrystalline alloys. From these results, it is possible to design smaller transformers using iron-based nanocrystalline alloys as the core than Mn-Zn ferrites for applications where the operating frequency is low and high ΔB. On the other hand, when the switching frequency is increased beyond 50 kHz, the loss increase in the iron-based nanocrystalline alloy material becomes significant, suggesting that Mn-Zn ferrite is more suitable for miniaturization. The development of iron-based nanocrystalline alloys with a further increase B_S in the loss of Mn-Zn ferrite is also underway, and further expansion of the operating frequency of high-frequency transformers using iron-based nanocrystalline alloys is also anticipated. Thus, in addition to the general performance indices of magnetic materials (saturation flux density, coercive force, and major hysteresis loop), we have focused on the excitation conditions, temperature dependence, and operating point on the B-H plane of magnetic elements in a circuit (minor hysteresis loop, ΔB, ΔH, DC bias magnetic

field H_0), as well as the maximum flux density and coercive force for different materials under identical Focusing on the relationship between the maximum magnetic flux density and operating frequency assuming the same loss conditions for different materials is considered useful not only for circuit designers who consider the optimization of transformer core size, thermal design, and high-frequency operation, but also for developers of soft magnetic materials for application to next-generation power electronics circuits.

[Takaaki Ibuchi]

References

(1) D. Azuma: "Wide Bandgap Power Semiconductor Packaging -Materials, Components and Reliability- Section 4: Magnetic materials ", Elsevier, pp. 97-107 (2018)
(2) R. W. Erickson, D. Maksimovic: "Fundamentals of Power Electronics (2nd edition) ", Springer (2001).
(3) C. W. T. McLyman: "Transformer and Inductor Design Handbook (4th edition)," CRC Press (2004).
(4) M. K. Kazimierczuk: "High-Frequency Magnetic components", Wiley (2009).
(5) M. K. Kazimierczuk, H. Sekiya: "Design of AC Resonant Inductors Using Area Product Method", 2009 IEEE Energy Conversion Congress and Exposition, pp. 994-1001, doi: 10.1109/ECCE.2009.5316501 (2009).
(6) A. D. Bastiani Lange, M. L. Heldwein: "Optimal inductor design for single-phase three-level bridgeless PFC rectifiers," 2017 Brazilian Power Electronics Conference (COBEP), pp. 1-6, doi: 10.1109/COBEP.2017.8257389 (2017).
(7) R. Orzechowski, M. Jahnes and M. Preindl: "Enhanced Area Product Method for High-Frequency Inductors and Transformers," 2024 IEEE Applied Power Electronics Conference and Exposition (APEC), pp. 3242-3246, doi: 10.1109/APEC48139.2024.10509420 (2024).
(8) P.J. Dowell: "Effects of eddy currents in transformer winding", Proc. IEE, Vol. 113, No. 8, pp. 1387-1394 (1966).
(9) W. G. Hurley, T. Merkin, and M. Duffy: "The Performance Factor for Magnetic Materials Revisited: the Effect of Core Losses on the Selection of Core Size in Transformers," IEEE Power Electronics Magazine, Vol. 5, No. 3, pp. 26-34 (2018).

1.6 Factors in design accuracy required for magnetic components

Keyword: Inductors, Iron loss, Inductance

1.6.1 Inductor loss

The current status of loss data provided by iron core manufacturers is described. Loss data are generally provided in the form of graphs of measured losses when two of the three parameters are fixed and the remaining parameter is varied, using sinusoidal excitation with the maximum magnetic flux density B_m, frequency f, and temperature T as parameters. In many cases, specific numerical values for losses at a typical frequency of 100 kHz and a typical maximum magnetic flux density of 100 mT or 200 mT are provided separately from the graphs.

For example, Magnetics (USA) provides the classical Steinmetz coefficient, POCO (China) provides the Steinmetz coefficient when eddy current loss and hysteresis loss are separated, and MICROMETALS (USA) provides Bozorth's hysteresis loss coefficient, which is different from the Steinmetz coefficient, with specific values. MICROMETALS (USA) provides the Bozorth hysteresis loss coefficient, which is different from the Steinmetz coefficient, with specific values.

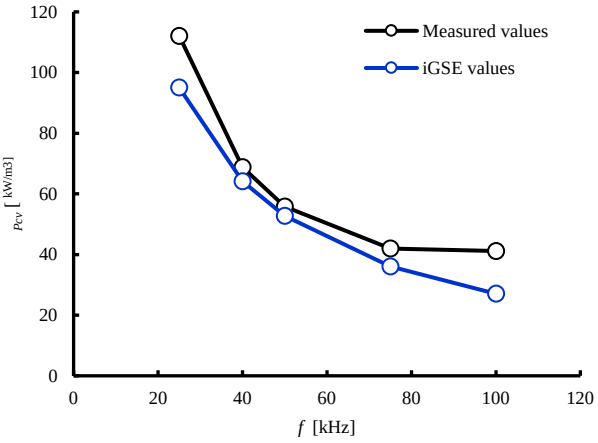


Figure 1.1.6.1 Loss frequency characteristics of high-

The actual voltage waveform applied to the filter inductor of a PWM inverter or DC chopper is not a sine wave but a square wave, and the current waveform is also a low-frequency sine wave superimposed with a triangular wave or sawtooth waveform caused by the switching frequency. Since the duty ratio of PWM inverters varies with time, circuit designers cannot accurately estimate the inductor losses under actual operating conditions using the loss data for sinusoidal excitation provided by the iron core manufacturer or mathematical formulas.

One effective and simple method for estimating losses under actual operation is to apply the iGSE (extended Steinmetz equation)[1] for square wave excitation (square wave for voltage and sawtooth wave for current) instead of the Steinmetz equation for sine wave excitation. In the case of an iron core with little variation in DC superposition characteristics, the extended Steinmetz coefficients can be converted from the Steinmetz coefficients for sinusoidal excitation.

Figure 1.1.6.1 shows the results of applying iGSE to Magenetics' High Flux, which has little variation in DC superposition characteristics (small change in inductance even when DC current is applied). The difference between the estimated loss of the extended Steinmetz equation using the Steinmetz coefficients provided by the manufacturer and the measured value was -5% at minimum and -34% at maximum. If the Steinmetz coefficients are provided by the iron core manufacturer, the user can estimate the inductor loss under actual operation of square wave excitation. From the viewpoint of power electronics circuit design, this level of error is generally not a problem if the loss can be determined in advance.

The Steinmetz coefficient can be calculated by the user by using a measuring instrument such as a BH analyzer[2] if the frequency range is limited. The loss can be measured under sinusoidal excitation conditions where the frequency *f and the* maximum flux density B_m *are* different.

Although all manufacturers provide the DC resistance R_{dc} *of the* windings in an inductor, it is not common to provide the frequency characteristics of the AC resistance R_{ac}. As the frequency *f*increases, the electrical resistance of the winding increases not only due to the skin effect but also due to the proximity effect between windings above 1 kHz, as **shown in Figure 1.1.6.** 2. Therefore, it is difficult for the user to estimate the inductor loss, including copper loss, under actual operation using only the data provided by the inductor manufacturer. This resistance is the result of measuring the resistance component of the winding only with an impedance analyzer.

The frequency characteristics of the AC resistance R_{ac} of the winding can be accurately measured by applying the same winding as the actual inductor to an air core of the same shape as the actual inductor core. For example, as shown in **Figure 1.1.6.3**, a hollow-core inductor can be manufactured inexpensively and quickly by fabricating the same shape using a 3D printer and winding the windings.

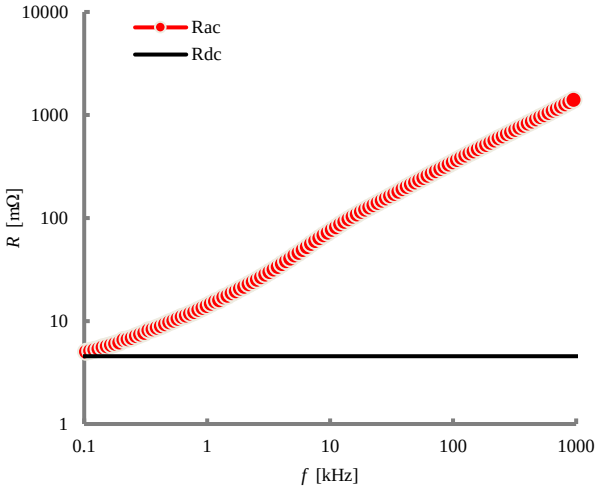


Figure 1.1.6.2 Electrical Resistance Frequency

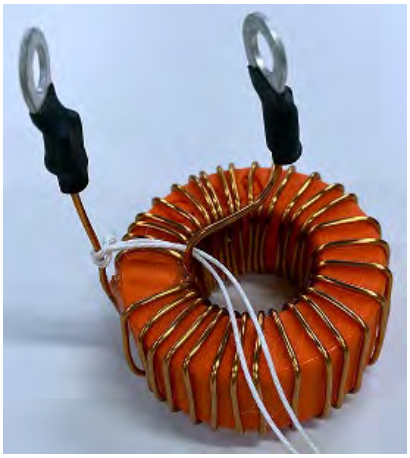


Fig. 1.1.6.3 Air-core inductor fabricated by 3D printer

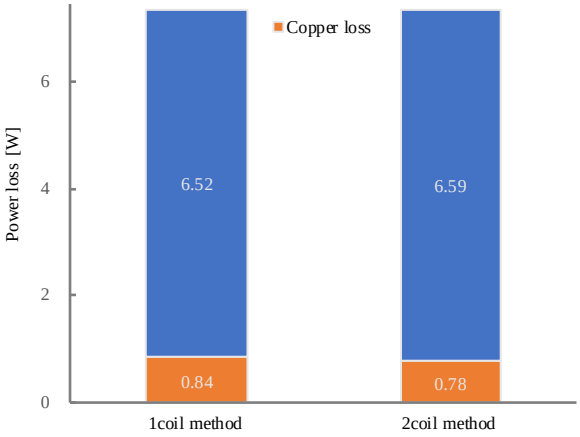


Figure 1.1.6.4 Comparison of losses between 2-

Once the frequency characteristic of the AC resistance R_{ac} of the winding is known, the user can estimate the copper loss of the inductor winding and accurately measure the loss in the iron core using the one-winding method as shown in **Figure 1.1.6.4**.

1.6.2 Inductor size

Since the iron core size is either a standard product or provided by the iron core manufacturer, the user does not customize and specify the iron core size but selects it from the provided products. Once the iron core size is selected, the weight is determined. The iron core size is determined by the required inductance *L and the* maximum current value I_{max}. The number of turns of winding *N* is determined from the inductance *L* and the AL value [nH/N^2] (self-inductance per unit number of turns) provided by the iron core manufacturer. Determine the winding diameter *D* to be used from *the* maximum current value I_{max}. In general, the current density of windings in power electronics equipment is often set around 4 to 10 A/mm^2. In the power electronics field, many manufacturers provide the magnetic permeability μ instead of the AL value for inductor design. It is necessary to design the inductor so that the iron core does not reach magnetic saturation at the maximum current value I_{max}.

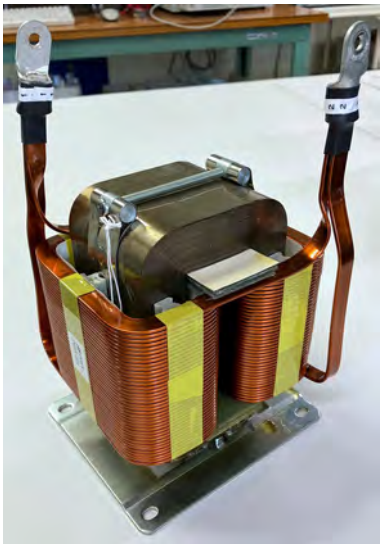


Figure 1.1.6.5. 200 uH DC inductor with flat winding

The user calculates the window area occupancy (the ratio of the winding to the window frame area) from the number of turns *N*, the winding diameter *D*, and the iron core size provided by the iron core manufacturer. After determining the validity of the calculation, the core size is selected and the weight is determined. The appropriateness of the window area occupancy of 30-70% must be determined by considering whether it is physically possible to wind the winding, the proximity effect of the winding winding winding method (single layer, multiple layers, winding spacing), the skin effect of the winding shape (round wire, flat wire, single wire, twisted wire, litz wire), and heat radiation characteristics. **Figure 1.1.6.5** shows a photograph of an inductor capable of conducting 200 A of DC current. This inductor was fabricated with a cut core (CS-630) using amorphous as the magnetic device. Although not visible in the photo due to the winding, a 13 mm gap is inserted on each side of the iron core. The weight of this inductor is 8 kg.

The size and weight of an inductor are determined by the size and weight of the iron core and winding, as well as the total number of components that make up the inductor, such as insulation resin, connection terminals, and fixtures. In power electronics-related products, magnetic components such as inductors still occupy a large volume and weight.

1.6.3 Inductance

The important factors in determining the inductance *L*are the iron core size and the magnetic permeability μ, or AL value. Since the magnetic permeability μ has a frequency characteristic, all manufacturers provide the frequency characteristic. In addition, since permeability μ has a DC superposition characteristic, as DC I_0 increases, permeability μ becomes smaller and inductance *L* decreases. The DC superposition characteristic of permeability μ is important information to know the ratio of the variation of inductance *L* to DC.

In the filter inductor of a PWM inverter or DC chopper, a sawtooth wave current with DC I_0 (including low-frequency AC) superimposed flows. If the DC superposition characteristics of the filter inductor are poor, the current ripple Δi_L (high-frequency component of the inductor current) of the inductor will be higher than the designed value, increasing the high-frequency losses in the iron core.

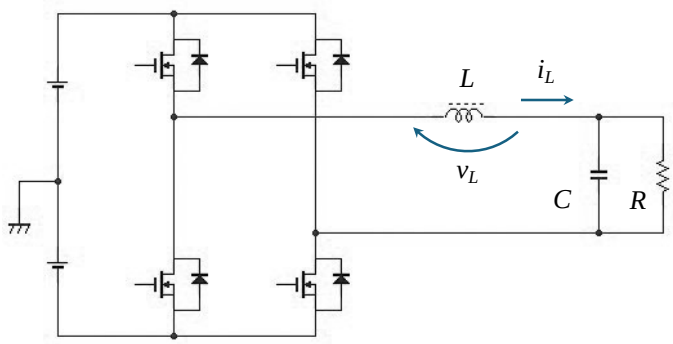


Figure 1.1.6.6 PWM inverter circuit diagram

Table 1.1.6.1 Example of data provided by manufacturer

品番	インダクタンス		直流抵抗 (at 20 °C) (mΩ)		定格電流 (A)	
	L0 (μH)	許容差 (%)	Typ. (max.)	許容差 (%)	ΔT = 40 K	ΔL=-30%
ETQP3MR2YFP	2.2	±20	22.6 (24.8)	±10	5.8	10.8
ETQP3MR3YFP	3.3		31.3 (34.4)		5.0	8.6
ETQP4MR7YFP	4.6		36.0 (39.6)		4.8	7.7
ETQP4M100YFP	10.0		95.0 (104.5)		3.0	3.9
ETQP4M220YFP	22.0		163.0 (179.0)		2.3	3.1

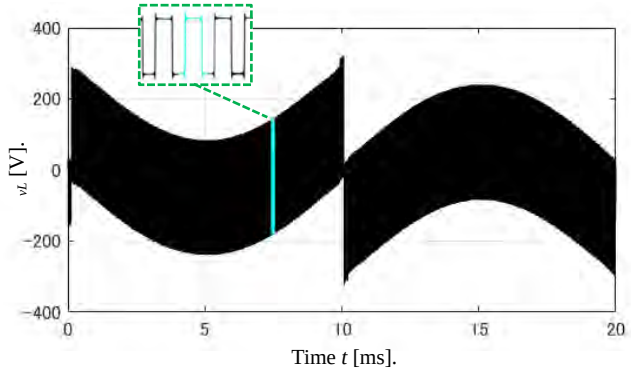


Fig. 1.1.6. 7 Inductor voltage waveform of a PWM

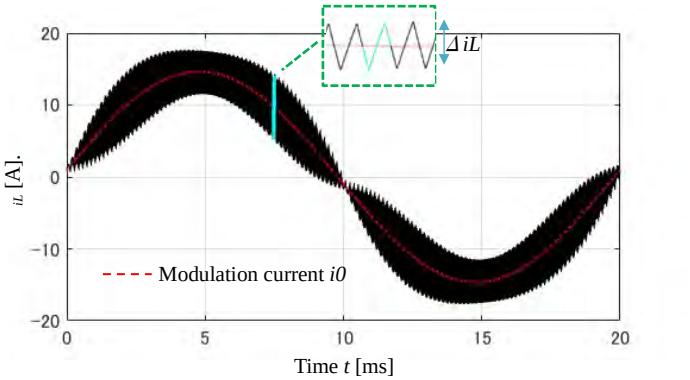


Figure 1.1.6.8 Inductor current waveform of PWM

Figure 1.1.6.6 shows the circuit diagram of a single-phase PWM inverter. The time waveforms of the filter inductor inductor voltage v_L and inductor current i_L are shown in **Figures 1.1.6.7** and **1.1.6.8**. i_L has a current ripple Δi_L at the switching frequency f_{sw} superimposed on the commercial frequency modulation wave current i_0. Since i_0 varies with time, the superimposed DC current varies with time. i_0 varies with time, which means that the superimposed DC current varies with time. The B-H curve, where i_L is converted to the magnetic field H and v_L to the magnetic flux density B, is shown in **Figure 1.1.6.9**. The minor loop corresponding to one switching cycle highlighted by v_L and i_L is also shown in light blue in the same figure. The slope of the minor loop represents the magnetic permeability at this time, and the area represents the loss energy per unit volume (for high frequency).

This section describes the current status of data related to inductance L provided by inductor manufacturers. The data related to inductance L are the typical value of inductance L, the frequency characteristics of impedance |Z|, and the DC superposition characteristics of inductance

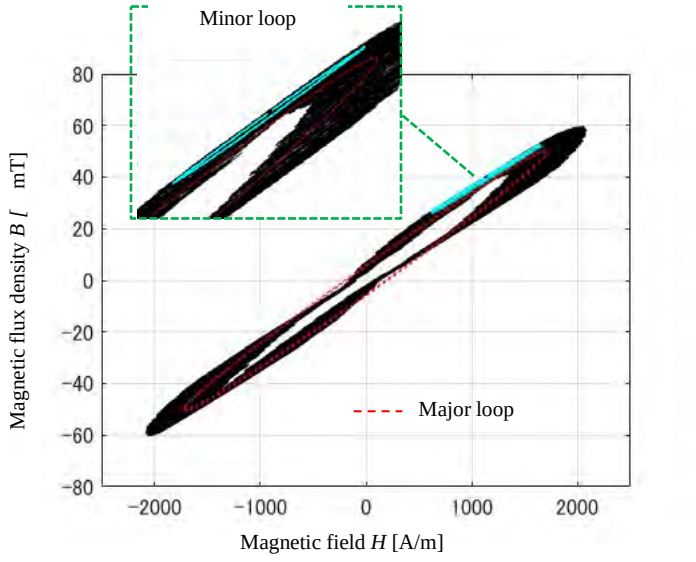


Figure 1.1.6.9 Inductor B-H curve of a PWM inverter

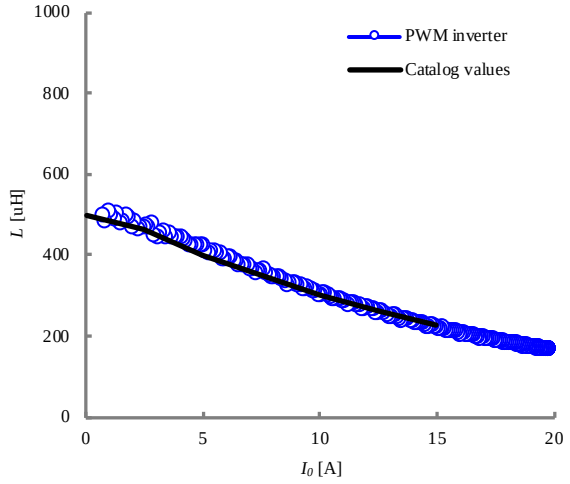


Figure 1.1.6.10 DC superposition characteristics using PWM inverter

L. As shown in **Table 1.1.6.1**, some places do not provide the DC superposition characteristics, but provide the rated current of the inductor based on the inductance change. In addition to this, inductance tolerances of 10-20% are also provided.

Most users can measure the frequency characteristics of inductance and impedance by using an LCR meter or an impedance analyzer, but these values show current values around 0 A. On the other hand, expensive measuring instruments are required to measure the DC superposition characteristics. The DC superimposed characteristic is an important characteristic that determines the loss of an inductor. For the DC superimposed characteristics of an inductor, if the inductor current i_L *and* inductor voltage v_L of a PWM inverter can be measured, the DC superimposed characteristics can be measured at several hundred points per modulation cycle in a short time. **Figure 1.1.6.10** shows an example of such a measurement.

[Keiji Wada]

References

(1) J. Li, T. Abdallah and C. R. Sullivan: "Improved calculation of core loss with nonsinusoidal waveforms", *Conference Record of the 2001 IEEE Industry Applications Conference. 36th IAS Annual Meeting* (*Cat. No. 01CH37248)*, Chicago, IL, USA, Vol. 4, pp. 2203-2210 (2001).
(2) IWATSU Electric Co. Ltd: "B-H Analyzer," https://www.iwatsu.co.jp/tme/sy/ [Accessed: Jul. 19, 2025].
(3) Panasonic Corporation: " PCC-M0530M / PCC-M0540M Series Power Choke Coil (Automotive Grade)", Datasheet, Mar. 2025. https ://industrial.panasonic.com/cdbs/www-data/pdf/AGL0000/AGL0000C60.pdf [Accessed: Jul. 19, 2025].

Section 2 Capacitor

This section describes the requirements for capacitors from the circuit side and the issues involved. The requirements for capacitors are classified and the differences in requirements for each application are summarized. Based on the results, requirements for smoothing and AC capacitors are introduced, and issues such as bottlenecks and reliability in circuit applications are outlined.

2.1 Requirements for capacitors for each application (including tan δ)

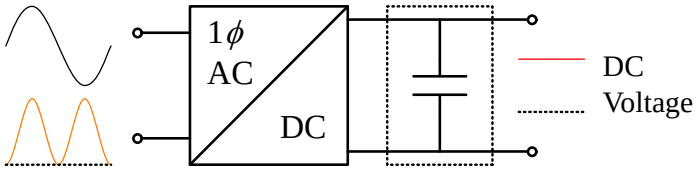
Keyword: Ripple current, Capacitance, Withstand voltage, Reliability

Power electronics has continued to develop along with the establishment of circuit and control technology and the improvement in performance of power semiconductor devices. On the other hand, the low loss and durability of passive components are not necessarily sufficient, and this is becoming a bottleneck in the miniaturization and reliability of power electronics circuits, so expectations for passive components are increasing year by year. Among passive components, magnetic elements such as inductors and transformers can be designed to have various characteristics depending on the application, and there is much room for power electronics circuit engineers to customize and bring out their characteristics. On the other hand, unlike magnetic elements, it is important for power electronics circuit engineers to make the best use of ready-made capacitors, and it is necessary to select the optimal capacitor by taking its functions and characteristics into consideration. In the following, the roles of capacitors in power electronics circuits are classified by application, and the electrical characteristics (applied voltage, current, frequency, etc.) required for each application are summarized. Finally, the requirements for capacitors for each application are summarized in terms of quantitative circuit constants along with the applicable capacitors.

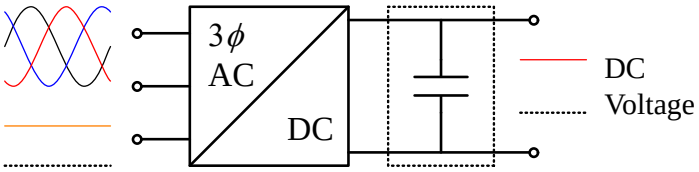
2.1.1 Capacitor for DC link

Figure 1.2.1.1 shows a block diagram of a dc link capacitor. Its role can be classified into three categories: (1) absorption of the instantaneous power difference between input and output, (2) maintenance of a constant DC voltage (smoothing), and (3) configuration of a canonical cell in a power electronics circuit [(1)]. Among these, the most influential factor in capacitor selection is the instantaneous power difference, which can be classified into switching frequency, input/output power pulsation, and transient changes caused by load variations and control delays. The single-phase converter shown in **Figure 1.2.1.1** (a) draws power pulsations of twice the power supply frequency in principle, while the instantaneous power flowing into the three-phase converter shown in (b) is constant. Therefore, the single-phase converter requires a larger capacitor than the three-phase converter.

Figure 1.2.1.2 shows the relationship between voltage and current in the dc link capacitor. The amplitude and frequency components of the ripple current i flowing into the capacitor determine the ripple voltage width Δv. The ripple voltage width is usually normalized by the DC voltage V and given by the ripple voltage factor r in the following equation.



(a) Single-phase converter



(b) Three-phase converter

Figure 1.2.1.1 Capacitors for DC link

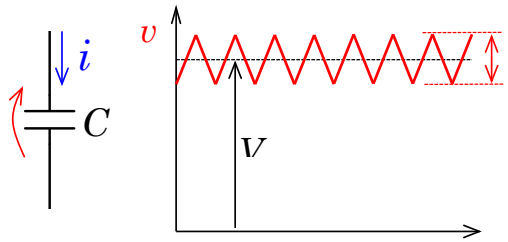


Figure 1.2.1.2 Ripple voltage ratio of capacitors

$$r = \frac{\frac{1}{2}\Delta v}{V} \qquad (1.2.1.1)$$

The ripple voltage ratio of the dc link capacitor is usually set at 5% or less from the standpoint of smoothing.

Another limiting factor in the selection of capacitors for DC link is the effective current rating of the ripple current flowing into the capacitor (hereinafter referred to as the ripple current rating). Even though the ripple voltage factor is low, the loss caused by ESR (Equivalent Series Resistance) is a problem, especially for high frequency currents. If the effective value of the ripple current is I_{rms}, the loss is given by the following equation.

$$P_{loss} = I_{rms}^2 ESR \text{ [W]} \qquad (1.2.1.2)$$

Usually, the maximum allowable RMS current is listed in the data sheet provided by the manufacturer.

2.1.2 Snubber capacitor

Figure 1.2.1.3 shows a PN lumped snubber. It is connected near the power module and plays the role of suppressing the surge voltage between PNs. It is connected in parallel with the DC link capacitor (for smoothing), but because of the parasitic inductance of the bus bar, high-frequency pulse currents associated with switching flow into the PN lumped snubber. Therefore, the PN lumped snubber requires not only low ESL (Equivalent Series Inductance) of the snubber itself, but also mounting technology to achieve low ESL. For example, it is anticipated that technologies such as mounting the PN lumped snubber near the internal semiconductor chip, rather than at the terminal end of the power module, will become necessary in the future. Although the loss is usually lower than that of a DC link capacitor, a lower ESR may be required to withstand high-frequency pulse currents. If the DC link capacitor C_{dc} for smoothing can be mounted with low ESR, it may be possible to configure only the DC link capacitor without the PN lumped capacitor. film or ceramic capacitors are used for the PN lumped snubber, but electrolytic capacitors may also be applied if they can be integrated with the DC link capacitor mentioned above The PN lumped snubber may be composed of only a DC link capacitor without a PN lumped snubber.

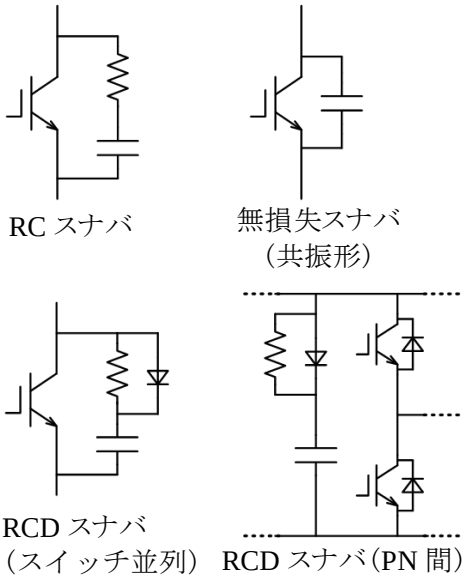


Figure 1.2.1.4 Charging and

Figure 1.2.1. 4 shows a charging and discharging type snubber. Switch turn-off voltage surges and diode reverse recovery voltage surges can damage switch elements and are a major source of noise. They are used to solve these problems. The operation of these snubbers is basically to provide a bypass to the switch during switch turn-off, absorb the energy stored in the parasitic inductance, clamp the switch voltage, and suppress surges [(1)]. Film and ceramic capacitors are often used as charge/discharge type snubber capacitors. Both are characterized by high reliability, non-polarity, and good frequency characteristics. Film capacitors are characterized by high current and high insulation resistance, while ceramic capacitors are characterized by low ESL and low ESR. On the other hand, the disadvantage of film capacitors compared to ceramic capacitors is their large shape, and the disadvantage of Class II ceramic capacitors used in snubber capacitors is that they are susceptible to mechanical stress and have poor DC bias characteristics (non-linearity). The designer should select the right capacitor for the right application based on the above characteristics [(1)].

On the other hand, zero-voltage switching technology is effective in suppressing turn-on surges [(2)]. **Figure 1.2.1.5** shows an example of a typical voltage waveform of a resonant type converter for a class E^2 converter. As shown in the dotted waveform in this figure, if the voltage jumps at the moment the switch is turned on, the energy stored in the parasitic capacitance of the switching device is released at once, resulting in switching losses. Therefore, if the switch is turned on when the switch voltage is zero, the switching losses can be ignored. Therefore, a capacitance is inserted in parallel with the switching device as shown in **Figure 1.2.1.3**. This C_S is then regarded as an adjustable parameter. This allows one more degree of freedom in circuit design to realize zero-voltage switching.

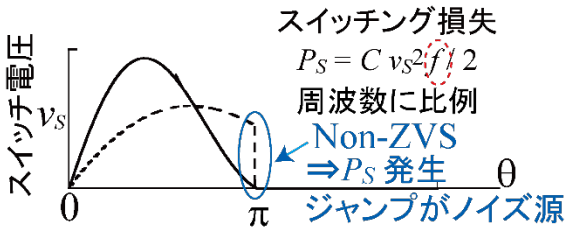


Fig. 1.2.1.5 Example of switch voltage in an E^2-class

The characteristics that this capacitance gives to the circuit are determined by the ratio of the resonant frequency of the L_C-C_S to the operating frequency, and in many cases the resonant frequency is extremely low compared to the operating frequency. In other words, the input inductor L_C is usually large enough for a Class-E converter. The C_S value to achieve zero-voltage switching is an adjustable parameter, and strictly speaking, its value is uniquely determined, but since the L_C *is* sufficiently large, a very precise element value is not required in implementation. Ceramic or film capacitors are usually used as shunt capacitors, and the appropriate one is chosen according to the maximum voltage and device size. Since the accuracy is not so high compared to the theory, there is no need to be nervous about the nonlinearity (DC bias characteristics) of the capacitor.

Similar to PN lumped snubbers, charging/discharge type snubbers also require low ESL, mounting techniques for low ESL, and high-frequency pulse current tolerance. Except for lossless snubbers, the stored energy of the snubber capacitor is consumed by the resistors connected in series, so the loss of the snubber capacitor itself is not a problem. However, the ESR and surge voltage suppression performance of snubber capacitors need to be analyzed. film or ceramic capacitors are used as in the case of PN lumped snubbers, but electrolytic capacitors

may be applied if pulse current tolerance and low ESL can be achieved.

2.1.3 AC filter capacitors

Figure 1.2.1.6 shows an example of an AC filter capacitor connected to an inverter. In the case of a grid-connected inverter, it has the role of removing the high-frequency ripple current generated by the inverter and allowing only the commercial frequency component current to flow out to the grid side. Unlike a DC link capacitor, an AC voltage of commercial frequency is applied to the capacitor, so a non-polarized capacitor with no voltage dependence of capacitance is used. Therefore, a film or ceramic capacitor (made of normal dielectric material) with no voltage dependence of dielectric constant is applied. Furthermore, since the LC constant must be designed and the capacitance Cac is uniquely determined from the cutoff frequency and the reactance value at the power supply frequency possessed by the inductor L, a capacitor with a large capacitance cannot be used to ensure ripple current withstand capacity, as is the case with DC link capacitors. Therefore, low ESR characteristics are required from low to high frequency.

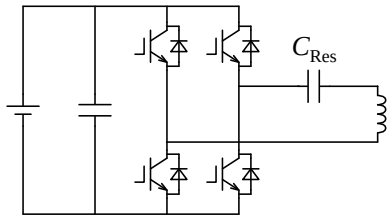


Figure 1.2.1.7 For resonance

2.1.4 Resonant capacitor

Figure 1.2.1.7 shows an application example of a capacitor for resonance. As AC voltage is applied in the same way as for AC filters, film or ceramic capacitors (made of normal dielectric material) are used because they are non-polarized and have no voltage dependence of capacitance. The difference from AC filters is that high-frequency voltage in the order of kHz to MHz is applied, and since LC resonance is used, a voltage higher than the output voltage of the inverter is applied. The capacitance is uniquely determined from the resonant frequency and characteristic impedance of the LC circuit, but because of the high resonant frequency, this capacitance is much smaller than that for AC filters. Therefore, ripple current capability is required despite the low capacitance. Since an inductor for resonance is always inserted in series, the ESL of the capacitor itself is not a problem, unlike in other applications.

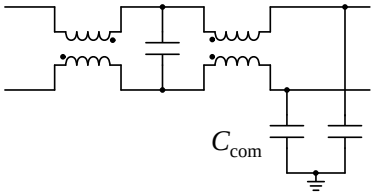


Figure 1.2.1.8 For noise filter

2.1.5 Noise filter capacitors

Figure 1.2.1.8 shows noise filter capacitors. The *two* main categories are the differential mode capacitor C_{dif} and the common mode noise capacitor C_{com}. The required capacitance, ripple current rating, and frequency response depend on the filter application and configuration. Depending on the target noise frequency, high-frequency characteristics in the order of kHz to MHz are required.

2.1.6 Summary of requirements for capacitors per application

The requirements for capacitors from the power electronics circuit side are classified as follows

- Ripple current rating (ESR)
  - Loss (W)
  - Current rating (A)
  - frequency response
  - tanδ
  - Thermal Design
  - Loss density per unit volume (W/m^3)
- Energy density (capacitance)
  - Dielectric constant ε (F/m)
  - Energy density per unit volume (J/m^3)
  - frequency response
  - Voltage Bias Dependence

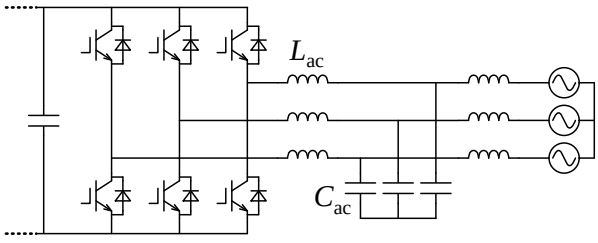


Fig. 1.2.1.6 For AC filter

- ESL
  - Surge voltage
  - High Frequency Characteristics
- pressure-resistant
- reliability
  - life span
  - Failure Mode

The five independent axes fall into five categories, but there are multiple parameters, for example, when discussing ripple current ratings, one can look at tanδ as a material-side parameter or at the frequency response of the ESR. Since they are mutually convertible in terms of electric circuits, the discussion is essentially the same for either parameter. However, when converting between tan δ and ESR, it is necessary to include the physical dimensions of the capacitor (volume, dielectric thickness, effective surface area, etc.). Similarly, to calculate the energy density from the dielectric constant ε, the dielectric thickness and effective surface area are necessary, and for ESL, the physical shape (length of the lead wire part) is necessary.

Table 1.2.1.1 summarizes the requirements from the power electronics circuit side and the applicable capacitors for each application. Most of the requirements from the circuit side are related to the ripple current rating, energy density, and breakdown voltage mentioned above. However, low ESL is also required for snubber applications.

Table 1.2.1.1 Requirements from the circuit side and applicable capacitors for each application

use	Request from circuit side	Applicable capacitor
Single-phase DC link	● high capacity ● Low ESR characteristics over 100 to several 100 kHz ● Withstand voltage 400 V～	● High voltage solid electrolytic ● Several hundred to several tens of thousands μΦ
Three-phase DC link	● High ripple current capability ● High withstand voltage (e.g., 800 V or more for 400 V inverter)	● High voltage solid electrolytic ● Series Connection Technology ● Several hundred to several tens of thousands μΦ
PN batch snubber	● low ESL ● High ripple current capability ● Shared use with smooth (including circuit mounting)	● Film Ceramics ● Possibility of electrolytic capacitor application ● Number μΦ~
Charging and discharging type snubber	● low ESL ● Low loss is not essential, but ESR and circuit performance must be considered	● Film Ceramics ● Lower ESL and higher ripple current withstand capability than tan δ ● Possibility of electrolytic capacitor application ● Number μΦ~
AC Filter	● Low ESR (ripple current capability) in the low to high frequency range ● non-polarized	● Film ceramic (constant dielectric constant) ● Number μΦ to number 100 μΦ
for resonance	● High withstand voltage and high current ● non-polarized	● Film ceramic (constant dielectric constant)
Noise filter	● High-frequency characteristics (kHz to MHz) ● Applications and Circuit Configuration	● Film ceramic (constant dielectric constant)

References

(1) H. Wang and F. Blaabjerg : "Reliability of Capacitors for DC-Link Applications in Power Electronic Converters-An Overview ", IEEE Trans. Ind. Appl., Vol. 50, No. 5, pp. 3569-3578 (2014).

2.2 Capacitors applied for smoothing

Keyword: Single-phase converter, Three-phase converter, Instantaneous power, Ripple current

As mentioned in the previous subsection, smoothing capacitors have two applications: single-phase DC link and three-phase DC link. Here, smoothing capacitors are used for maintaining a constant DC voltage in DC link applications, excluding applications that actively pulsate the DC link voltage, such as power coupling applications. For single-phase DC link applications, it is necessary to absorb a pulsation component twice the power supply frequency, which requires a large capacitance. In addition, single-phase DC link applications, except for multi-level configurations, are used for AC power supplies of 100 to 240 V, so withstand voltages of up to 450 V are sufficient. For these reasons, electrolytic capacitors are suitable for single-phase DC link applications because of their low cost and large capacitance.

On the other hand, in three-phase DC link applications, the instantaneous power is constant, so in principle, a small capacitor can be used, but the ripple current rating must be taken into account. Electrolytic capacitors are often used, but most of them are not used in cases where capacitance is required, but large capacitance electrolytic capacitors are used to provide ripple current withstand capability. It is expected that film or ceramic capacitors will replace these capacitors if they can be advantageous in terms of cost, including mounting. However, even in the case of three-phase inverters, there are cases in which large capacitors are required to maintain power pulsation caused by unbalance and control stability during regenerative operation, and this depends on the load of the inverter.

[Kazunori Hasegawa]

References

(1) Technical Investigation Special Committee on Passive Components in Power Electronics, ed.
(2) Kosuke Harada, Tamotsu Ninomiya, Wenjian Gu: "Fundamentals of Switching Converters," Corona Publishing Co.

2.3 AC capacitor

Keyword: Snubber capacitor, Resonant capacitor, Film capacitor, Ceramic capacitor

This section discusses AC capacitors in resonant converters. Specifically, the E^2 class converter is discussed.

2.3.1 Resonant capacitor for E^2 class converter

Figure 1.2.3. 1shows the circuit topology of a Class-E2 isolated resonant DC-DC converter consisting of a Class-E inverter and a Class-E rectifier. the Class-E inverter has a push-pull structure and two Class-E inverters are coupled in series. The class-E inverter operates maintaining a phase difference of π. The input voltage v_I *and the* input inductor L_C realize the DC current source. Therefore, the input inductor L_C must be sufficiently large. *The* shunt capacitance C_S includes the output capacitance of the switching device. In addition, L_0 and C_0 constitute a resonant filter. It is coupled to the rectifier *by the* coupling transformer *T*. The rectifier is a full-waveform Class E rectifier, and the full-wave rectified current by the diode passes through the low-pass filter C_f-L_f to obtain the DC output.

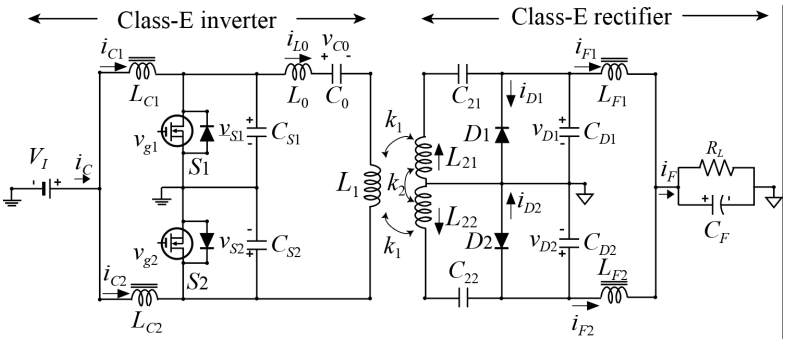


Figure 1.2.3.1 E^2 Class Converter

The resonant capacitances C_0 and C_2 in **Figure 1.2.3.1** take a series resonant structure with the inductors L_0 and L_2, respectively. In a resonant converter, the ratio of the resonant frequency of the resonant network to the operating frequency greatly affects the characteristics of the entire circuit. In particular, a network with a sufficiently high Q value ($Q = \omega L/R$) is acutely sensitive to changes in the resonant frequency, and a slight change in the L or C value of the resonant network causes a large change in soft switching and output power as shown in **Figure 1.2.3.2** (conversely, the output is often controlled by the operating frequency).

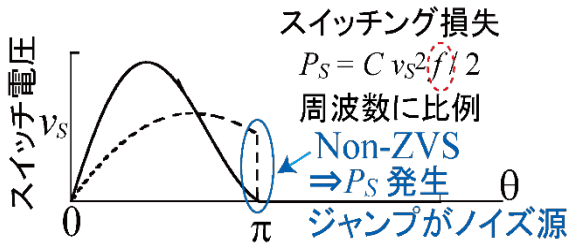


Fig. 1.2.3.2 Example of switch voltage in an E^2-class

Therefore, resonant capacitors, like resonant inductors/transformers, must have low ESR and high element value accuracy. Furthermore,

bipolarity is essential. Film capacitors, ceramic capacitors, and mica capacitors are examples of capacitors suitable for these characteristics.

Film capacitors are characterized by small initial capacitance variation and have the advantage of sensitivity to capacitance values. They also have a larger capacitance lineup than ceramic or mica capacitors, and are often used in resonances between 10 and 100 kHz [(1)]. On the other hand, the size of the capacitor is a disadvantage compared to ceramic capacitors, and it is not often used at higher frequencies.

In high-frequency operation in the MHz band, the capacitance value of resonant capacitors is small and limited. Ceramic and mica capacitors are generally available in the lineup for small capacitance, and ceramic capacitors are the most promising candidates when considering cost [(2)]. For high-frequency resonance applications, Class I ceramic capacitors with excellent high-frequency characteristics and stability and a high Q value are often used. Mica capacitors have long been used in audio amplifiers, etc., and have features such as narrow capacitance tolerance and good high-frequency characteristics, but they are more expensive and larger in size than ceramic capacitors.

By the way, the output capacitance C_D in **Figure 1.2.3.1** constitutes a low-pass filter and is unipolar. Like the output inductor, it is required to be "large enough. For this reason, the requirement for capacitance accuracy is the lowest. On the other hand, it is required to have a higher capacitance than other capacitors. Therefore, electrolytic capacitors and film capacitors are candidates. When electrolytic capacitors are used, it is known that the real capacitance value for high frequency is much smaller than the nominal capacitance value for electrolytic capacitors.

[Hiroo Sekiya]

2.3.2 Resonant capacitor for WPT

(1) WPT R&D Trends

In recent years, wireless power transfer (WPT) with magnetic field coupling has been attracting attention as a new charging technology. WPT is now commonly used as a charging technology for small-capacity devices such as smartphones, electric toothbrushes, and electric shavers, and R&D is also actively underway for its application and practical use in high-capacity applications such as electric vehicles (EVs). In particular, research on next-generation technologies such as rapid charging and dynamic wireless power transfer (DWPT) has been active. These technologies require high-capacity power transmission of 20 kW or more, which is about 10 times larger than that of conventional stationary power transfer WPT.

Currently, power transmission in the 85 kHz band (79 to 90 kHz) is becoming the mainstream for WPT for EVs, and it is essential for the resonant capacitors that make up the power feed system to be capable of handling high frequencies, high voltages, and large currents. In addition, resonant capacitors are expected to be installed underground or buried together with power transmission coils, and therefore must be more reliable under severe conditions than capacitors used in ordinary power conversion circuits.

Based on this background, this section summarizes the requirements and technological trends for resonant capacitors for 85 kHz band WPTs.

(2) Overview of Resonant Capacitors for WPT

In a WPT, capacitors and inductors are connected so that the transmitting and receiving coils satisfy resonance conditions, as shown in **Figure 1.2.3.3**, so that power can be transmitted efficiently over a distance. This resonant circuit is driven by a high-frequency inverter and operates similarly to a resonant converter.

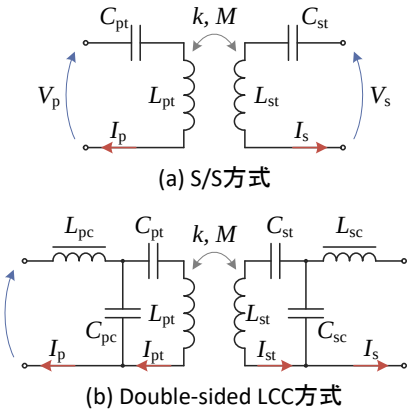


Figure 1.2.3.3 Resonant circuits commonly

The system shown in **Figure 1.2.3.3** (a) is a resonant circuit system called the S/S (Series-Series) system, which is the most widely used system in recent years. Focusing on the primary side (power transmission side), the resonant capacitor C_{pt} (F) is designed to resonate with the transmission coil L_{pt} (H) on the primary side only, as shown in the following equation. where ω_0 (rad/s) is the resonant angular frequency.

$$C_{pt} = \frac{1}{\omega_0^2 L_{pt}} \tag{1.2.3.1}$$

The magnitude of the input current in the S/S system is expressed using the secondary side voltage *Vs* (V) and the mutual inductance *M* ($= k\sqrt{L_{pt}L_{st}}$) (H) as follows

$$I_p = \frac{V_s}{\omega_0 M} \tag{1.2.3.2}$$

Therefore, when the distance between the primary and secondary transmission coils is long and the coupling coefficient *k* approaches 0, the impedance becomes almost zero and a large current flows.

In addition, since it is a series resonance of LC, the filter characteristics are weak, and current distortion due to harmonics is likely to occur. As a result, harmonic components also appear in the magnetic field leaking from the primary and secondary coils, making the installation of equipment difficult from the standpoint of the Radio Law. In other words, the S/S method is not suitable for high power applications or for DWPTs where the magnetic coupling between coils fluctuates violently.

Against this background, the double-sided LCC method [3][4] shown in **Figure 1.2.3.3** (b) has recently begun to attract attention, because it has a configuration similar to that of an LC low-pass filter connected to an LC series resonant circuit. The harmonic component of the current flowing through the primary and secondary transmission coils is extremely low compared to the S/S method. In addition, the change in impedance with *respect to the* coupling coefficient *k*has the opposite characteristics of the S/S method, so that even when $k = 0$, the input current (fundamental wave) is zero and does not diverge, making it suitable for applications such as the DWPT. In this case, the parameters of each part (primary side) are determined as in the following equation, and the secondary side can be determined in the same way.

$$C_{\mathrm{pc}} = \frac{1}{\omega_0^2 L_{\mathrm{pc}}} \tag{1.2.3.3}$$

$$C_{\mathrm{pt}} = \frac{1}{\omega_0^2 \left(L_{\mathrm{pt}} - L_{\mathrm{pc}}\right)} \tag{1.2.3.4}$$

In this case, the magnitude of the current at each part of the primary side in the double-sided LCC system is expressed as follows

$$I_{\mathrm{p}} = \frac{M V_{\mathrm{s}}}{\omega_0 L_{\mathrm{pc}} L_{\mathrm{sc}}} \tag{1.2.3.5}$$

$$I_{\mathrm{pt}} = \frac{V_{\mathrm{p}}}{\omega_0 L_{\mathrm{pc}}} \tag{1.2.3.6}$$

Thus, the WPT system actively uses resonant capacitors. Furthermore, the input impedance of the resonant circuit changes as the coupling coefficient changes, resulting in a system with both low-voltage/high-current and high-voltage/low-current conditions. In other words, the resonant capacitor must be designed for the worst-case scenario, so it must have a higher withstand voltage and current resistance with respect to the power capacity compared to a normal power converter.

Resonance misalignment is also an issue in WPT systems that use resonance. It is known that resonance misalignment causes a decrease in transmission power and efficiency. This resonance misalignment is caused not only by variations in element values during manufacturing, but also by changes in the inductance of the transmission coil and capacitance of the resonant capacitor during energization. For this reason, various measures have been taken for resonant capacitors. For example, the use of a capacitor with good DC bias characteristics, changing the frequency of the applied voltage, and using a switched capacitor, i.e., a resonant capacitor whose capacitance can be actively changed, are all known methods.

(3) Mounting environment for resonant capacitors for WPT

WPT resonant capacitors are expected to be installed or buried underground along with the power transmission coils, and must be more reliable under severe conditions than the capacitors used in ordinary power conversion circuits. In particular, for in-transit power supply, the coils and capacitors must be buried securely so that they do not protrude from the road. Therefore, the capacitor itself and the soldered parts must not crack even when the vehicle travels over the buried area and pressure is applied.

Because of these requirements, it is often considered to embed coils and resonant capacitors in a case made of a strong resin material such as ABS. As an example, in the demonstration experiments in Kashiwa City, Chiba Prefecture, and at the Osaka Kansai Expo, the coils and resonant capacitors were placed in a resin case [5] as shown in **Figure 1.2.3.4**, and the surrounding area was made into a precast road structure using fiber reinforced cement composite material to ensure the strength of the case before mounting. In the example, the resonant capacitor is placed next to the coil, but it may be placed on the back side of the ferrite, etc. The resin case also prevents the ingress of moisture.

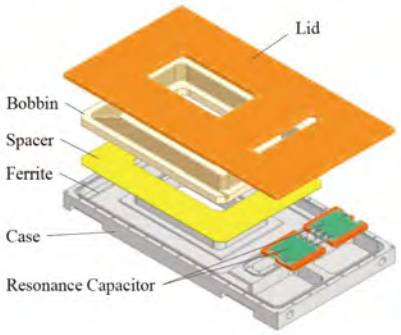


Fig. 1.2.3.4 Coil and resonant capacitor case for DWPT [3]

In addition, during the summer months when temperatures are high and solar radiation is intense, the surface temperature of asphalt and concrete can exceed 60 ℃ during the day. Therefore, the resonant capacitors buried under them must be able to withstand the ambient temperature plus self-heating temperature and humidity, and must have highly reliable and robust characteristics.

Furthermore, since a large number of coils need to be buried in the ground, it is necessary to consider not only simple element performance but also cost and ease and speed of manufacture.

(4) Resonant capacitors for WPT currently in use

Film capacitors and multilayer ceramic capacitors (MLCCs) are often employed in resonant capacitors for WPT. When WPT first began to attract attention, only film capacitors were available as resonant capacitors for large-capacity applications, from the viewpoint of DC bias characteristics and low loss performance [6][7]. Today, however, the DC bias characteristics, equivalent series resistance, withstand voltage and withstand current of MLCCs have improved due to the demand for isolated resonant converters used in WPTs, automotive on-board chargers, server power supplies, etc., and they are often used in terms of miniaturization (**Figure 1.2.3.5**).

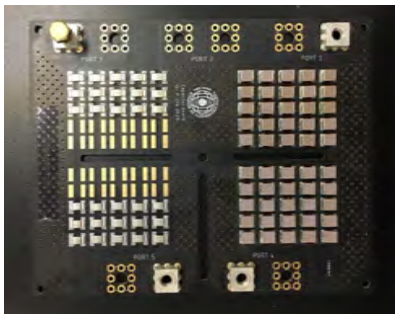


Figure 1.2.3.5. Example of capacitor board

Reference [7] describes that the use of MLCCs can significantly reduce the mounting area and volume when trying to manufacture a resonant capacitor that satisfies the specifications of 20 nF capacitance and 2 kVrms AC. In particular, the use of MLCCs with C0G characteristics (capacitance hardly changes with changes in temperature, voltage, or time), which were introduced in 2024 and have a withstand voltage of 1000 V, will make it possible to reduce size and weight even more than before. In some cases, MLCCs with metal feet (leads) may be used to minimize solder cracks in environments where there is a lot of shock and vibration, or where the capacitor board is curved.

In the above MLCC example, the number of series-parallel capacitors has been reduced, but for higher power applications, the number of series-parallel capacitors must be further increased, and current bias becomes an issue. Therefore, film capacitors, which have a high degree of structural freedom and can easily achieve high withstand voltage and current characteristics, are superior to the above-mentioned MLCCs. Currently, there is almost no lineup of film capacitors designed for WPT, but a series for WPT that specializes in withstand current characteristics is available from China's AnXon Electronic Co., Ltd.

Other special examples of resonant capacitors for WPTs include the use of a floating capacitance intentionally created in the coil as a resonant capacitor and the use of a switched capacitor in combination with a semiconductor switch as a resonant capacitor. In particular, the method using stray capacitance was used in the MIT presentation in 2006, and is superior in terms of breakdown voltage and cost. However, it is much more difficult to design than using an ordinary capacitor, and its capacitance varies greatly depending on the ambient environment, in addition to its large size, which poses many problems for WPT systems that are designed to be buried, etc. On the other hand, a switched capacitor can be interpreted as a solid-state capacitor, which can compensate for the effects of resonance misalignment in real time. However, it is not a replacement for MLCCs because it is not intended to improve the withstand voltage or current capability of the capacitor itself. In addition, since semiconductor power devices are used, the cost of driving circuits, etc., is also high.

(5) Requirements for resonant capacitors for WPT

The resonant capacitor for WPT is required to have the following

Withstand voltage, withstand current, and heat dissipation performance

Reliability, durability, moisture resistance

Flat DC bias characteristics and low element value variation

Cost, ease of manufacturing

Details are given below.

<u>Withstand voltage, withstand current, and heat dissipation performance</u>

As mentioned above, very large withstand voltages and currents are required because resonant currents and voltages are applied. In particular, in the normal charging of electric vehicles, where 3.7 to 7.7 kW of power is transmitted at 85 kHz, voltages of 500 to several kV and currents of several to around 30 A are applied.

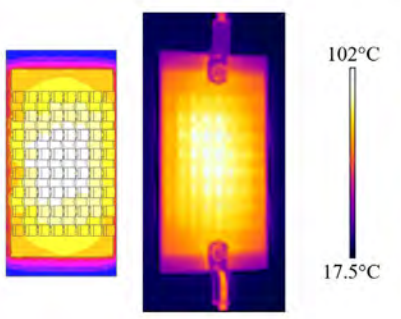


Figure 1.2.3.6 Temperature Distribution of Resonant

In particular, with regard to withstand current performance, not only the ESR of the capacitor itself, but also the ESR caused by the PCB and solder have a significant impact. When multiple capacitors are arranged in a row, as **shown in Figure 1.2.3.6**, variations in current and heat are likely to occur [9], so the PCB layout and pattern shape are also an issue.

In particular, the heat dissipation performance (withstand current performance) does not fully bring out the withstand voltage performance of MLCCs. Currently, MLCCs [10] with a withstand voltage of 630 V and 100 nF are often used, but according to the data sheet, if a rise of up to about 20 ℃ is allowed, each MLCC should be used at 6 A or less. However, when used at 85 kHz, the instantaneous voltage applied to the capacitor is 112 V, which is only 1/6 of the withstand voltage of 630 V. Assuming steady and normal operation, there is a considerable margin for withstand voltage. In other words, when WPT applications are assumed, the withstand voltage performance can be fully utilized by improving heat dissipation.

Reliability, durability, moisture resistance

As mentioned above, the idea is to bury coils and capacitors in roads. Therefore, it is required that the capacitor itself and the soldered parts do not crack even when pressure is applied or humidity changes. There are some cases where MLCCs with metal feet (leads) have been used, but this still poses a problem in terms of miniaturization, and there is room for further study on various points, such as PCB materials and the use of no solder.

Flat DC bias characteristics and low element value variation

As mentioned above, it is strongly required that the capacitance does not change with the applied voltage. in past cases where MLCCs were used, an extreme drop in transmission power occurred when the input voltage was increased. This was caused by the use of general MLCCs, which have the characteristic of capacitance decreasing with voltage. This phenomenon was corrected by using MLCCs [(6)], which exhibit good characteristics with respect to voltage, and the system operated as expected. However, MLCCs with such characteristics are currently very expensive and there are only a few available. Depending on the power capacity of the system, the component cost of a capacitor is equal to that of a coil. Against this background, there is a method of actively increasing the stray capacitance of the coil and using it as a resonant capacitor, but many issues remain regarding design, parameter changes after mounting, and miniaturization.

The variation in element values is also a cause of resonance misalignment and should be minimized as much as possible. In particular, this is one of the major issues when considering the worst case when the number of series-parallel elements is large.

Cost, ease of manufacturing

Assuming that WPT systems will be installed in electric vehicles and mounted on roads, resonant capacitors must not only be cost-effective but also have a structure that can handle mass production. In other words, when multiple capacitors are used in series and parallel on a PCB, the surface mount type is suitable for mass production, not the through-hole type. In addition, rather than using capacitors with multiple capacitances, it is possible to use capacitors with the same capacitance.

[Ryosuke Ota]

References

(1) Technical Investigation Special Committee on Passive Components in Power Electronics, ed.

(2) H. Sekiya: "General Remarks: High Frequency Switching and Passive components in Power Converters," Journal of Electrical Engineering, Vol. 141, No. 10, pp. 618-620 (2021)

(3) S. Li, W. Li, J. Deng, T. D. Nguyen and C. C. Mi: "A Double-Sided LCC Compensation Network and Its Tuning Method for Wireless Power Transfer ", in *IEEE Transactions on Vehicular Technology*, Vol. 64, No. 6, pp. 2261-2273, June (2015).

(4) W. Li, H. Zhao, S. Li, J. Deng, T. Kan and C. C. Mi: "Integrated LCC Compensation Topology for Wireless Chargers in Electric and Plug-in Electric Vehicles," in *IEEE Transactions on Industrial Electronics*, Vol. 62, No. 7, pp. 4215-4225, July (2015).

(5) Osamu Shimizu, Shota Yamada, Hiroshi Fujimoto, Koichi Tanaka, Masanori Sato, Hayato Kakutani, Eisuke Takahashi, Yoshihisa Yamaguchi, Keisuke Tani: "Loading Test and Mechanical and Electrical Evaluation of Precast Coil Structure for Power Feed during Running," Journal of Society of Automotive Engineers of Japan, Vol.54, No.4, pp.732-737, July (2023).

(6) Murata Manufacturing: "Medium-voltage, low-loss multilayer ceramic capacitors suitable for automotive OBCs, wireless power supply, and server power supplies: Applications in LC and LLC resonant circuits," Product Introduction, March (2025), https://article.murata.com/ja-jp/article/ applications-in-lc-and-llc-resonant-circuits?intcid1=msl_xxx_xxx_xxx_hm_xxx_art-api (last accessed July 10, 2025)..

(7) TDK Corporation: "Applications for Wireless Power Transfer Systems for EVs," TDK Tech Library - Solution Guide, https://product.tdk.com/ja/techlibrary/solutionguide/mlcc05.html ((last accessed July 10, 2025).

(8) AnXon Electronic: "1000V 0.1uF Power Film Capacitors for Wireless Power Transfer Applications," https://www.anxonelec. com/sale-33904882-1000v-0-1uf-power-film-capacitors-for-wireless-power-transfer-applications.html (last accessed July 10, 2025).

(9) A. K. Bailey, J. Wong, S. Kim, W. Wijaya and G. A. Covic: "Thermal Modelling of Resonant Capacitor Boards for Inductive Power Transfer Systems", *2024 IEEE Wireless Power Technology Conference and Expo (WPTCE)*, pp. 173-176, Kyoto, Japan, (2024)

(10) TDK corp. : "C5750C0G2J104J280KC Characterization Sheet (Multilayer Ceramic Chip Capacitors)"..

2.4 Bottleneck in circuit application

Keyword: Smoothing capacitor, Active power decoupling

2.4.1 Capacitor Selection Optimization and Tradeoffs

The primary parameters in capacitor selection are capacitance, rated voltage, and allowable current. Capacitors are selected to minimize the volume, weight, and cost of the capacitor while meeting the requirements of the circuit design. In many cases, the commercial capacitor lineup does not allow all of these parameters to be matched to the requirements of the circuit design, and only one or two parameters are optimized to the requirements of the circuit design, while the others are over-performing.

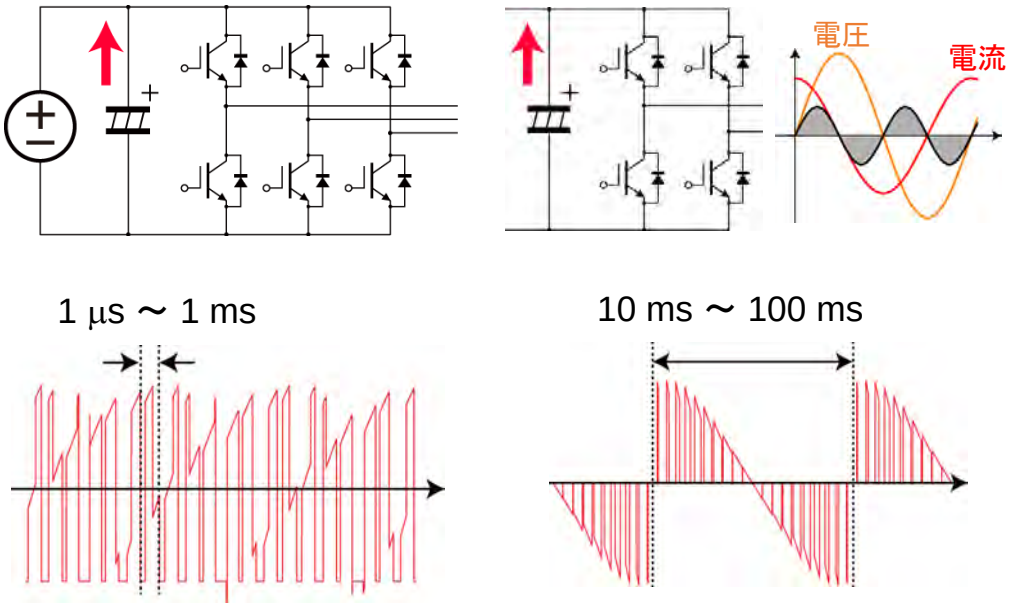
2.4.2 Relationship between capacitance and allowable current

One example is the smoothing capacitor. In the case of smoothing capacitors, the rated voltage should be selected with a certain margin for the DC voltage to be used. On the other hand, the capacitance and allowable current should also be greater than the requirements of the circuit design, but when selecting from the same series of capacitors, the allowable current is automatically determined once the capacitance is determined. In general, when electrolytic capacitors are used, the allowable current is often the bottleneck, so the number of parallelisms is increased to reduce the current per capacitor, and the capacitance is determined as a result. In most cases, this will be sufficient to meet the requirements of the circuit design, such as capacitance that keeps voltage ripple below a certain level. On the other hand, when film capacitors are used, the allowable current is often sufficiently higher than the operating current to achieve the capacitance required by the circuit design. In this case, the allowable current is excessive.

Since the frequency component of the ripple current varies with the application circuit, the requirements for the allowable current and required capacitance of the capacitor also vary with the application circuit. In a three-phase inverter, when the load is balanced, the pulsating power (twice the AC fundamental frequency, 100 or 120 Hz) caused by the output AC power is canceled on the DC side, so the current in the smoothing capacitor is mainly due to switching ripple as shown in **Figure 1.2.4.1** (a). The amplitude of the ripple current is large, but its frequency component is above the switching frequency, mainly from several kHz to several tens of kHz. Therefore, the capacitance required to suppress voltage fluctuations is small. On the other hand, in single-phase inverters, a low-frequency component corresponding to the pulsating power caused by AC power is superimposed on the ripple current, resulting in the waveform shown in **Figure 1.2.4.1** (b). A large capacitance is necessary to suppress the voltage pulsation to the low-frequency component below a certain level.

2.4.3 Relationship between capacitance, allowable current and volume

Reference (1) reports on the selection of a smoothing capacitor to be installed between a single-phase AC-DC converter and an isolated DC-DC converter as shown in **Figure 1.2.4.2**. This study investigates the capacitance and volume of the smoothing capacitor when the control that does not allow the smoothing capacitor to provide low-frequency compensation for single-phase pulsation is applied by simultaneously converting the same amount of instantaneous power that pulsates at twice the system frequency converted by the single-phase AC-DC converter (so-called single-phase pulsation) using an isolated DC-DC converter. The capacitance and volume are investigated. In this way, the required capacitance can be reduced to some extent.



(a) Smoothing capacitor current of three-phase inverter (b) Smoothing capacitor current of single-phase inverter

Figure 1.2.4.1 Frequency components of ripple currents depending on the applied circuit

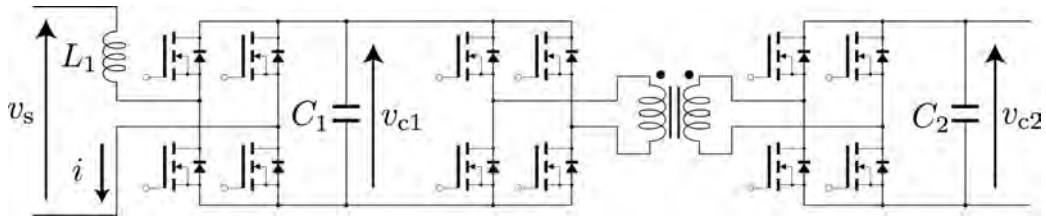


Figure 1.2.4.2 Circuit consisting of a single-phase AC-DC converter and an isolated DC-DC converter

Figure 1.2.4. 3 summarizes the results of a survey on the relationship between capacitance and volume for commercially available film capacitors and electrolytic capacitors when the same withstand voltage is achieved. The results are consistent with the general knowledge that electrolytic capacitors are used because film capacitors have a larger volume than electrolytic capacitors to achieve the same capacitance. Furthermore, reference (1) also investigates the relationship between the current flowing through the capacitor and the allowable current of the capacitor in this application. In the assumed control, the ripple current generated by switching flows through the smoothing capacitor, which is constant regardless of the capacitance. The range of electrolytic capacitor selections that can tolerate this current is shown in **Figure 1.2.4.3**. Under the conditions given here, it can be read that electrolytic capacitors cannot be used in the range of capacitance below 100 µF (range plotted in red) because the allowable current is lower than the working current, but in the range of capacitance above 100 µF (range plotted in orange) electrolytic capacitors have an advantage in terms of volume. The above-mentioned proposed control is not adopted because the capacitance is lower than 100 µF. On the other hand, if the capacitance can be reduced to 15 µF or less by the above proposed control, it is advantageous to use film capacitors. In other words, the proposed control will not lead to miniaturization with film capacitors unless the capacitance can be reduced to 15 µF or less. However, the current ripple caused by switching is high frequency, and it may not be appropriate to supply all of it with electrolytic capacitors, which do not have good frequency characteristics of capacitance, so electrolytic capacitors cannot be selected simply by the relationship between ripple current and allowable current.

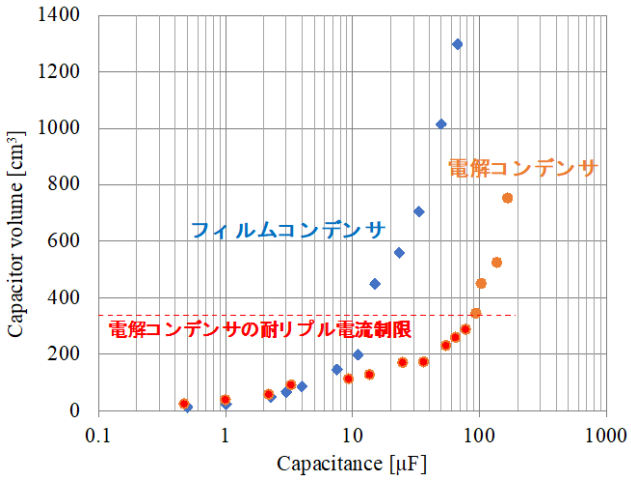


Figure 1.2.4.3 Example of relationship between capacitance and

The above example is a study of a case where special control is applied to the smoothing capacitor between a single-phase AC-DC converter and an isolated DC-DC converter, but in a three-phase inverter, there may be no need to consider the effect of single-phase pulsating power, in which case the above discussion can be expanded directly to a discussion of whether a film or electrolytic capacitor should be used in a general inverter. In such a case, the above discussion can be directly applied to the discussion of whether film capacitors or electrolytic capacitors should be used in general inverters. The capacitance required by circuit design is most simply the minimum capacitance that can keep the voltage pulsation generated by the square wave current generated by switching below a certain value, and the capacitance can be reduced by increasing the switching frequency. However, in practical use, the capacitance must be larger than the capacitance determined by the switching frequency alone, as it depends on the handling of unbalanced power, the response to system and load abnormalities, and the control follow-up to such abnormalities. From a long-term perspective, in addition to improvements in switching frequency, improvements in circuit technology (e.g., active power decoupling [(2)]) and control performance are expected to reduce the required capacitance. Therefore,

from the viewpoint of improving system performance (in this case, capacitor volume), it is necessary to improve the allowable current per capacitance for electrolytic capacitors, and to reduce the volume per capacitance for film capacitors.

2.4.4 The evolution of applied circuits demands smaller capacitors and constraints on capacitor selection

As another example, capacitors used in active power decoupling are introduced. In active power decoupling, single-phase pulsating power is converted by a semiconductor power conversion circuit and compensated by energy accumulation with a capacitor of small capacitance. The capacitor that actually accumulates the single-phase pulsating power is assumed to be a film capacitor with a small capacitance but a relatively large current flow relative to its capacitance, so a film capacitor with a large allowable current is assumed to be used. The voltage of the capacitor fluctuates greatly at a frequency twice the system frequency. Reference (3) reports an evaluation of capacitor volume in a transducer that uses capacitors under conditions similar to this. Generally, film capacitors intended for use with direct current have a specified amplitude of AC voltage ripple voltage to be superimposed on them in addition to the DC rated voltage, so it is necessary to adopt a larger DC rated voltage to allow large voltage fluctuations, resulting in a larger volume. As a result, the reduction in volume by reducing the capacitance is constrained by the allowable AC voltage ripple voltage of the capacitor. Alternatively, capacitors must be employed that have been preliminarily designed for use with AC.

As the above two examples show, it is difficult to exhaust the capacitor performance in terms of system performance improvement, and there is almost always a mismatch between the circuit design requirements and the parameters that the capacitor has. Since the correlation between each performance parameter of a capacitor is an inherent characteristic of each type of capacitor technology, it is not possible to expect to achieve a capacitor that perfectly matches the requirements given by the circuit design, but good modeling of this characteristic to maximize the improvement in system performance is done from the circuit However, the circuit designers are trying to improve the system performance to the maximum extent possible by modeling these characteristics well.

[Takanori Isobe]

References

(1) H. Obara and Y. Okamura: "Design Consideration of MMC-based AC-DC Converter with 3.3 kV SiC-MOSFETs for SSTs", *2024 13th International Conference on Renewable Energy Research and Applications (ICRERA)*, Nagasaki, Japan, (2024).

(2) T. Shimizu, Y. Jin and G. Kimura: "DC ripple current reduction on a single-phase PWM voltage-source rectifier," *IEEE Trans. Ind. Appl.*, Vol. 36, No. 4, pp. 1419-1429 (2000).

(3) T. Isobe, R. A. Barrera-Cardenas and H. Tadano: "Capacitor size reduction of MMC-based STATCOM for medium voltage power distribution network", *2016 18th European Conference on Power Electronics and Applications (EPE'16 ECCE Europe)*, Karlsruhe, Germany (2016).

2.5 Lifetime, reliability, safety

Keyword: Electrolytic capacitor, Film capacitor, Ceramic capacitor, Reliability, Life span

2.5.1 Capacitor Issues

In power electronics, capacitors are critical components that directly affect the stability of the entire system, as they perform DC smoothing and filtering functions. On the other hand, as shown in **Figures 1.2.5.2**, capacitors still account for a high percentage of failures in power electronic equipment [(1)(2)]. This section describes the latest trends in capacitor life characteristics, technologies to improve reliability, new

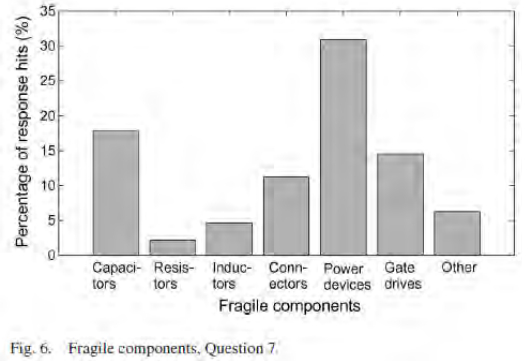
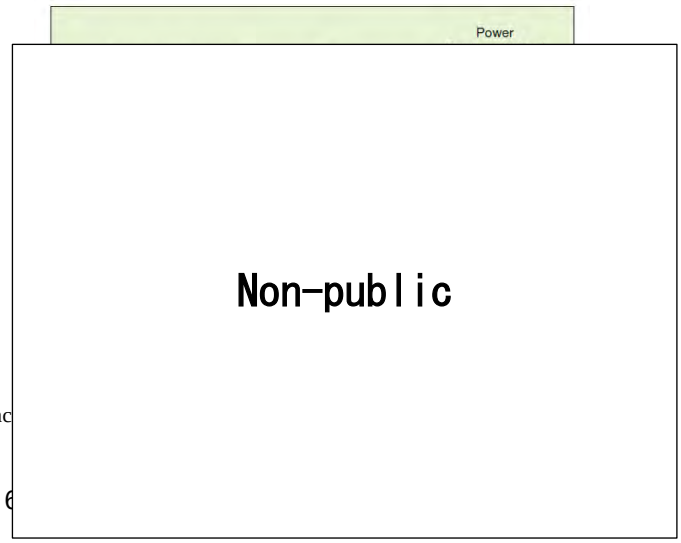


Fig. 6. Fragile components, Question 7.

Figure 1.2.5.1 Failure factors for the circuit shown in referenc



safety-related approaches, and technical issues.

(1) Recent Trends in Electrolytic Capacitor Lifetime Characteristics

Aluminum electrolytic capacitors are widely used because of their high capacitance density. However, the evaporation of the electrolyte and insulation degradation over time cause a decrease in capacitance and an increase in equivalent series resistance (ESR), which eventually leads to short circuit failure. In the past, the rated life at 105 ℃ was generally around 2,000 hours, but in recent years, product improvements have extended the life of these capacitors. For example, 105 ℃ products are now guaranteed for 5,000 to 10,000 hours, and for automotive applications, high-temperature products are being developed that are guaranteed for 5,000 hours at 125 ℃ or even 2,000 hours at 135 ℃. In fact, Panasonic has commercialized the industry's first hybrid electrolytic capacitor guaranteed to operate at 135 ℃, achieving a lifetime of 2,000 hours at 135 ℃(4,000 hours at 135 ℃ for large capacitors) for small capacitors [(3)]. Nichicon has also introduced a series of 150 ℃ capacitors (guaranteed for 1,000 hours) to meet the needs for use under high temperatures [(4)]. (4) These high-temperature, high-reliability products are reported to have improved electrode foils and electrolyte solutions to stabilize characteristics under high temperature environments. In addition, conductive polymer electrolytic capacitors and hybrid electrolytic capacitors (liquid electrolyte + polymer) have become popular over the past 20 years. Solid polymer electrolytic capacitors are characterized by a self-healing mechanism that recovers the oxide film without liquid evaporation, and their operating temperature-dependent lifetime behavior is different from that of conventional capacitors. In general, the lifetime of liquid electrolytic capacitors is said to increase by a factor of 2 for every 10 ℃ decrease in temperature (based on the Arrhenius rule), whereas polymer electrolytic capacitors are reported to increase by a factor of 10 for every 20 ℃ decrease in temperature. The difference is more pronounced at low temperatures, with the polymer electrolytic reaching approximately 200,000 hours (approximately 22 years) at 65 ℃, far exceeding the 32,000 hours of the conventional electrolytic. However, the rated life of the polymer electrolytic is about the same as that of the conventional product at high temperatures (e.g., 2,000 hours at 105 ℃), and its strength lies in its longer life in the mid-temperature range and below. Therefore, for applications requiring a life of 5,000 hours or more in the high temperature range, a comparison with long-life liquid electrolytic capacitors (e.g., those guaranteed for 5,000 to 10,000 hours at 105 ℃) is necessary, and the advantages and disadvantages of the two are different depending on temperature conditions [(5)]. In recent years, hybrid electrolytic capacitors have been used to achieve both low ESR characteristics and long life of polymers even at high temperatures. In general, aluminum electrolytic capacitors have been greatly improving their lifetime characteristics over the past 20 years through improvements in materials, encapsulation, and manufacturing technology, and their application in fields where high temperature and long life are required, such as inverters for automobiles and renewable energy, is expanding.

The reliability of electrolytic capacitors is also described in Chapter 2, Section 2.4, so please refer to that section.

(2) Lifetime characteristics of film capacitors

Film capacitors using a resin film such as polypropylene as dielectric are known for their long life and high reliability due to their self-healing function compared to other types of capacitors. In general, the service life of film capacitors is an order of magnitude longer than that of aluminum electrolytic capacitors of the same capacitance, and some reports indicate that the service life is approximately 10 times longer [(6)]. The self-healing action is a mechanism that prevents failure by instantaneously evaporating and dispersing the metallized electrode at minute breakdown points and insulating the surrounding area, allowing the capacitor to continue operating at the cost of a gradual decrease in capacitance. This mechanism prevents the sudden death failure of the film capacitor in the short mode, and the capacitor takes a safe degradation mode in which the capacitance gradually decreases. Even at the end of life, capacitance degradation is often limited to a few percent, and a 5 to 10% drop in capacitance is generally used as a criterion for determining the life of a film capacitor. Recent technological trends include higher temperature capability and energy density improvement. Conventional polypropylene (PP) film has been the mainstream for DC link applications due to its low self-dielectric loss and high dielectric strength, but its heat resistance has been limited to 85-105 ℃. However, a review of the dielectric material has led to the development of a new type of film capacitor that can withstand higher temperatures. However, its heat resistance is limited to 85 to 105℃. Therefore, research and development of film capacitors that can be used in the 125 to 150 ℃ range has become active by reviewing the dielectric material. For example, polyethylene naphthalate (PEN) film has been reported as a dielectric for high heat-resistant capacitors with excellent temperature characteristics, while PEN and polyimide film are more stable under high temperatures than PP, but there are issues in terms of loss and capacitance per volume. Improvements are underway, including trade-offs with cost.

The reliability of film capacitors is also described in Chapter 2, Section 2.3, so please refer to that section.

(3) Reliability and lifetime characteristics of ceramic capacitors

Multilayer ceramic capacitors (MLCCs) are increasingly used in power electronics circuits due to their high-frequency characteristics and high capacitance. Ceramic capacitors are basically solid in structure and have almost no capacitance degradation due to aging, except for dielectric depolarization (aging) of the material. In reality, however, mechanical stress and rapid temperature changes can cause cracks in the ceramic element, resulting in failure modes such as short circuits and increased leakage current. In particular, the larger the size of the device,

the more likely it is to crack due to distortion or thermal shock during mounting on the board, and in the past there have been reports of MLCC breakdowns in automotive ECUs, etc., causing reliability problems. As a countermeasure, soft termination technology has been put to practical use in the past 20 years. This technology dramatically reduces the occurrence of cracks by sandwiching a conductive resin layer between terminal electrodes to relieve stress caused by board deflection and impact. It is reported that no cracking occurred even when the soft termination was bent more than twice as much as the normal product. Thus, the reliability of ceramic capacitors has been improved through the improvement of packaging technology. As for the lifetime characteristics themselves, ceramic dielectrics (e.g., BaTiO3-based) are known to show aging characteristics such as capacitance decrease (aging) and insulation resistance decrease due to temperature and voltage application, and a destruction mechanism called avalanche breakdown or thermal runaway has been observed under high temperature and high electric field conditions. Therefore, the rated capacitance of the capacitors is not sufficient for high-reliability applications. Therefore, in highly reliable applications, it is important to secure a large margin of rated voltage (e.g., less than 50% applied) and to control self-heating. In recent years, improvement of dielectric materials has led to the development of dielectrics such as X8R and X9U, which have less degradation even at high temperatures, and MLCCs that can operate stably even at 150 ℃ class are beginning to be put into practical use. However, the risk of dielectric breakdown increases as the thickness of dielectric layers increases for higher capacitance, so the future challenge for ceramic capacitors is to ensure lifetime reliability through material research and optimization of the manufacturing process.

The reliability of ceramic capacitors is also described in Chapter 2, Section 2.2, so please refer to that section.

(4) Effect of parasitic inductance of capacitors

The equivalent series inductance (ESL) of a capacitor is not a property of the material, but is caused by the physical structure of the internal lead frame and electrodes **as shown in Figure 1.2.5.3**, which occurs in capacitor mounting. Essentially, the larger the area of the loop created by the current flow path inside the component, the larger the ESL. In power electronic circuits, the parasitic inductance of the capacitor itself, ranging from several nH to several tens of nH, is a serious parameter for the reliability of the component itself. In power electronic circuits, the steep current change (di/dt) and ESL associated with switching cause excessive voltage overshoots in the capacitors. At the same time, ESL constitutes a series resonant circuit for capacitors in the high frequency range, causing an inflow of ripple current that exceeds expectations and increases self-heating. These electrical and thermal stresses accelerate the degradation mechanisms specific to each capacitor type.

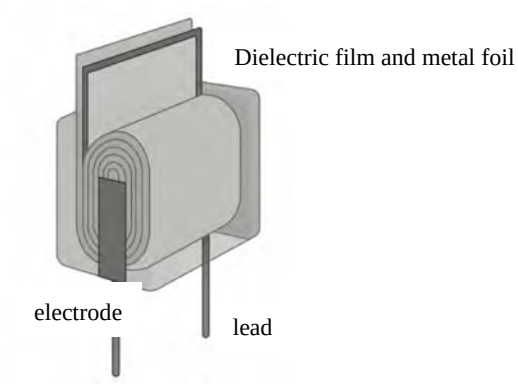


Figure 1.2.5.3 Internal Structure of a Film

In metallized film capacitors, the voltage overshoot caused by ESL increases the electric field stress on the dielectric and increases the frequency of micro dielectric breakdown and subsequent self-healing (self-healing) events [7]. The repetition of these self-healing events leads to a cumulative degradation of characteristics with a gradual loss of capacitance.

In the case of multilayer ceramic capacitors (MLCCs), although ESL is low, the large current flowing due to resonance with the circuit causes self-heating. This heat and the difference in thermal expansion coefficient between the materials cause mechanical stress, which induces cracks, a fatal failure mode.

2.5.2 State-of-the-Art Technologies for Improving Reliability

(1) Advanced self-healing technology

As mentioned above, the self-healing function is the key to reliability of film capacitors. In the past, the electrode shape was generally a fully evaporated electrode, but in recent years, segmented electrodes, in which the electrode is finely segmented and a fuse function is provided between each segment, have become the standard. **Figure 1.2.5.4** is shown in Reference (8). These are capacity degradation curves for various self-healing techniques. It has been reported that the conventional type (without self-healing) has unstable degradation behavior and a risk of sudden death, whereas the segmented electrode method, which is optimized based on experience, has a slow and predictable capacity decrease

over time and no short circuit breakdowns. Currently, the phi lm capacitor uses this method, which has contributed to a dramatic improvement in long-term reliability.

(2) Improved packaging technology and structural design

Structural improvements in various capacitors also contribute to improved reliability. In aluminum electrolytic capacitors, improvement of the rubber seal material and optimization of the can shape have improved the operational stability of the gas venting safety valve and the

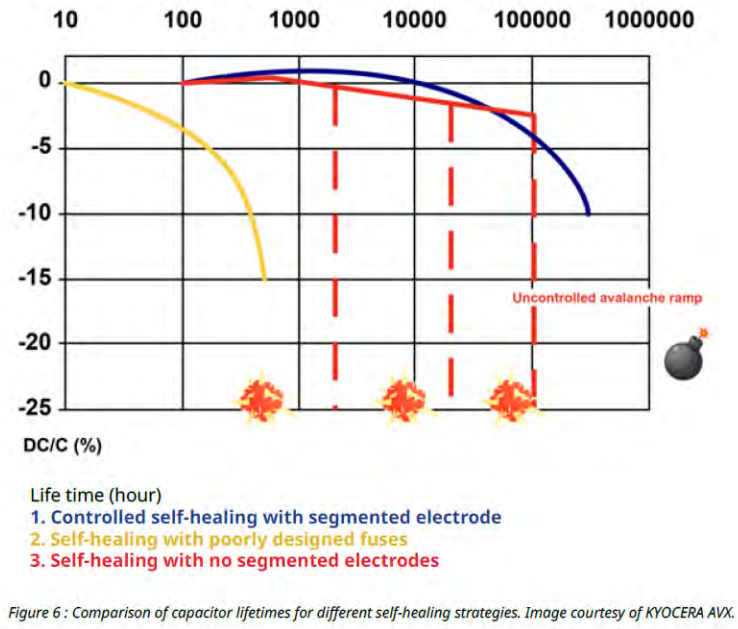


Figure 6 : Comparison of capacitor lifetimes for different self-healing strategies. Image courtesy of KYOCERA AVX.

Figure 1.2.5.4 Comparison of capacitor life with self-healing technology [10]

*Courtesy of Kyocera AVX Components, Inc.

retention of the electrolyte. In recent years, the composition of the electrolyte has been reviewed and the structure has been improved to prevent evaporative leakage from the seal material, resulting in a life extension of more than twice that of conventional capacitors, even at high temperatures. The film capacitors are shifting from oil-impregnated type to dry type, but the control of internal filling gas and epoxy mold sealing make it difficult for moisture to penetrate into the capacitor even in a high humidity environment, thereby preventing corrosion deterioration (end-face corrosion) of the deposited electrode, which is a problem in the field. Ceramic capacitors are also being designed to reduce the number of mounted parts and increase the reliability of the joints by introducing soft termination [9], an intermediate layer that reduces the thermal expansion difference between the element and substrate, and mounting technology that integrates multilayer chips by laminating and bonding them together. The method of connecting multiple capacitors in series-parallel is also important for reliability design. For example, in DC link circuits, film capacitors are arranged in parallel to distribute the ripple current of each element, and electrolytic capacitors are connected in series for high voltages to reduce the voltage stress per element. In the hybrid capacitor bank, aluminum electrolytic and film capacitors are combined in parallel to compensate for each other's disadvantages and extend the life of the capacitors. Specifically, there have been reports of cases in which the addition of film capacitors with high ripple current tolerance to a group of high capacitance, high density electrolytic capacitors has reduced heat generation on the electrolytic capacitor side and extended its life by more than 10 years.

2.5.3 New Safety Initiatives

(1) Abnormality and deterioration detection technology (condition monitoring)

Condition monitoring techniques to detect capacitor degradation in advance have been actively studied in the maintenance of power electronics equipment. ESR (equivalent series resistance) and capacitance have been used as indicators of electrolytic capacitors. This is because as degradation progresses, capacitance decreases due to electrolyte depletion and electrode corrosion, and ESR tends to increase at the same time. Typically, a 20% drop in capacitance or a 2-fold increase in ESR is defined as the life of the capacitor, and is often used as a guide for replacement [2]. For this reason, a method of periodically measuring the impedance of capacitors inside equipment and predicting their life based on changes in capacitance and ESR has been widely considered. Recently, algorithms for estimating ESR from ripple current

and voltage waveforms during inverter operation and methods for analyzing harmonic components of impedance have been proposed to perform this measurement online. For example, a method to monitor the impedance change of a DC link capacitor using the switching waveform of a power electronics circuit without additional test signals has been reported. Advanced monitoring using machine learning and model-based estimation has also been attempted. Various approaches are under investigation, including research using neural networks to capture minute changes in circuit response during capacitor degradation, and a method to diagnose degradation by detecting changes in capacitor current with a magnetic sensor [(10)]. Capacitor degradation detection is also attracting attention in industry as a "self-diagnostic function of inverters," and examples of its implementation are increasing. For example, in inverters for EVs, condition monitoring of DC link capacitors is considered important from the viewpoint of safe operation, and preventive maintenance is recommended to replace the capacitors before failure. Against this background, condition monitoring, which enables early detection of abnormal conditions and planned component replacement, has become a new trend in safety and reliability design.

(2) Fail-safe and safety design

Improving the safety of the capacitor itself is another important initiative. Aluminum electrolytic capacitors have long employed safety valves to prevent rupture when internal pressure rises. In recent years, the reliability of their operation has been further improved, and they are designed to be disconnected from the circuit while gradually releasing pressure even if gas is generated at the end of their life. This ensures fail-safe characteristics that prevent the capacitor from rupturing or catching fire in the worst case scenario. In addition, film capacitors are highly safe because they are self-healing and basically do not lead to short circuits, but in high power applications, there is a possibility of large dielectric breakdowns that cannot be self-healed. For this reason, designs are being pursued to prevent short-circuit failure modes, such as internal fuses that disconnect the device from the circuit in the event of an overcurrent, or a configuration that prevents a short circuit even in the event of a single point of failure by connecting multiple devices in series. For ceramic capacitors, safety measures are also being discussed for Class I (for temperature compensation) and Class II high dielectric constant types used in high-voltage circuits, such as using a material system that is resistant to short circuits in the event of dielectric breakdown and inserting a series resistor to minimize damage in the event of a short circuit. In addition, advanced failure mode analysis is also contributing to improved safety. Manufacturers and research institutes have made progress in dissecting and analyzing capacitors that have degraded or failed in accelerated life tests, examining the mode and mechanism in detail, and providing feedback. For example, high-temperature and high-voltage tests of X7R ceramics have identified two failure modes, avalanche failure and thermal runaway, each of which is caused by different defects (intrinsic defects in the former and dielectric loss overheating in the latter) [(6)]. This has led to a reduction of defects and a review of ratings at the design stage, and has been reflected in the setting of safety margins for actual products. Similarly, research is underway to model the behavior of film capacitors at the end of their service life by analyzing the inside of the capacitor after long-term use and collecting data on the progress of edge corrosion and the distribution of self-repair traces on the deposited electrodes. Such deeper understanding and modeling of physical failure mechanisms are indispensable for reliability design with a safety margin, which in turn leads to maximizing product life while ensuring a safety margin.

2.5.4. Future technical issues

(1) High temperature environment

With the advent of SiC/GaN devices, the operating ambient temperature of power electronic circuits can rise even higher than before. Most capacitors have a practical operating temperature range of 125 ℃, and there is a need to develop capacitors that can operate at 150 to 200 ℃ for a long period of time. Further heat resistance of polymer-based film dielectrics and improvement of high-temperature operating characteristics of ceramic materials are the subjects of research [(11)(12)]. Since liquid electrolytic capacitors are difficult to use at high temperatures, the role of film and ceramic capacitors is expected to increase. The key issue is how to compensate for the increased volume of film capacitors and decreased capacitance of ceramic capacitors, and the creation of new materials with high dielectric constant and high withstand voltage is the key.

(2) Support for high ripple and high frequency operation [(3)]

With the increase in switching frequency, more high-frequency ripple current flows through capacitors than ever before. Since high-frequency losses in the dielectric cause heat generation and degradation, the development of low-loss materials and heat dissipation design become increasingly important. PP film, currently the mainstream material, has the advantage of low high-frequency loss, but it is vulnerable to high temperatures. On the other hand, some materials with high heat resistance have a slightly large dielectric loss tangent and are prone to generate heat at high frequencies. In order to solve these problems, research is being conducted to increase temperature resistance while suppressing loss by using nanocomposite dielectrics, and approaches to incorporate a cooling mechanism in the capacitor itself are also being considered. Reducing the inductance of the capacitor is also an issue as the frequency increases, and it is necessary to maintain stable capacitor operation even in high dv/dt environments by devising the stacking structure and terminal arrangement.

(3) Improvement of energy density and reliability [(2)]

In devices for electric vehicles, there is a strong need to reduce the capacitor volume, i.e., to downsize the system. On the other hand, the thinner the dielectric layer and the higher the dielectric constant to increase the energy density per capacitance, the higher the risk of dielectric strength degradation and thermal runaway. To address this tradeoff, it is important to improve materials and use advanced life prediction models to evaluate the risk from the design stage and set the optimum margin. For example, a lifetime model for voltage stress can be modeled), and design optimization is expected to ensure reliability while minimizing losses due to overdesign. Another method that is expected to be developed in the future is to link physics-based lifetime models with system simulations to predict the lifetime by comprehensively evaluating the effects of capacitor stresses (voltage, current, temperature, and humidity) under actual operating conditions.

(4) Long life and maintenance-free

Capacitor life expectancy of 30 years or more may be required for renewable energy equipment and aerospace applications. Currently, film capacitors have a life of several dozen to several tens of years, but further data accumulation and understanding of degradation mechanisms are needed to guarantee long-term reliability. In particular, it is necessary to quantify the effects of the field environment on long-term degradation and design capacitors accordingly. The development of next-generation capacitors with self-diagnostic functions is also expected. This is a concept in which each capacitor autonomously monitors its own health by incorporating a capacitor with a built-in sensor or a structure that emits an alarm when its impedance changes significantly during degradation. This could lead to a truly maintenance-free capacitor with dramatically improved reliability.

2.5.5 Summary

This section reviews the progress of capacitor technology for power electronics from the viewpoints of life time, reliability, and safety. Aluminum electrolytic capacitors have been extended in life time at high temperatures through the adoption of new materials and design improvements, and film capacitors have achieved a dramatic extension of stable operation period and improved safety failure characteristics through the advancement of self-healing technology. Ceramic capacitors have also improved their reliability through improved mounting technology, and their use in high-temperature, compact applications is expanding. Furthermore, the reliability of systems has been enhanced through the development of deterioration monitoring technology and fail-safe designs for various types of capacitors. On the other hand, it is necessary to address issues such as high temperature operation and high energy density in order to meet the requirements of the next generation. In the future, it is expected that new materials development and physics-based reliability design will play a dual role in realizing even higher performance and reliability capacitors.

[Keiji Wada]

References

(1) S. Yang, A. Bryant, P. Mawby, D. Xiang, L. Ran and P. Tavner : "An Industry-Based Survey of Reliability in Power Electronic Converters ", *IEEE Trans. on Industry Applications*, Vol. 47, No. 3, pp. 1441-1451(2011).

(2) H. Wang and F. Blaabjerg : "Reliability of Capacitors for DC-Link Applications in Power Electronic Converters-An Overview ", *IEEE Trans. on Industry Applications*, Vol. 50, No. 5, pp. 3569-3578 (2014).

(3) Panasonic Corporation : "ZL Series 135 ℃ Compatible Hybrid Electrolytic Capacitors" Press Release (2024).

(4) *Nippon Chemi-Con Corporation*, [Online]. Available: https://www.chemi-con.co.jp/en/products/aluminum/chart/#:~:text=Group%20Chart%20,GQB%3A%20150%E2%84%831%2C000H%20%C2%B7% 20GVA [Accessed: Jul. 18, 2025].

(5) F. Puhane: "Expected Lifetime of Aluminum Electrolytic and Aluminum Polymer Capacitors", *Würth Elektronik Technical Note SN008* (2018).

(6) H. L. Dang and S. Kwak: "Review of Health Monitoring Techniques for Capacitors Used in Power Electronics Converters",. *Sensors*, Vol. 20, No. 13, 3740 (2020)

(7) C. Zhang, Yu Feng, Fei Kong, Zhaoliang Xing, Cheng Zhang, Tao Shao: "Accelerated Damage in Metallized Film Capacitors Under Pulse Surge Combined With Rated DC Voltage", *IEEE Transactions on Plasma Science*, Vol. 51, No. 6, pp. 1494-1501 (2023).

(8) KYOCERA AVX: "Controlled Self-Healing of Power Film Capacitors", Technical Document (2020).

(9) M. Cannon: "Use Soft Termination to Improve Reliability in Vehicle Applications", *Power Systems Design* (2023).

(10) H. Wang: "Capacitor Failure Modes and Lifetime Models from and Application Perspective", in *Proc. IEEE Appl. Power Electron. . Conf. Expo.(APEC)* (2018)

(11) B. Fan, F. Liu, G. Yang, H. Li, G. Zhang, S. Jiang and Q. Wang: "Dielectric materials for high-temperature capacitors", *IET Nanodielectric*, Vol. 1, No. 1, pp. 32-40 (2018).

(12) L. Liu, L. Li, S. Zhang, W. Xu and Q. Wang: "Polyimide-Based Dielectric Materials for High-Temperature Capacitive Energy Storage ", *Electric Material*, 5, pp. 303-320 (2024).

Section 3 Benchmark

Based on the theoretical considerations of inductor design principles and loss characteristics described in the previous sections, this chapter verifies the effectiveness and practicality of the design method through application examples (benchmarks) to actual power electronics

circuits. The results of optimization design based on design requirements such as inductance, current ripple, size constraints, and loss limits for each application are presented.

3.1 Inductor

Keyword: DC inductors, AC inductors

This section presents a benchmark design of an inductor to be used in a particular power electronics circuit and the optimization process in terms of material selection, gap adjustment, and winding configuration. The designed inductors are evaluated under realistic operating conditions, considering the trade-off between loss, size, and performance. In particular, the loss evaluation is performed by applying the "loss map method" from among the iron loss calculation methods that take into account the excitation of power electronics circuits, instead of the Steinmetz method based on the conventional assumption of uniform magnetic flux density. This approach provides a guideline for inductor design that is optimized for application conditions and does not rely on mere catalog specifications. Although there are various references [(1)-(10)] on inductor optimization, this chapter briefly introduces benchmark results of DC inductors for DC chopper excitation and AC inductors for inverter excitation from references [(9)(10)].

3.1.1 Benchmark with DC chopper excitation

An example of the results of selecting the iron core volume to minimize the total loss (sum of iron loss and copper loss) of a DC inductor is shown [(9)]. The loss reduction of the DC filter inductor is studied when the iron loss measurement circuit shown in **Figure 1.3.1.1** is driven under the operating conditions listed in **Table 1.3.1.1**. **Figure 1.3.1.2** shows the appearance of the inductors to be studied, and **Table 1.3.1.2** shows the design parameters of each inductor.

Figure 1.3.1.3 shows the measurement results and the calculated iron loss, copper loss, and total inductor loss when the core cross section is varied from 45 mm^2 to 400 mm^2. The loss map method was applied to the measurements [(9)].

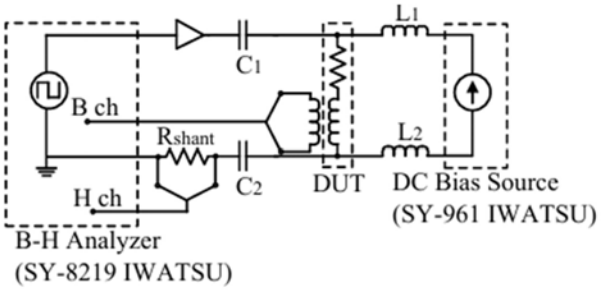


Figure 1.3.1.1 Iron loss measurement circuit under DC superposition

Table 1.3.1.1 Circuit conditions of the measurement circuit

Input voltage V_{in}	150 V
Output voltage V_{out}	75 V
Duty ratio d	0.5
Switching frequency f_{sw}	40 kHz
Inductance L	316 μH
DC component on inductor current $I_{L,dc}$	6 A



(a) Iron dust (SK-Toho Zinc) (b) Sendust (HK-Toho Zinc) (c) Mn-Zn ferrite (PC40-TDK)

Figure 1.3.1.2 Appearance of the inductor under consideration [(9)]

Table 1.3.1.2 Specifications of inductors to be considered [(9)]

(a) Iron dust (SK-Toho Zinc)

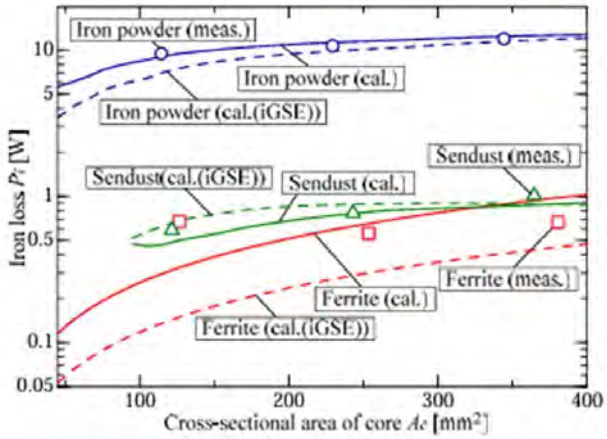
Indcutor name	Iron powder 1	Iron powder 2	Iron powder 3
Number of parallel cores	1	2	3
Magnetic path length of core l_c	108.4 mm	108.4 mm	108.4 mm
Cross-sectional area of core A_c	115 mm^2	230 mm^2	345 mm^2
Winding number N	67	41	31
Inductance L	316 μH	307 μH	302 μH

(b) Sendust (HK-Toho Zinc)

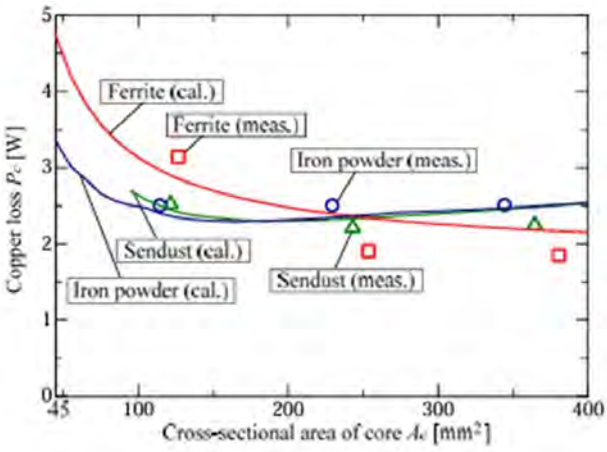
Indcutor name	Sendust 1	Sendust 2	Sendust 3
Number of parallel cores	1	2	3
Magnetic path length of core l_c	108.4 mm	108.4 mm	108.4 mm
Cross-sectional area of core A_c	115 mm^2	230 mm^2	345 mm^2
Winding number N	65	38	30
Inductance L	293 μH	301 μH	316 μH

(c) Mn-Zn ferrite (PC40-TDK)

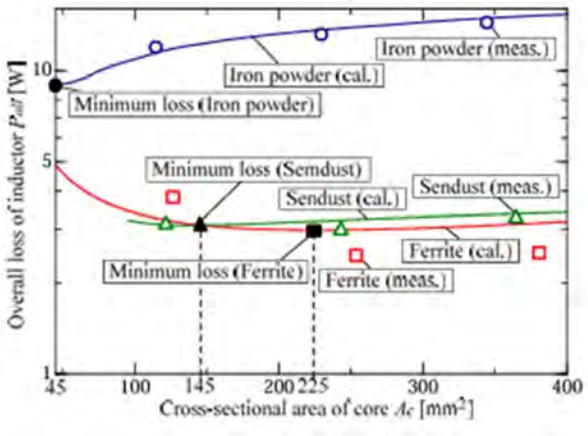
Indcutor name	Ferrite 1	Ferrite 2	Ferrite 3
Number of parallel cores	1	2	3
Magnetic path length of core l_c	124 mm	124 mm	124 mm
Air gap length l_g	2.80 mm	1.36 mm	0.84 mm
Cross-sectional area of core A_c	127 mm^2	127 mm^2	127 mm^2
Winding number N	75	37	15
Inductance L	493 μH	394 μH	366 μH



(a) Iron loss



(b) Copper loss



(c) Total inductor loss

Figure 1.3.1.3 Calculated [and] measured results of iron loss, copper loss, and total inductor loss [(9)]

Figure 1.3.1.3 (a) shows that there is a good agreement between the calculated and measured iron loss results for iron dust and sendust. On the other hand, a difference was observed for Mn-Zn ferrite, which has a small iron loss. This may be due to errors in the iron loss measurements. In the ferrite inductors used in the experiment, the phase difference between the magnetic field waveform and the magnetic flux density waveform is approximately 88.7°, and the iron loss measurement error increases as the phase difference approaches 90°Considering this error, it can be judged that the measurement results shown in **Figure 1.3.1.3** (a) fully reflect the calculation results. Based on the measurement results, the DC magnetic field tends to increase for small inductors with a large number of turns. Therefore, when using iron dust or ferrite, whose iron loss is affected by the DC magnetic field bias, it is important to consider the DC magnetic field bias characteristics when calculating the iron loss.

Figure 1.3.1.3 (b) shows that the calculated and measured copper loss results are in good agreement for each magnetic material . When the cross-sectional area of the iron core was the same, there was almost no difference in the Cu loss due to the type of magnetic material. This may be due to the fact that the magnetoresistance of the ferrite core with a gap was almost the same as that of iron dust and sendust, and consequently the number of windings was also almost the same. Therefore, it is expected that even when a magnetic material with high permeability is gapped, the copper loss is not necessarily reduced compared to a magnetic material with low permeability that is not gapped.

Furthermore, **Figure 1.3.1.3** (c) shows that the calculated and measured total inductor losses are in good agreement for each magnetic material. **Table 1.3.1.3** shows the conditions for minimum inductor total loss under the circuit conditions. **Table 1.3.1.3** shows that the minimum total inductor losses of sendust and ferrite are almost the same. However, taking into account the factors that sendust has a slightly smaller iron core volume, that ferrite cores with gaps are prone to fringing losses, and that the addition of gaps increases costs, sendust is considered to have a higher advantage.

Table 1.3.1.3 Conditions for minimum inductor loss

Core marerial of inductor	Iron powder	Sendust	Ferrite
Overall loss of inductor P_{all}	8.96 w	3.10 w	2.99 w
Core volume V_c	4860 mm^3	15660 mm^3	27900 mm^3

3.1.2 Benchmark with inverter excitation

The following is an example of an AC filter inductor design that achieves the optimum balance between the inductor total loss (iron loss and copper loss) and the iron core volume. When the single-phase PWM inverter shown in **Figure 1.3.1.4** is operated under the circuit conditions shown in **Table 1.3.1.4**, the AC filter inductor loss and volume can be reduced by changing the magnetic material (material composition and specific permeability) and iron core volume.

Figure 1.3.1.5 shows an example of the results of designing the single-phase PWM inverter shown in **Figure 1.3.1.4** with different magnetic materials and iron core volumes [(10)]. The iron core with the best balance between inductor loss and iron core volume is the best case, and the iron cores with the largest inductor loss and iron core volume in the iron cores under consideration are the worst case (1) and worst case (2), respectively. Comparing the best case and the two worst cases, the inductor loss of the best case is 55.7 % (2.37 W) smaller than that of case

(1), and the iron core volume is 69.3 % (35.9 cm^3) smaller than that of case (2). This shows that the inductor loss and iron core volume can be significantly reduced by proper selection of magnetic materials.

In addition, as shown in **Figure 1.3.1.6**, the loss ratio in the best case is almost equal, whereas different results are obtained for designs with large iron core volume but low loss, such as case (2) [(10)].

Furthermore, the B-H curve shows that the maximum flux density in the best case is 0.37 T, which is 73.0% smaller than the saturation flux density (1.00 T) under the excitation conditions. Therefore, it is considered necessary to operate the inductor at a flux density with a sufficient margin from the saturation flux density in the optimization design of the AC filter inductor.

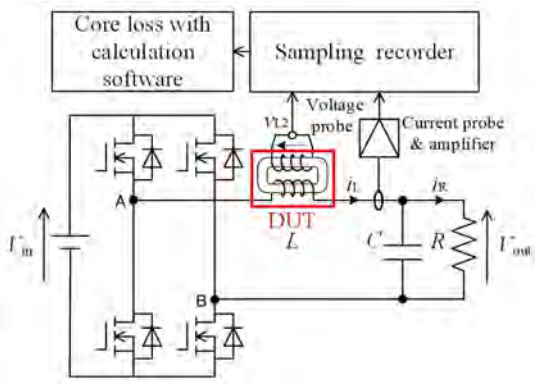


Figure 1.3.1.4 Single-phase PWM inverter circuit

Table 1.3.1.4 Single-Phase PWM Inverter Specifications

Input voltage V_{in}	DC 200 V
Output power P_{out}	350 W
Output frequency f_{out}	50 Hz
switching frequency f_{sw}	20 kHz
modulation rate m	0.707
AC Filter Inductance L	1 mH
AC Filter Capacitance C	10 μF
Output Resistance R	28.5 Ω

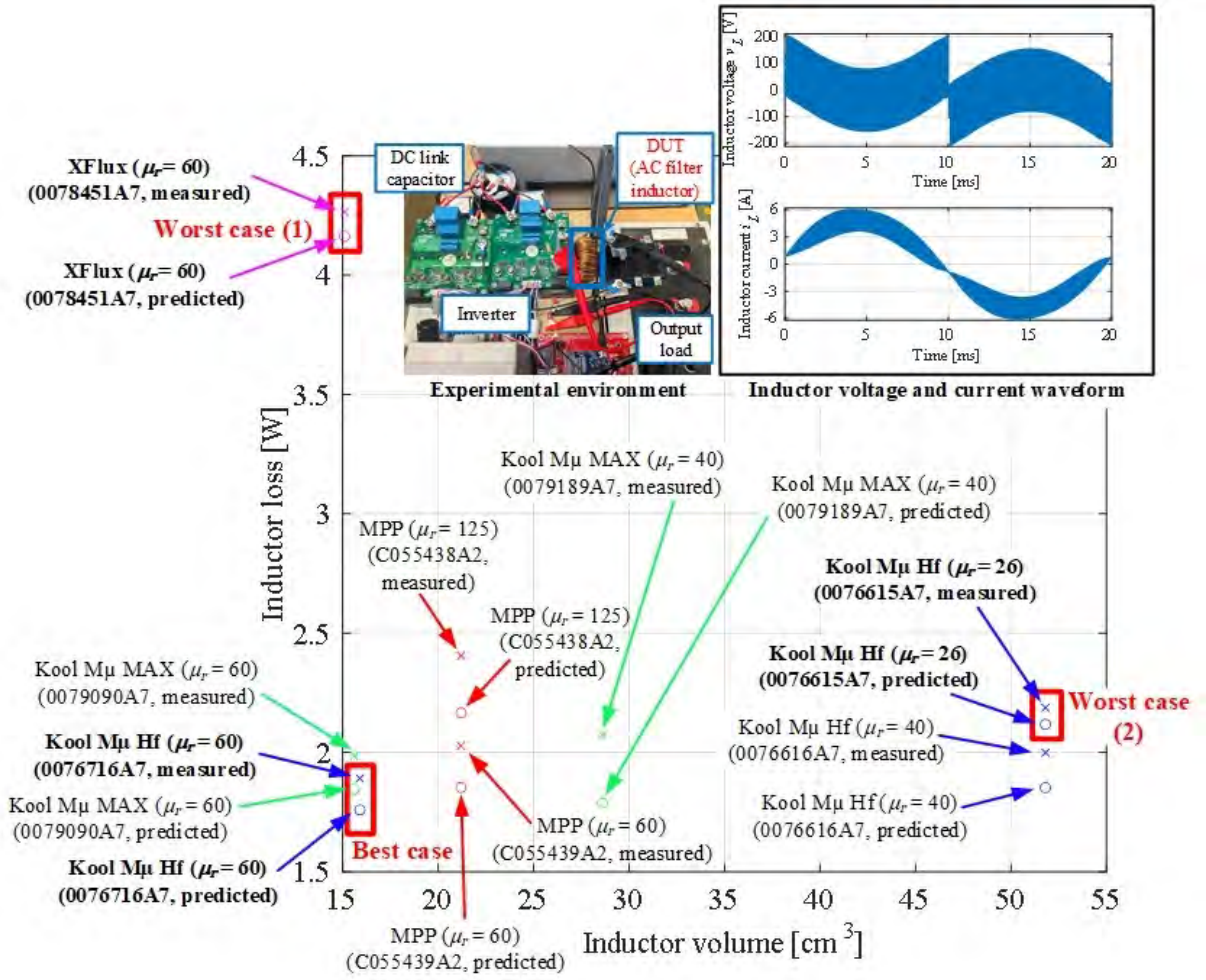


Figure 1.3.1.5 Example of inductor total loss-iron core volume characteristics for various magnetic materials in single-phase PWM inverter excitation [10]

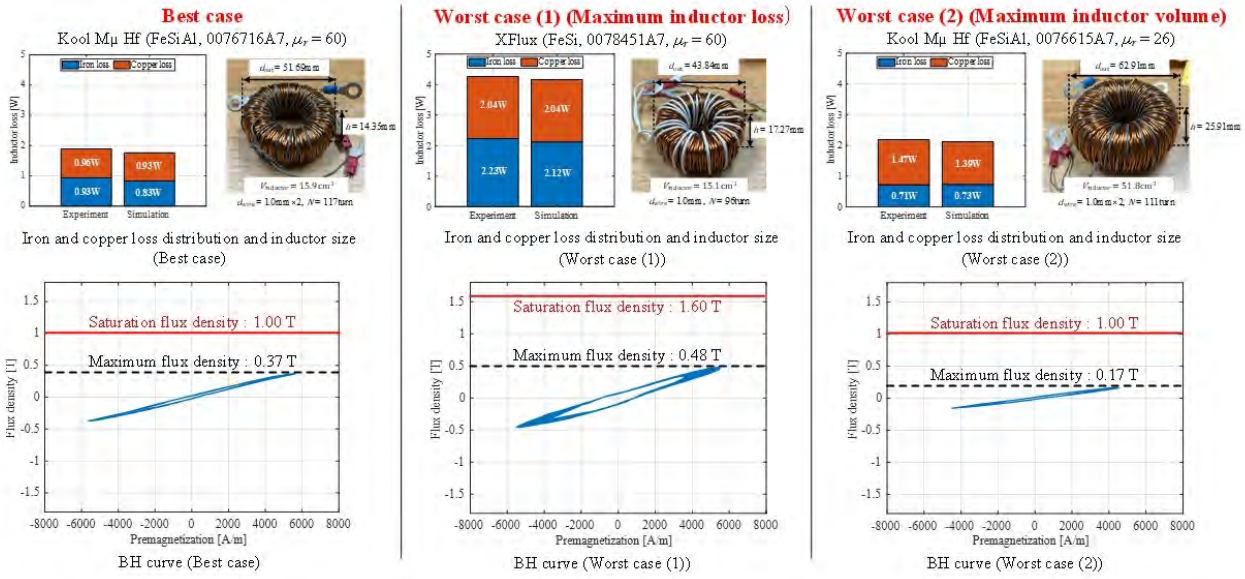


Figure 1.3.1.6 Example of AC filter inductor optimization design results [10] and B-H curve trajectory

[Hiroaki Matsumori]

References

(1) Bima Nugraha Sanusi, "Advances in High Frequency Inductor Design for Power Converter", Ph.D. thesis, Technical University of Denmark, 2023.

(2) J. Wang, N. Rasekh, X. Yuan and K. J. Dagan, "An Analytical Method for Fast Calculation of Inductor Operating Space for High-Frequency Core Loss Estimation in Two-Level and Three-Level PWM Converters," in *IEEE Transactions on Industry Applications*, Vol. 57, No. 1, pp. 650-663, Jan.-Feb. 2021. Jan.-Feb. 2021, doi: 10.1109/TIA.2020.3037879.

(3) T. Guillod, P. Papamanolis and J. W. Kolar, " *Artificial Neural Network (ANN) Based Fast and Accurate Inductor Modeling and Design.*", IEEE Open Journal of Power Electronics, 2020.

(4) H. Li *et al*, " MagNet: An Open-Source Database for Data-Driven Magnetic Core Loss Modeling, " *2022 IEEE Applied Power Electronics Conference and Exposition (APEC)*, Houston, TX, USA, 2022, pp. 588-595, doi: 10.1109/APEC43599.2022.9773372.

(5) A. J. Hanson, J. A. Belk, S. Lim, C. R. Sullivan and D. J. Perreault, " Measurements and Performance Factor Comparisons of Magnetic Materials at High Frequency," in *IEEE Transactions on Power Electronics*, Vol. 31, No. 11, pp. 7909-7925, Nov. 2016, doi: 10.1109/TPEL.2015.2514084.

(6) J. Mühlethaler , *Modeling and Multi-Objective Optimization of Inductive Power Components*, Ph.D. dissertation, ETH Zurich, Zurich, Switzerland, 2012 .

(7) R. S. Yang, A. J. Hanson, B. A. Reese, C. R. Sullivan and D. J. Perreault, " A Low-Loss Inductor Structure and Design Guidelines for High- Frequency Applications," in *IEEE Transactions on Power Electronics*, Vol. 34, No. 10, pp. 9993-10005, Oct. 2019, doi: 10.1109/TPEL.2019. 2892397.

(8) H. Matsumori, T. Shimizu, K. Takano and H. Ishii, " *Evaluation of Iron Loss of AC Filter Inductor Used in Three-Phase PWM Inverters Based on an Iron Loss Analyzer*," IEEE T. on Power Electronics, 2016.

(9) Akihiro Miwa, Toshihisa Shimizu, Koji Takano, Hitoshi Ishii, "Low Loss Design of Inductors for Buck Chopper Circuits Considering DC Magnetic Field Bias Characteristics of Iron Loss," IEEJ Transactions on D (Journal of Industrial Applications), Vol. 137, No. 5, pp. 385-394, May 2017. doi:10.1541/ieejias.137.385.

(10) Taisei. Yamauchi and Hiroaki. Matsumori, "Proper magnetic materials selection method for AC filter inductor design used in single phase PWM inverters", AIP Advances, vol. 14, Issue.1, p.015132, 2024.

3.2 Common mode inductor

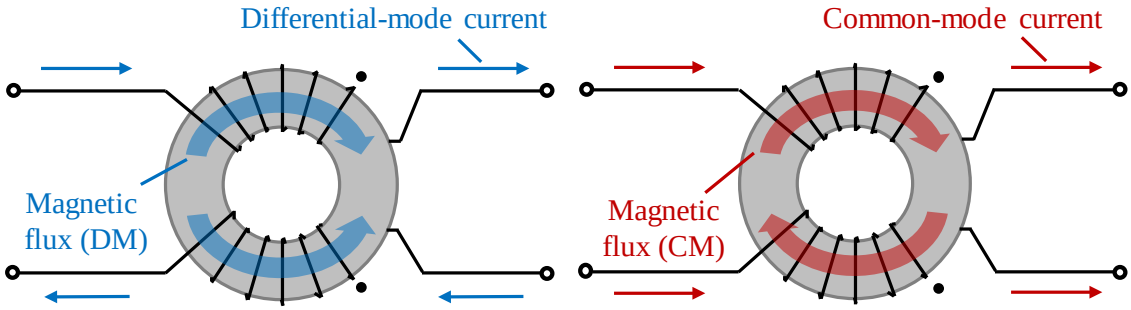
Keyword: Common mode inductor, EMI, Iron loss, Magnetic flux density, Nanocrystal

3.2.1 Common Mode Inductor Overview

In power electronic equipment that uses switching of power semiconductor devices, the voltage and current fluctuate greatly in an instant. To prevent EMI, the International Electrotechnical Commission (IEC) and other organizations have established EMI standards. All power electronic equipment is required to meet noise standards according to the application.

Power devices using wide bandgap semiconductors such as silicon carbide (SiC) and gallium nitride (GaN), which have been the focus of much research and development in recent years for practical applications, can achieve switching speeds 10 times faster than those of conventional silicon semiconductor-based power devices. While faster switching speeds reduce switching losses, there is concern about a significant increase in high-frequency electromagnetic noise associated with switching [(1)-(4)]. Electromagnetic noise is broadly classified into differential mode (DM) noise and common mode (CM) noise based on the propagation mode. Among these, CM noise, which propagates through stray capacitances distributed in various parts of the system, is often dominant in the high-frequency region above several MHz. Therefore, much time and money is spent on the analysis and reduction of CM noise in order to suppress EMI caused by electromagnetic noise in power electronic equipment.

A common-mode inductor (CMI) is a magnetic component for CM noise suppression[(5)] A CMI is fabricated by applying the number of windings corresponding to the number of phases of a power line to a single iron core with the same polarity. For example, if the CMI is connected to a single-phase system, two windings are applied to the iron core, and if the system is three-phase, three windings are applied to the iron core. As shown in **Figure 1.3.2.1**, the magnetic flux inside the iron core of the CMI strengthens against the CM signal, while the total flux against the DM signal is ideally zero. Therefore, CMIs are widely used as CM noise suppression components because they have



(a) Flux inside the iron core for DM current (b) Flux inside the iron core for CM current

Figure 1.3.2.1 Schematic diagram of winding structure **and** magnetic flux inside the iron core of a single-phase CMI

inductance only against CM noise.

To prevent degradation of noise suppression performance due to unwanted magnetic coupling with neighboring components, CMIs often use a toroidal-shaped iron core with high magnetic permeability. In addition, the CMI should have low stray capacitance between windings to avoid impedance reduction in the high-frequency range. This is because the high-frequency current bypasses between the windings through the stray capacitance, forming a path that does not pass through the iron core, thereby lowering the effective impedance. The single-layer winding structure can greatly reduce the inter-winding stray capacitance compared to the multi-layer winding structure, but the occupancy ratio of the window of the toroidal core is reduced. Therefore, it is necessary to select an appropriate winding scheme, taking into consideration the trade-off relationship with a larger iron core size. In addition, the leakage inductance of the CMI can be used for DM noise suppression. In other words, actively utilizing the leakage inductance of the CMI can reduce the size and number of DM noise suppression elements. However, in applications where the rated current is large, the large current (DM current) flowing in the winding and the leakage inductance may cause a non-uniform magnetic flux in the iron core. As a result, localized magnetic saturation may occur, which reduces the inductance of the CMI and degrades its noise suppression performance.

In many cases, CMIs occupy the largest volume and weight among EMI countermeasure components. For this reason, many studies have been conducted on miniaturization and minimum volume design of CMIs [6]-[8]. In this section, taking a three-phase motor drive system as an example, which is a typical application of power electronics equipment, we will discuss the minimum volume design of CMI considering the specific permeability and iron loss characteristics of magnetic materials, the characteristics required for magnetic materials to achieve further miniaturization, and the technical issues to be solved in the design process in the future. This paper describes the characteristics required for magnetic materials to achieve further miniaturization and the technical issues to be solved in the design.

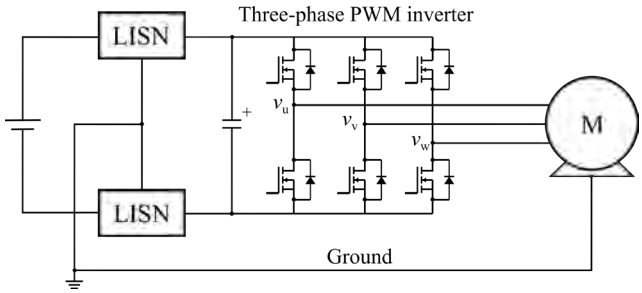


Figure 1.3.2.2 Configuration of a three-phase motor drive system for noise evaluation

3.2.2 Configuration of the system under consideration and CM equivalent circuit

Figure 1.3.2.2 shows the configuration of a noise evaluation system for a three-phase motor drive system fed by a pulse width modulation (PWM) inverter. The motor case and the inverter heat sink are connected to the ground plane. The DC power supply and the three-phase PWM inverter are connected via a line impedance stabilization network (LISN) to stabilize the impedance on the power supply side. The inverter produces a ground potential variation v_{cm} corresponding to the change in each phase voltage. This potential variation is called CM voltage and can be expressed as the following equation (1.3.2.1) using the three-phase output voltages v_u, v_v, and v_w of the inverter [9].

$$v_{cm} = \frac{v_u + v_v + v_w}{3} \tag{1.3.2.1}$$

If the CM impedance including the output cables of the motor and inverter is Z_{cmo} and the CM impedance including the input cables of the LISN and inverter is Z_{cmi}, the CM equivalent circuit of the motor drive system **shown in Figure 1.3.2.2** can be expressed as in **Figure 1.3.2.3**. The CM impedances Z_{cmo} and Z_{cmi} result in the propagation of the CM current i_{cm} expressed by the following equation (1.3.2.2).

$$i_{cm} = \frac{v_{cm}}{Z_{cmi} + Z_{cmo}} \tag{1.3.2.2}$$

CM current is a source of conducted EMI, which propagates to

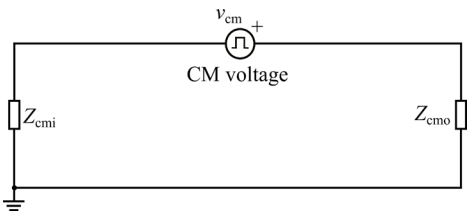


Figure 1.3.2.3 CM equivalent circuit of Figure 1.3.2.2

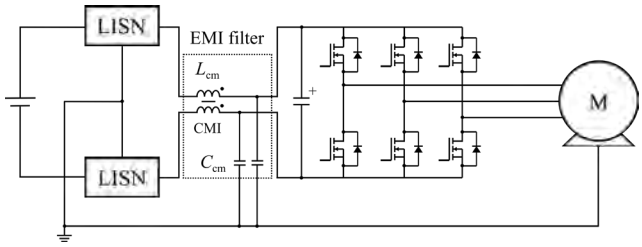


Figure 1.3.2.4 Input side EMI filter connected Motor Drive System Configuration

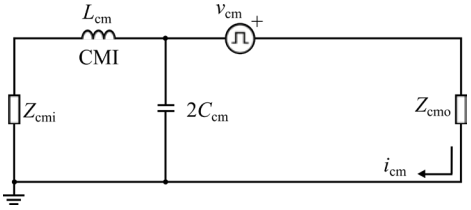


Figure 1.3.2.5 CM equivalent circuit of Figure 1.3.2.4

equipment that shares a power supply with the inverter, and radiated EMI, which affects peripheral equipment by propagating as electromagnetic waves through space, mainly using cables as antennas, so appropriate countermeasures are necessary.

3.2.3 Input side EMI filter

In a three-phase motor drive system, CM noise suppression using CMI includes an input-side EMI filter [10], an output-side CMI [11], and an output-side EMI filter [12]. The configuration of a motor drive system with an input-side EMI filter connected is shown in **Figure 1.3.2.4**, and its CM equivalent circuit is shown in **Figure 1.3.2.5**. The input EMI filter consists of CMI L_{cm} *and* Y capacitor C_{cm}. If the capacitance of the Y capacitor is increased, the current flowing out to the ground system will increase, which may cause electric shock. Therefore, the maximum capacitance value of the Y capacitor is determined for each application. In other words, the inductance value of the CMI is often adjusted so that the input EMI filter meets the required attenuation characteristics. In particular, a very large CMI is required to achieve large attenuation in the low-frequency range. Therefore, it is desirable to select a magnetic material with high permeability for the CMI of the input-side EMI filter to achieve the desired inductance with as few turns as possible. Since most of the CM current is returned through the Y capacitor, the CMI of the input-side EMI filter is excited with a relatively small signal. Therefore, in many cases, magnetic materials with high saturation magnetic flux density or low iron loss characteristics are not necessarily required for the CMI that constitutes the input-side EMI filter.

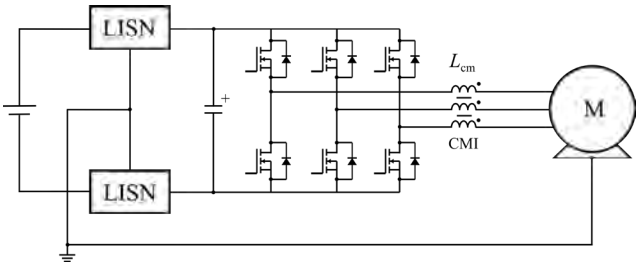


Figure 1.3.2.6 Configuration of motor drive system with output side CMI connected.

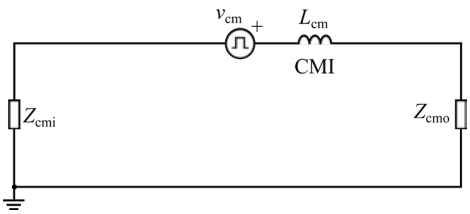


Figure 1.3.2.7 CM equivalent circuit of Figure 1.3.2.6

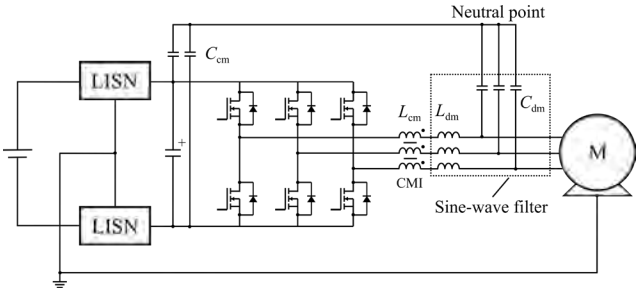


Figure 1.3.2.8 Output side EMI filter connected Motor Drive System Configuration

3.2.4 Output-side CMI

Next, **Figure 1.3.2.6** shows the configuration of a motor drive system with a CMI connected to the output side of the inverter, and its CM equivalent circuit is shown in **Figure 1.3.2.7**. The CM impedance Z_{cmo} on the output side of the motor drive system can be regarded as a capacitive impedance in which the motor winding-to-case stray capacitance is dominant. In other words, by connecting the CMI to the output side of the inverter, the CMI and the stray capacitance of the motor constitute a low-pass filter. Assuming that the cutoff frequency of the low-pass filter is sufficiently lower than the switching frequency of the inverter, the impedance of the CMI becomes dominant in the CM equivalent circuit shown in **Figure 1.3.2.7** near the switching frequency. Since almost all of the CM voltage of the inverter is applied to both ends of the CMI, a high magnetic flux density is generated inside the iron core of the CMI. In other words, the magnetic material used in the output-side CMI must have a high saturation magnetic flux density and low iron loss characteristics under high-signal excitation. Also, as with the CMI for the input side EMI filter, a high specific permeability is required to achieve a large inductance with a small number of turns of winding. Here, the stray capacitance of a motor usually takes a value of several nF. Therefore, to set the cutoff frequency of the low-pass filter lower than the switching frequency of the inverter, a very large inductance exceeding several tens of mH is required, which inevitably increases the volume and weight of the CMI.

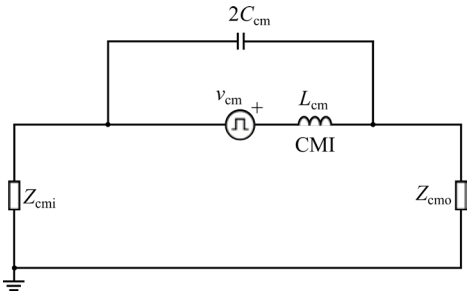


Figure 1.3.2.9 CM equivalent circuit of Figure 1.3.2.8

3.2.5 Output side EMI filter

Figures 1.3.2.8 and **1.3.2.9** respectively show the configuration of an EMI filter connected to the output side of a motor drive system and its CM equivalent circuit. In this scheme, the neutral point of a sinusoidal filter consisting of a DM inductor L_{dm} and a DM capacitor C_{dm} is connected to the DC input of the inverter via a Y capacitor. The propagation to the ground system is greatly suppressed. The CMI is placed inside the filter loop to suppress the CM current circulating in the loop. For example, by setting $L_{cm} \geq 100 \cdot L_{dm}/3$ and $2C_{cm} \leq 3C_{dm}/100$, respectively, the effects of the DM inductor and DM capacitor on the CM can be ignored [13], so L_{dm} and C_{dm} are omitted in **Figure 1.3.2.9**. Furthermore, by setting the cutoff frequency determined by the CMI and Y capacitor lower than the switching frequency of the inverter, the CMI can be designed in the same way as the output-side CMI shown in **Figure 1.3.2.6**. In addition, this method allows the use of a Y capacitor with a capacitance larger than the stray capacitance of the motor, which allows the CMI to be smaller than the method of connecting only the CMI. In the following, the results of the minimum volume design for each inverter switching frequency, the characteristics required for magnetic materials to achieve further miniaturization, and the technical issues in designing CMIs for use in output-side EMI filters are summarized. The discussion in this section can be widely applied to PWM inverters in general, regardless of the number of phases, single or three.

3.2.6 Inductance required for CMI

First, the design of the CMI used for the output side EMI filter is described: a toroidal core of nanocrystalline material (Vitroperm 500F, VACUUMSCHMELZE) is selected as the iron core of the CMI. Based on the specific permeability of the magnetic material and the iron loss characteristics, a CMI with a minimum volume less than the permissible loss density is designed for a given inverter switching frequency f_{sw} in the frequency band of 10 kHz to 1 MHz, taking into account the window area and internal flux density of the iron core.

The Vitroperm 500F data sheet [14] lists AL values at 10 kHz and 100 kHz. Here, the AL values below 10 kHz were fixed to those at 10 kHz, and the AL values in the other bands were interpolated and extrapolated on a logarithmic scale from the values at 10 kHz and 100 kHz. The window area of the toroidal core is evaluated to determine if it is large enough to provide the required number of turns of winding. The cutoff frequency is calculated for each filter cutoff frequency f_{cut} using the AL value obtained from the data sheet. The cutoff frequency was set to be sufficiently low relative to the inverter switching frequency f_{sw}, $f_{cut} = f_{sw}/7$ [15].

3.2.7 Design of CMI considering iron loss characteristics of magnetic materials

Next, the iron loss characteristics of Vitroperm 500F can be measured at any frequency and flux density using a B-H analyzer or similar device. **Figure 1.3.2.10** shows the measured iron loss characteristics of Vitroperm 500F under sinusoidal excitation conditions. From the measured iron loss characteristics, the magnetic flux density at which the allowable loss density P_{lit} is reached can be determined for each excitation frequency. In this section, curve fitting is performed on the measured iron loss characteristics using the following loss equation, and six fitting parameters are identified.

$$P_v = k_1 f^{\alpha_1} B_p^{\beta_1} + k_2 f^{\alpha_2} B_p^{\beta_2} \tag{1.3.2.3}$$

In the above equation, P_v *is* the loss density, *f is the* excitation frequency, B_p is the peak magnetic flux density, and k_1, k_2, α_1, α_2, β_1, and β_2 are fitting parameters, respectively. In this section, P_{limit} is set to 300 kW/m^3 [16] and the limiting flux density B_{limit} that reaches P_{limit} for each excitation frequency is obtained based on Equation (1.3.2.3).

Note that Vitroperm 500F has a saturation flux density of about 1.1 T at 100 °C [14]. Based on this, in this section, the maximum value of B_{limit} is set to 1.0 T. The peak magnetic flux inside the iron core of the CMI is maximum when the CM voltage of the inverter is assumed to be $\pm E_{dc}/2$, square wave with duty 0.5 (E_{dc} is the DC input voltage of the inverter). Under these conditions, the magnetic flux density B_c inside the iron core is calculated and evaluated to see if it is less than the flux density limit B_{limit}.

Vitroperm 500F has a specific magnetic permeability of approximately 15,000~150,000 [14]. Considering the aforementioned window area and internal magnetic flux density of the iron core, we selected the iron core from the data sheets and designed the CMI for three conditions with specific permeability μ_r of 25,000 or more, 60,000 or more, and 90,000 or more. **Figure 1.3.2.11** shows the volume V_c of the CMI designed for each inverter switching frequency under each condition. **Figure 1.3.2.11** also plots the calculation results of the limiting flux density B_{limit} and the flux density inside the iron core B_c for each switching frequency. In the design, the DC input voltage and motor rating of the inverter were set to 200 V and 0.75 kW, respectively.

Selecting an iron core with high specific permeability reduces the number of turns, but increases the flux density inside the iron core, resulting in the need for an iron core with larger dimensions. **Figure 1.3.2.11** shows that the volume reduction effect of higher switching frequency is limited to about 40 kHz (condition of $\mu_r \geq 25{,}000$). In addition, it can be confirmed that the volume reduction effect can be achieved by including an iron core with lower specific permeability in the design, especially in the high-frequency range.

As an example, two CMIs designed for f_{sw} = 50 kHz were fabric ated with 14 turns of winding per phase on L2045-V102 (model

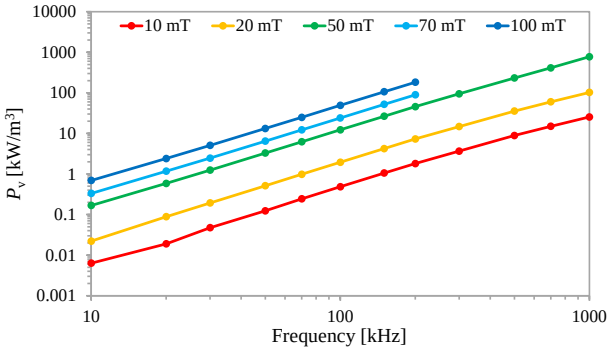


Fig. 1.3.2.10 Iron loss characteristics of Vitroperm 500F

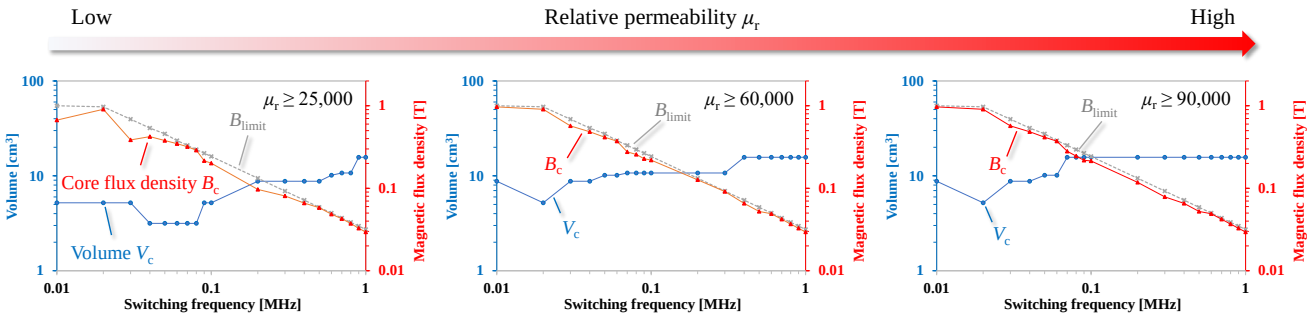


Fig. 1.3.2.11 Volume V_c of CMI *and* flux density B_c inside the iron core designed for each inverter switching frequency

number of the iron core) for $\mu_r \geq 60{,}000$ and $\mu_r \geq 90{,}000$. For $\mu_r \geq 25{,}000$, L2030-W358 was used with 33 turns of winding per phase. **Figure 1.3.2.12** shows the appearance of the two fabricated CMIs. By using an iron core with high specific permeability, the number of turns required is reduced, and it can be seen that the windings are sparsely wound on the iron core. On the other hand, under the condition of using an iron core with low specific permeability, the volume of the iron core becomes smaller, but the required number of turns increases, resulting in a very dense winding structure with multi-layer windings.

3.2.8 Impedance of prototype CMI

The impedance to CM of the two fabricated CMIs was measured using a network analyzer over a bandwidth of 1 kHz to 30 MHz, and the results are **summarized in Figure 1.3.2.13.** Under the condition using an iron core with high specific permeability (L2045-V102, $\mu_r \approx 100{,}000$), the slope of the impedance increase becomes slower from around 10 kHz due to the decrease in permeability. Then, around 2 MHz, self-resonance with stray capacitance is induced, and the impedance decreases at the following frequencies. In contrast, when an iron core with low specific permeability (L2030-W358, $\mu_r \approx 25{,}000$) is used, the stray capacitance is large, causing self-resonance at around 200 kHz, and the impedance decreases in the frequency band thereafter. As a result, there is a large difference between the impedances of the two CMIs in the band after 1 MHz, suggesting that the CM noise suppression performance in the high frequency band under the condition using the low permeability iron core is much worse than that of the CMI using the high permeability iron core.

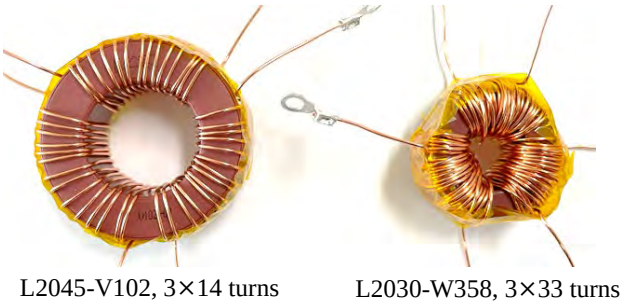


Figure 1.3.2.12. Appearance of the fabricated CMI (Left: with high permeability core, Right: with low permeability core)

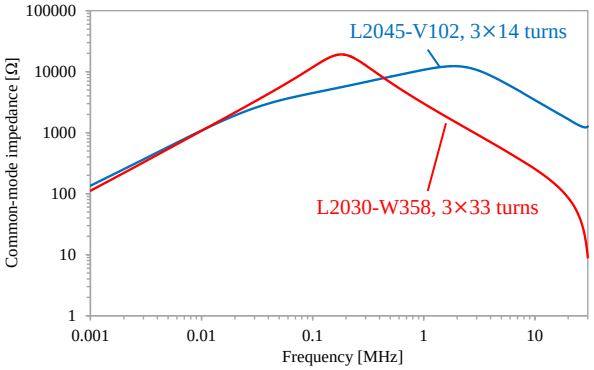


Fig. 1.3.2.13 Measured impedance of fabricated CMI

3.2.9 Summary

This section describes a minimum volume design for the CMI of an output-side EMI filter in a three-phase PWM inverter-fed motor drive system, taking into account the specific permeability of the magnetic material and iron loss characteristics. Under the condition that an iron core with low permeability is selected, the required number of turns increases, and the magnetic flux density inside the iron core can be kept relatively low, allowing the use of a compact iron core. However, when an iron core with low permeability is used, the stray capacitance is much larger than in the condition in which an iron core with high permeability is selected, and as a result, the CM noise suppression performance in the high frequency range deteriorates. Therefore, as a suitable magnetic material for a CMI that is compact, lightweight, and maintains a large impedance over a wide bandwidth, it must have high permeability to reduce the number of turns (stray capacitance), exhibit low iron loss characteristics even under high frequency excitation conditions, and not limit the flux density in the iron core. In the design of CMI, it is desirable to establish a minimum volume design method that takes into account not only the frequency characteristics of magnetic permeability and iron loss, but also the frequency characteristics of impedance based on the estimation of stray capacitance.

[Shotaro Takahashi]

References

(1) D. Han, S. Li, Y. Wu, W. Choi, and B. Sarlioglu: "Comparative analysis on conducted CM EMI emission of motor drives: WBG versus Si devices ", *IEEE Trans. Industrial Electronics*, Vol. 64, No. 10, pp. 8353-8363 (2017).

(2) G. Engelmann, A. Sewergin, M. Neubert, and R. W. De Doncker : "Design challenges of SiC devices for low- and medium- voltage DC-DC converters ", *IEEJ Journal of Industry Applications*, Vol. 8, No. 3, pp. 505-511 (2019).

(3) B. Zhang, and S. Wang: "A survey of EMI research in power electronics systems with wide-bandgap semiconductor devices", *IEEE Journal of Emerging and Selected Topics in Power Electronics*, Vol. 8, No. 1, pp. 626-643 (2020).

(4) S. Takahashi, K. Wada, H. Ayano, S. Ogasawara, and T. Shimizu : "Review of modeling and suppression techniques for electromagnetic interference in power conversion systems", *IEEJ Journal of Industry Applications*, Vol. 11, No. 1, pp. 7-19 (2022).

(5) M. L. Heldwein, L. Dalessandro, and J. W. Kolar : "The three-phase common-mode inductor: modeling and design issues", *IEEE Industrial Electronics*, Vol. 58, No. 8, pp. 3264-3274 (2011).

(6) Y. Maillet, R. Lai, S. Wang, F. Wang, R. Burgos, and D. Boroyevich : "High-density EMI filter design for DC-fed motor drives",. *IEEE Trans. Power Electronics*, Vol. 25, No. 5, pp. 1163-1172 (2010).

(7) D. O. Boillat, F. Krismer, and J. W. Kolar : "EMI filter volume minimization of a three-phase, three-level T-type PWM converter system ", *IEEE Trans. Power Electronics*, Vol. 32, No. 4, pp. 2473-2480 (2017).

(8) B. Zaidi, A. Videt, and N. Idir : "Optimization method of CM inductor volume taking into account magnetic core saturation issues ", *IEEE Trans. Power Electronics*, Vol. 34, No. 5, pp. 4279-4291 (2019).

(9) S. Ogasawara, and H. Akagi : "Modeling and damping of high-frequency leakage currents in PWM inverter-fed AC motor drive systems *Industry Applications*, Vol. 32, No. 5, pp. 1105-1114 (1996).

(10) F. Y. Shih, D. Y. Chen, Y. P. Wu, and Y. T. Chen: "A procedure for designing EMI filters for AC line applications," *IEEE Trans. Power Electronics*, Vol. 11, No. 1, pp. 170-181 (1996).

(11) A. Roc'h, and F. Leferink: "Nanocrystalline core material for high-performance common mode inductors", *IEEE Electromagnetic Compatibility*, Vol. 54, No. 4, pp. 785-

791 (2012).
(12) H. Akagi, H. Hasegawa, and T. Doumoto: "Design and performance of a passive EMI filter for use with a voltage-source PWM inverter having sinusoidal output voltage and zero common-mode voltage", *IEEE Trans. Power Electronics*, Vol. 19, No. 4, pp. 1069-1076 (2004))
(13) M. Antivachis, P. S. Niklaus, D. Bortis, and J. W. Kolar: "Input/output EMI filter design for three-phase ultra-h.igh speed motor drive GaN inverter stage", *CPSS Trans. Power Electronics and Applications*, Vol. 6, No. 1, pp. 74-92 (2021).
(14) VACUUMSCHMELZE GmbH & Co. KG, Nanocrystalline VITROPERM EMC Products, May 2016. [Online]. Available: https://www.vacuumschmelze.com/fileadmin/medien/brochures/NanocrystallineVITROPERM-EMC-Products-Mai_2016.pdf
(15) M. M. Swamy, J. K. Kang, and K. Shirabe: "Power loss, system efficiency, and leakage current comparison between Si IGBT VFD and SiC FET VFD with various filtering options," *IEEE Trans. Industry Applications*, Vol. 51, No. 5, pp. 3858-3866 (2015).
(16) A. J. Hanson, J. A. Belk, S. Lim, C. R. Sullivan, and D. J. Perreault: "Measurements and performance factor comparisons of magnetic materials at high frequency," *IEEE Trans. Power Electronics*, Vol. 31, No. 11, pp. 7909-7925 (2016).

3.3 Transformer for SST

Keyword: Finemet, Ferrite, Magnetic flux density, Iron loss

This section describes the design results of a transformer for Solid State Transformer (SST) as a benchmark transformer and examines the material properties desired for high frequency transformers.

3.3.1 Transformer Specifications

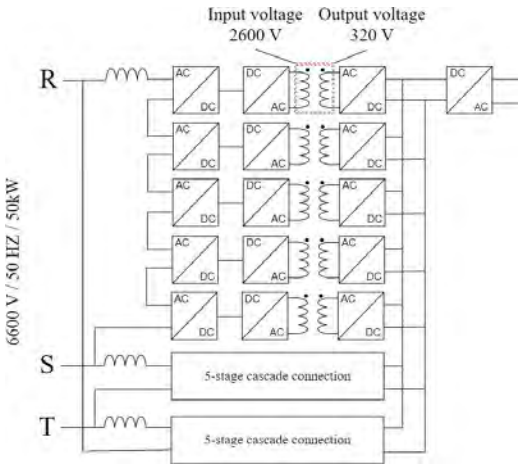


Figure 1.3.3.1 SST (Solid State Transformer)

Table 1.3.3.1 Transformer Specifications

Parameter	Value
Rated capacity [kVA]	3.3
Primary voltage [V].	2600
Primary current [A].	1.3
Secondary voltage [V].	320
Secondary current [A].	11

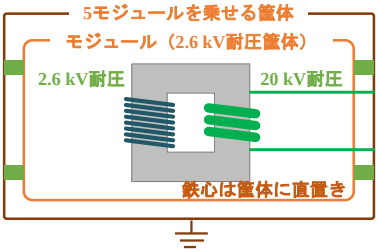


Fig. 1.3.3.2 Transformer Required Withstand

Figure 1.3.3.1 shows the SST configuration and **Table 1.3.3.1** shows the designed transformer specifications. The winding ratio is 8:1, and the transformer is characterized by high primary input voltage and large secondary current. As shown in **Figure 1.3.3.2**, a primary side withstand voltage of 2.6 kV and a secondary side withstand voltage of 20 kV are required .

3.3.2 Magnetic Material Selection

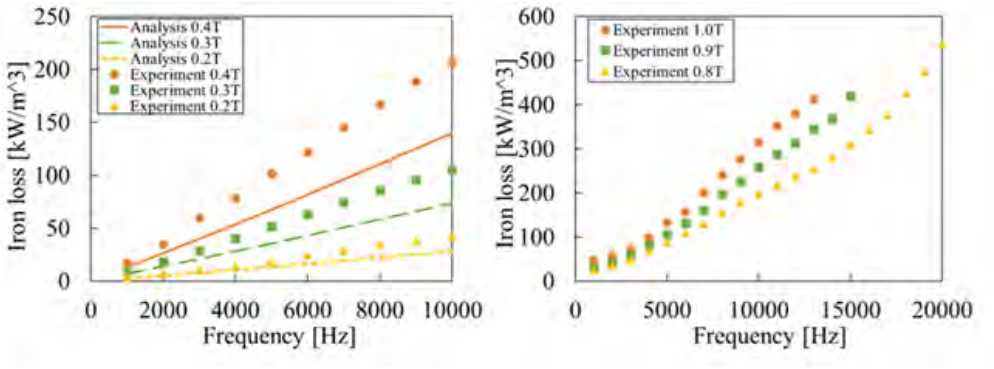
Electromagnetic steel sheet (35H210: 0.35 mm), amorphous soft magnetic material (2605SA1: 0.025 mm), nanocrystalline soft magnetic material (FINEMET FT-3M), and soft ferrite (PC47) were considered as candidates for application as the iron core material for the transformer for SST. Typical properties of each are shown in **Table 1.3.3.2**. The study methodology is as follows.

(1) Design and prototyping of sample transformers using various materials
(2) Obtained DC magnetization characteristics and iron loss characteristics for each driving frequency for the sample transformer prototyped in (1)
(3) Design transformers with SST specifications for each drive frequency using the iron loss characteristics obtained in (2).
(4) Derive volume and iron loss in (3) (iron loss is calculated by post-analysis after deriving magnetic flux density)

Table 1.3.3.2 Transformer Iron Core Material Acquisitiveness

材料	飽和磁束密度 [T]	比透磁率 (1 kHz)	電気抵抗率 [Ω · m]	鋼板厚さ [mm]
電磁鋼板 (35H210)	1.90	2.7×10^{3}	0.5×10^{-6}	0.35
アモルファス軟磁性材料 (2605SA1)	1.56	5.0×10^{3}	1.30×10^{-6}	0.025
ソフトフェライト (PC47)	0.52	2.5×10^{3}	4.0	×
ナノ結晶軟磁性材料 (ファインメット FT-3M)	1.23	70.0×10^{3}	1.20×10^{-6}	0.018

The drive frequency was set to a maximum of 20 kHz in consideration of the switching loss of the DAB converter used in the SST, and sample transformers of different sizes were designed for each 1 kHz frequency. In designing the transformers, we obtained sample iron cores in advance and measured the frequency, magnetic flux density, and iron loss, and input the obtained results into electromagnetic field analysis. The measurement results for ferrite and finemet are shown in **Figure 1.3.3.3.**



Ferrite Finemet

Figure 1.3.3.3 Frequency - Flux Density - Iron Loss Characteristics of Sample Iron Core

Figure 1.3.3.4 shows the magnitude and iron loss results for each frequency of the transformer designed using the experimental results shown in **Figure 1.3.3.3**. The maximum magnetic flux density was set at 0.4 T for ferrite and 1.0 T for FINEMET.

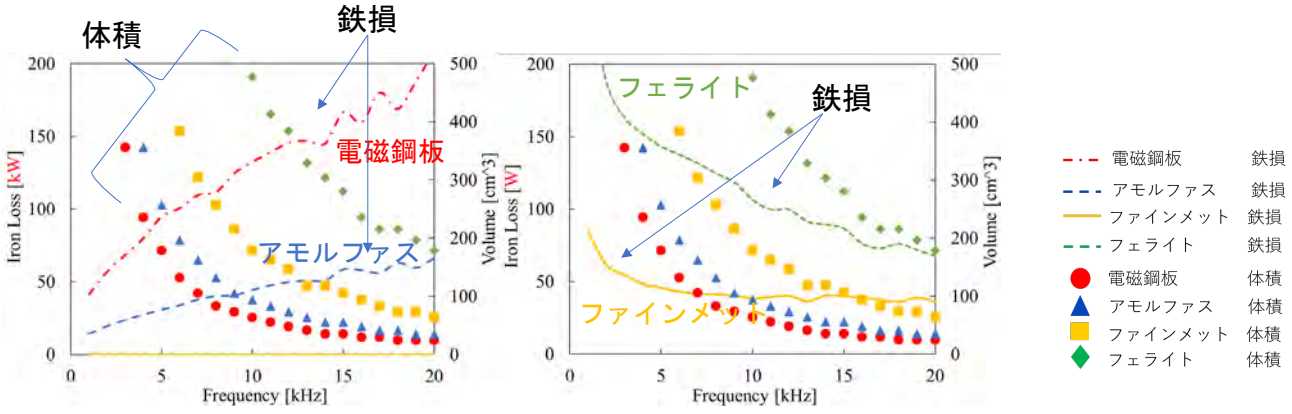


Figure 1.3.3.4 Sample transformer size and iron loss (right figure **is** an enlarged view of Iron Loss on the left)

Figure 1.3.3.4 shows that although the volume of electromagnetic steel sheet and amorphous soft magnetic material is smaller than that of FINEMET and ferrite, the iron loss is 1000 times higher. In addition, there is a significant trade-off between these two materials: iron loss increases while volume decreases as the drive frequency increases. On the other hand, the volume of FINEMET and ferrite decreases as the

drive frequency increases, and the iron loss decreases at the same time. This is because the rate of volume reduction at higher frequencies is greater than the rate of loss increase. Extrapolating from **Figure 1.3.3.4**, it can be inferred that the driving frequency must be increased to approximately 50 kHz for the volume of the transformer using ferrite to become equal to that of Finemet at 20 kHz. From the above, it was found that Finemet is a suitable material for SST transformers in the drive frequency range up to 20 kHz.

3.3.3 Transformer design using finemet

The transformer was designed based on the specifications in **Table 1.3.3.1** with a target conversion efficiency of 99 %. From **Figure 1.3.3.4**, the driving frequency was set to 10-20 kHz and the volume to less than 100 cc, and the CS-50 iron core shape was selected. The winding was selected as shown in **Table 1.3.3.3.3**, based on the specifications in **Table 1.3**.3.**1**, taking the withstand voltage into consideration. By making the secondary winding itself of high withstand voltage specifications, the insulation between the primary and secondary sides and between the secondary side and the iron core is ensured by the winding. In designing the transformer, the drive frequency and magnetic flux density design values were used as parameters, and the iron loss and number of turns were checked. to achieve 99 % efficiency in a 3.3 kW transformer, both the copper and iron losses were designed to be around 15 W. The iron loss was designed to be less than 15 W and the number of turns on the primary side was designed to be less than 256 turns. **Figure 1.3.3.5** shows the results of the study.

Figure 1.3.3.5 shows that increasing the magnetic flux density setting and drive frequency will lower the number of turns required and enable downsizing. However, since iron loss also increases, the target iron loss of 15 W or less can be achieved by setting the drive frequency to 10 kHz and the magnetic flux density to around 0.8 T. In addition, it can be seen that increasing the drive frequency is more effective for miniaturization than increasing the magnetic flux density. Therefore, it can be said that the most suitable magnetic material for SST transformers is a high-frequency, low iron loss material. For reference, **Figure 1.3.3.6** shows the results of a study using ferrite. Although ferrite has low iron loss, its magnetic flux density is low, and it could not satisfy the condition of the number of turns.

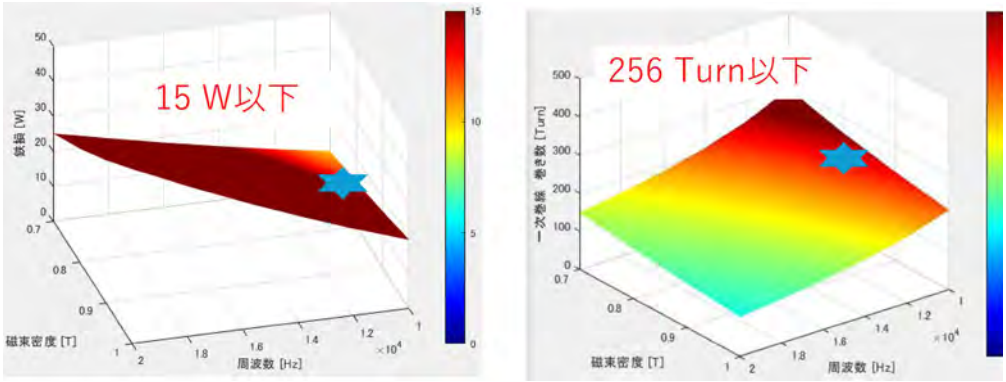


Fig. 1.3.3.5 Results of transformer study using FINEMET
(Left: Magnetic flux density of iron loss, frequency dependence, Right: Magnetic flux density of number

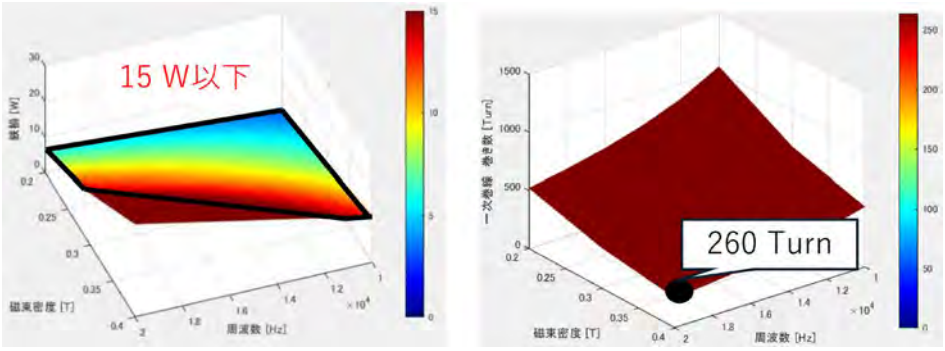


Fig. 1.3.3.6 Results of transformer study using ferrite
(Left: Magnetic flux density of iron loss, frequency dependence, Right: Magnetic flux density of number of turns, frequency dependence)

Based on the above results, the transformer was designed as shown in **Table 1.3.3.3**, and the loss was calculated by electromagnetic field analysis, resulting in an efficiency of over 99% as shown in **Table 1.3.3.4**. The measurement results of the actual experiment (**Figure 1.3.3.7**) also showed an efficiency of more than 99 % (**Figure 1.3.3.8**). However, 14 μm uncut iron core material was used in the experiment.

3.3.4 Summary

A transformer suitable for a drive frequency of 10 to 20 kHz was designed as a transformer for SST, and a volume of less than 100 cc and an efficiency of more than 99 % were obtained using FINEMET. The results show that iron loss characteristics at high frequencies are more important than the size of the saturation magnetic flux density when miniaturization and high efficiency are the objectives. We hope that the results will be used as a guideline for the development of magnetic materials for high-frequency transformers in the future. [Kan Akatsu]

Table 1.3.3.3 Finemet Design Specifications

Core type	CS50
Material	Nanocrystal
Operating Flux Density	0.81 T
Number of turns	256 Turn : 32 Turn
Primary winding type	TIW-3(SWT) 21/φ0.1
Primary winding resistance	2.93 Ω
Secondary winding Type	TIW-ELX 1080/φ0.1
Secondary winding resistance	0.00814 Ω
Lamination factor	0.78
Operating frequency	10 kHz (square wave)
Input voltage	2600 V
Load	29.54 Ω

Table 1.3.3.4 Transformer analysis results

Input voltage	2600 V
Output current	11 A
Input Power	2813 W
Output Power	2774 W
Copper Loss	6.27 W
Iron Loss	11.7 W
Efficiency	99.4 %

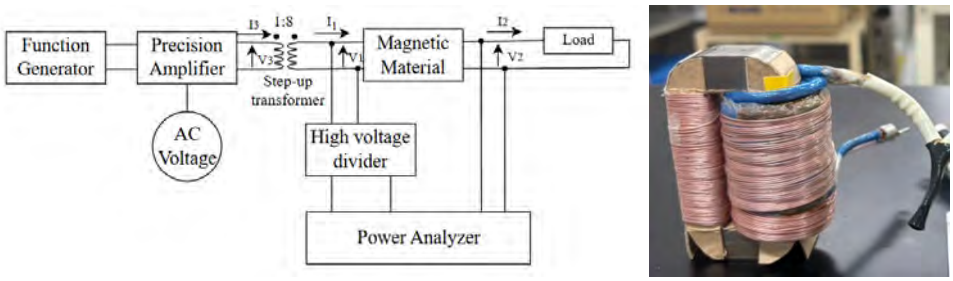


Figure 1.3.3.7 Measurement circuit of the actual experiment (left) and photo of the prototype transformer (right)

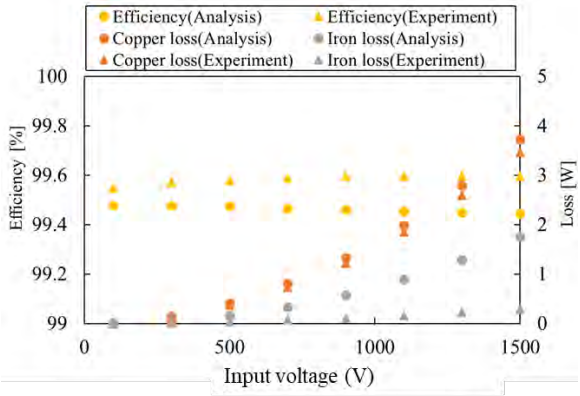


Figure 1.3.3.8 Experimental results (efficiency and loss)

References

(1) N. Owada and K. Akatsu, "Design of Compact High Efficiency High Frequency Transformers Suitable for Solid State Transformers," *IECON 2024 - 50th Annual Conference of the IEEE Industrial Electronics Society*, Chicago, IL, USA, pp. 1-6, DOI: 10.1109/IECON55916.2024.10905214(2014).

3.4 Capacitor for DC link

Keyword: Full-wave rectifier, PWM converter, DC-DC converter, Electrolytic capacitor, Film capacitor, Ceramic capacitor

3.4.1 Capacitors in power electronic circuits

In the circuit configuration of power electronics, the selection of capacitors and the design of their capacitance are important factors that determine the size and life of the device. **Figure 1.3.4.1** shows the main circuit configuration in which smoothing capacitors are used in a power electronics circuit based on a motor drive.

Figure 1.3.4.1 (a) shows the simplest configuration of a single-phase to three-phase converter, in which a single-phase full-wave rectifier is used to configure the DC power supply and the DC power supply drives the inverter. Since the DC voltage $_{EDC}$ generates a lot of pulsation at twice the AC power frequency, a large-capacity electrolytic capacitor is necessary for smoothing. Even with the same circuit configuration, a capacitor-less technology has been put to practical use in which the smoothing capacitor is intentionally made small and the pulsation

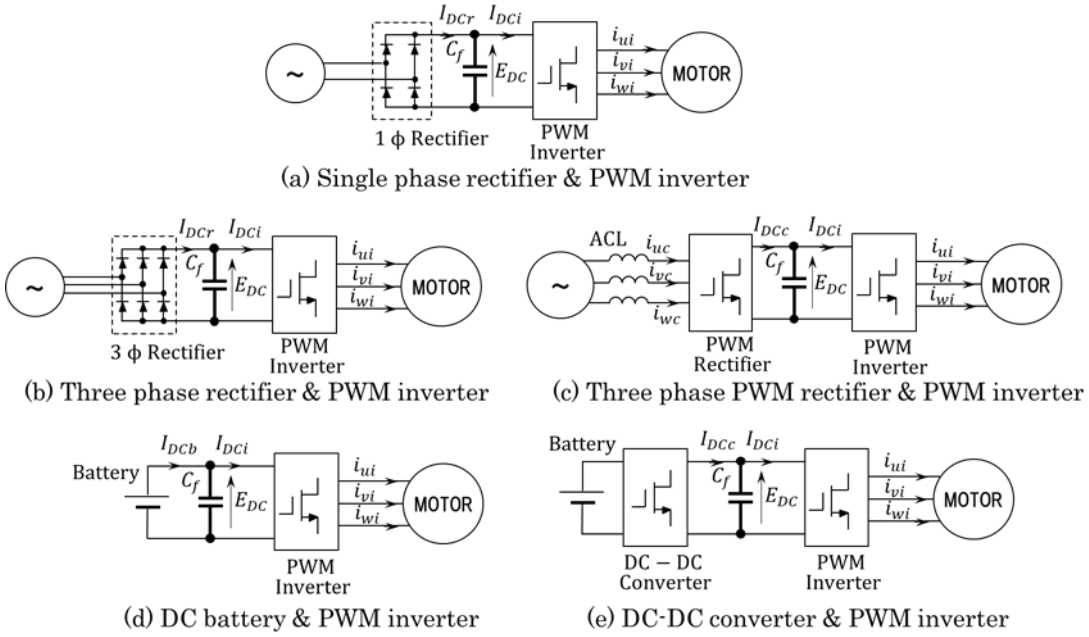


Figure 1.3.4.1 Circuit configuration using a smoothing capacitor

component is intentionally left to improve the overall power factor [(1)]. In this case, a film capacitor of several 10 μF is used.

Figure 1.3.4.1 (b) shows a three-phase full-wave rectifier circuit, in which a pulsation of six times the AC power frequency occurs in the DC voltage. Again, large-capacity electrolytic capacitors are used. Figure (c) uses a PWM converter as the converter on the power supply side and is configured to achieve DC voltage control and power factor improvement. In this case, the transient movement of the motor is also linked to the control of the converter side, thereby reducing the smoothing capacitor capacity.

In circuits driven by batteries, such as electric vehicles, a smoothing capacitor is also used in the DC section as shown in **Figure 1.3.4.1** (d) and (e). In (d), a smoothing capacitor is needed to prevent the high-frequency current flowing out of the inverter side from flowing into the battery side. In this case, the effect of not only the high-frequency waves caused by the switching of the inverter but also the high-frequency components caused by the motor, such as the distortion of the induced voltage of the motor, cannot be ignored. In the case of a DC-DC converter in the front stage as shown in the same figure (e), the smoothing capacitor capacity can be reduced by improving the control response of the converter, as in the same figure (c).

Smoothing capacitors are used in a variety of configurations, and the frequency components and magnitude of the current flowing through the capacitors also vary. It is important to evaluate these with a common measurement method and to generate benchmarks.

3.4.2 Smoothing capacitor evaluation

Figure 1.3.4.2 shows the circuit configuration for evaluating a smoothing capacitor against pulsating current. In the figure, the voltage pulsation and temperature rise of the capacitor C_f to be evaluated are measured and evaluated in the circuit on the right half. In the circuit on the left side, two upper and lower arms of the inverter (Arm 1 and Arm 2) are used to set the average voltage (DC component) applied to the target C_f and the current flowing through it. Specific operations are described below.

The controller detects the current (1) I_{in} input to the target C_f and controls the voltage E_{DC} at both ends of C_f to a constant value by its feedback control. This voltage control operates to keep the average value of E_{DC} constant, allowing the voltage condition of C_f to be set. The inductance L_1 makes the current I_{in} a direct current and reduces the pulsation component to a negligible level.

The current (2) I_{out} flowing out of the capacitor C_f is determined by (3) I2 and the switching operation of Arm3. Here, the switching of Arm 3 is fixed at Duty 50 %, but the switching frequency f_s itself can be set over a wide range (only Duty should be fixed). In this state, the current I2 is controlled to become various waveforms by using the controller on the left side and Arm 1. In other words, evaluate the current I2 as DC or sinusoidal AC (varying frequency and amplitude). The current I_{out} from the capacitor C_f is output as a waveform chopped by Arm 3 from the current I2. At this time, the frequency characteristics of C_f can be observed purely because ①Iin *on* the input side is set to a constant value by L_1. In addition, the smoothing capacitor used under various conditions in a power electronic circuit (**Figure 1.3.4.1**) can be evaluated by formalizing the current.

Film capacitors, ceramic capacitors, and electrolytic capacitors are used as C_f to be evaluated, and changes in loss and capacitor temperature are measured.

In an actual motor drive system, the capacitor current will include various high-frequency components due to PWM, but by formulating the evaluation method as described here, the benchmark results can be effectively utilized.

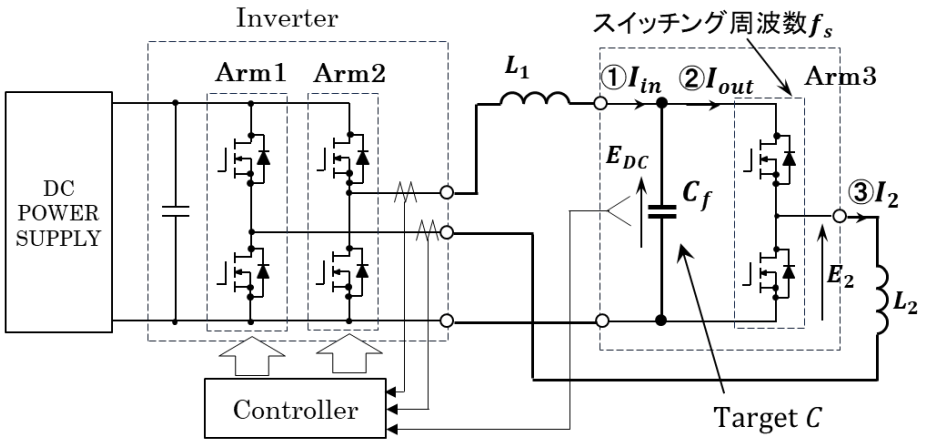


Figure 1.3.4.2 Evaluation circuit for a smooth capacitor

3.4.3 Evaluation Results

Table 1.3.4. 1shows the specifications of the evaluation device (**Figure 1.3.4.2).** The half bridge (Arm 3) uses SiC-MOSFETs to enable high switching frequency. The inverters (Arm 1 and 2), which perform current control, operate at a carrier frequency of f_c = 30 kHz to control E_{DC} and I_2. **Figure 1.3.4.3** shows the current and voltage waveforms during the measurement. The input current of the target capacitor C_f (1) I_{in} and the output current from the half bridge (Arm 3) (3) I_2 are almost DC, indicating that the rectangular pulsating current is all absorbed by the capacitor C_f.

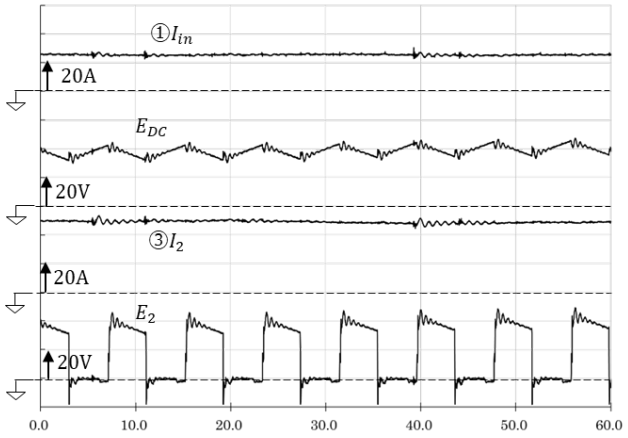


Figure 1.3.4.3 Measurement waveform (f_s =120 kHz, I_2=50 A, film capacitor 10 μF)

Table 1.3.4.1: Specifications of

DC POWER SUPPLY	DC60 V/100 A
インバータ(Arm1,2)	MOSFET, fc=30 kHz
ハーフブリッジ(Arm3)	SiC MOSFET
直流電圧E_{DC}	40 V
L_1	0.0090 mH
L_2	0.0045 mH
C_f (Target C)	①電解コンデンサ 680 μF, 450 V ②フィルムコンデンサ 10 μF, 1250 V ③セラミックコンデンサ 10 μF, 700 V

(1) Temperature measurement results

Three capacitors (C_f in **Table 1.3.4.1**) were tested for temperature rise. The results are shown in **Figure 1.3.4.4.** This time, the surface temperature of each capacitor was measured using a thermographic camera. The values were measured 5 minutes after setting each current condition. The electrolytic capacitor stopped measuring at 40 A because of a significant temperature rise. The results show that the ceramic capacitors did not increase in temperature as much as the electrolytic capacitors.

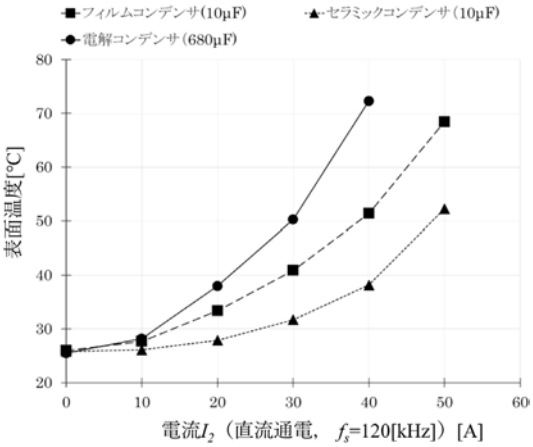


Figure 1.3.4.4 Results of temperature measurement of capacitor

(2) Loss measurement

The output current I_2 was used as DC to compare the losses when each capacitor was used. The difference between the input power with I_{in} and E_{DC} and the output power with I_2 and E_2 in **Fig. 1.3.4.** 2was measured using a power meter. This measurement also includes the loss of Arm3. **Figure 1.3.4.5** shows the measured losses when electrolytic and ceramic capacitors were used.

The 10 μF ceramic capacitor and the 680 μF electrolytic capacitor have approximately the same loss. However, the ceramic capacitor has a slightly slower increase in loss versus current; the loss of the electrolytic

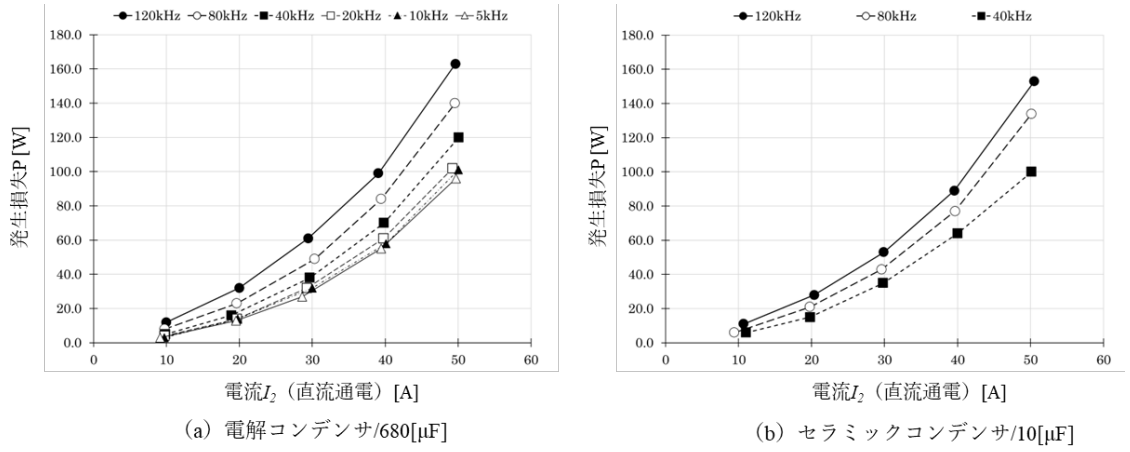


Figure 1.3.4.5 Measurement results of loss

capacitor tends to increase noticeably more than the increase in switching loss, although the result is not very clear because the switching loss of Arm3 is quite large.

(3) Dependence on frequency

The change in loss was investigated using an electrolytic capacitor when an alternating current was applied *as* I_2 (**Figure 1.3.4.6**). A sinusoidal wave from 50 to 600 Hz was applied as the AC current. It was expected that the loss would increase as the frequency increased, but the loss was significant at 150 Hz and then decreased again. Although the dependence of the electrolytic capacitor on frequency was confirmed, the reason why the maximum value exists at 150 Hz needs to be examined.

In the above, we have proposed an evaluation method for capacitors that assumes the configuration of actual power electronics circuits. Further improvements will be made in the future.

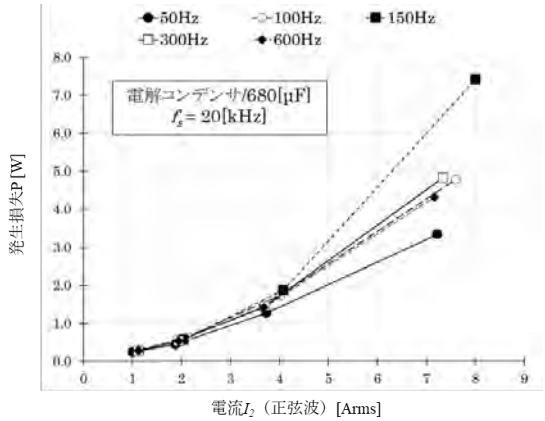


Fig. 1.3.4. 6 Measurement results of loss of electrolytic capacitor when AC current is applied

[Yoshinao Iwaji]

References

(1) Isao Takahashi and Hitoshi Haga: "Input Power Factor Correction Method of Single-Phase Diode Rectifier Circuit Using Weakened Field of IPM Motor," Transactions of the Institute of Electrical Engineers of Japan D, Vol.123, No.12, pp.1467-1473 (2003).

(2) S. Noguchi, A. Sato, and D. Takeuchi: "Reducing the Smoothing Capacitance of Direct Power Control Type PWM Rectifier and its Operating Characteristics in Unbalanced Power Supply," IEEJ Transactions D, Vol.126, No.2, pp.103-108 (2006).

(3) Daisuke Takei, Hiroshi Fujimoto, and Yoichi Hori: "Load Current Feedforward Control for Downsizing Smoothing Capacitor in Boost Converter," IEEJ Transactions D, Vol. 135, No. 5, pp. 457-466 (2015).

(4) Susumu Xu and Yoshihiko Sato: "Determination Method of Minimum Capacitance of DC Link Capacitor in PWM Rectifier Circuit-Inverter System," IEEJ Transactions D, Vol. 133, No. 8, pp. 804-811 (2013).

(5) Yoshiya Sato and Yoshinao Iwaji: "Study of Reducing Smoothing Capacitor Capacitance by High Response of Power Converter," 2024 IEEJ Industrial Applications Division Convention, No.3-73, pp.III-411-414 (2024).